

GEOLOGIC MAP OF THE GRANITE FALLS 7.5-MINUTE QUADRANGLE, SNOHOMISH COUNTY, WASHINGTON

by Joe D. Dragovich, Skyler P. Mavor, Megan L. Anderson,
Shannon A. Mahan, James H. MacDonald, Jr., Jeffery H. Tepper,
Daniel T. Smith, Bruce A. Stoker, Curtis J. Koger, Recep Cakir,
S. Andrew DuFrane, Spenser P. Scott, and Benjamin P. Justman

WASHINGTON
DIVISION OF GEOLOGY
AND EARTH RESOURCES
Map Series 2016-03
November 2016

UNREVIEWED



WASHINGTON STATE DEPARTMENT OF
NATURAL RESOURCES
DIVISION OF GEOLOGY AND EARTH RESOURCES

GEOLOGIC MAP OF THE GRANITE FALLS 7.5-MINUTE QUADRANGLE, SNOHOMISH COUNTY, WASHINGTON

by Joe D. Dragovich, Skyler P. Mavor, Megan L. Anderson,
Shannon A. Mahan, James H. MacDonald, Jr., Jeffery H. Tepper,
Daniel T. Smith, Bruce A. Stoker, Curtis J. Koger, Recep Cakir,
S. Andrew DuFrane, Spenser P. Scott, and Benjamin P. Justman

WASHINGTON
DIVISION OF GEOLOGY
AND EARTH RESOURCES
Map Series 2016-03
November 2016

*This geologic map was funded in part by the USGS
National Cooperative Geologic Mapping Program,
award no. G15AC00248*

*This publication has not been subject to a technical review by
Division geologists, editors, or cartographers;
it is the authors' original work.*

This publication has been formatted by Division staff.



WASHINGTON STATE DEPARTMENT OF
NATURAL RESOURCES
DIVISION OF GEOLOGY AND EARTH RESOURCES

DISCLAIMER

Neither the State of Washington, nor any agency thereof, nor any of their employees, makes any warranty, express or implied, or assumes any legal liability or responsibility for the accuracy, completeness, or usefulness of any information, apparatus, product, or process disclosed, or represents that its use would not infringe privately owned rights. Reference herein to any specific commercial product, process, or service by trade name, trademark, manufacturer, or otherwise, does not necessarily constitute or imply its endorsement, recommendation, or favoring by the State of Washington or any agency thereof. The views and opinions of authors expressed herein do not necessarily state or reflect those of the State of Washington or any agency thereof.

INDEMNIFICATION

Research supported by the U.S. Geological Survey, National Cooperative Geologic Mapping Program, under USGS award number G15AC00248. The views and conclusions contained in this document are those of the authors and should not be interpreted as necessarily representing the official policies, either expressed or implied, of the U.S. Government.

WASHINGTON STATE DEPARTMENT OF NATURAL RESOURCES

Peter Goldmark—*Commissioner of Public Lands*

DIVISION OF GEOLOGY AND EARTH RESOURCES

David K. Norman—*State Geologist*

Timothy J. Walsh—*Assistant State Geologist*

John P. Bromley—*Assistant State Geologist*

Washington State Department of Natural Resources Division of Geology and Earth Resources

Mailing Address:
MS 47007
Olympia, WA 98504-7007

Street Address:
Natural Resources Bldg, Rm 148
1111 Washington St SE
Olympia, WA 98501

Phone: 360-902-1450

Fax: 360-902-1785

Email: geology@dnr.wa.gov

Website: <http://www.dnr.wa.gov/geology>

Publications and Maps:

[www.dnr.wa.gov/programs-and-services/geology/
publications-and-data/publications-and-maps](http://www.dnr.wa.gov/programs-and-services/geology/publications-and-data/publications-and-maps)

Washington Geology Library Searchable Catalog:

[www.dnr.wa.gov/programs-and-services/geology/
washington-geology-library](http://www.dnr.wa.gov/programs-and-services/geology/washington-geology-library)



Suggested Citation: Dragovich, J. D.; Mavor, S. P.; Anderson, M. L.; Mahan, S. A.; MacDonald, J. H., Jr.; Tepper, J. H.; Smith, D. T.; Stoker, B. A.; Koger, C. J.; Cakir, Recep; DuFrane, S. A.; Scott, S. P.; Justman, B. J., 2016, Geologic map of the Granite Falls 7.5-minute quadrangle, Snohomish County, Washington: Washington Division of Geology and Earth Resources Map Series 2016-03, 1 sheet, scale 1:24,000, 63 p. text.

[http://www.dnr.wa.gov/publications/ger_ms2016-03_geol_map_granite_falls_24k.zip]



Contents

Introduction	1
Methods	1
Description of Map Units	3
Quaternary Sedimentary Deposits	3
Holocene Nonglacial Deposits	3
Pleistocene Glacial and Nonglacial Deposits	5
Vashon Stade of the Fraser Glaciation	5
Pre-Fraser Glacial and Nonglacial Deposits	9
Tertiary Volcanic, Intrusive, and Sedimentary Rocks	13
Mesozoic Low- to Medium-Grade Metamorphic Rocks of the Western Mélange Belt	17
Holocene to Mesozoic Tectonic Zones	25
Geochemistry	25
Quaternary Sand Deposits	25
Eocene Igneous Rocks	27
Western Mélange Belt	28
Isostatic Gravity and Aeromagnetic Analyses	30
Discussion	33
Mesozoic to Tertiary Tectonics of the Western Mélange Belt	33
Eastern and Western Mélange Belts—Correlation of Ultramafic Rocks in the Map Area	33
Metamorphic Grade, Stratigraphy, and Structural Stacking of the WMB	34
The Western Mélange Belt Structural/Stratigraphic End-members—Regular Volcanic Arc Stratigraphy and Local Structural Dismemberment in Thrust Dislocation Zones	35
Regional and Local Eocene Tectonics and Magmatism	36
Transtensional Structures—A History of Regional Transtension and Basin Inversion	36
Regional and Proximal Examples of Extensional Eocene Faults Bounding Fluvial Basins	36
Local Examples of Nonmarine Basins in the Pilchuck River Valley	36
Magmatism and Extensional Structures in the Pilchuck River Valley East of the Granite Falls Quadrangle	37
Magmatism and Extensional Structures in the Granite Falls Quadrangle	38
Regional Plate Tectonics and Magmatism	38
Fault Zones in the Study Area	39
Regional Faults	39
Woods Creek Fault Zone	39
Granite Falls Fault Zone	39
Iron Mountain Fault Zone	40
Worthy Creek Fault	41
Eocene to Plio-Pleistocene Tectonics	41
Structurally Controlled Basins and Valleys—Eocene Structural Control of Neotectonic Structures	41
Explorer Falls Basin	41
Carpenter Creek Fault Zone	42
Bosworth Lake Basin	43
Northeast-trending Pleistocene Transtensional Basins—Possible Regional Tectonic Implications	44
Everett Basin and Vertical Tectonics Along the Granite Falls Fault Zone	46

Tertiary Sedimentary and Igneous Rocks—Facies Changes and Vertical Tectonics.....	46
Neotectonism in the Map Area	47
Vashon Recessional Lake and Delta Formation.....	47
Acknowledgments.....	48
References Cited	48
Appendix A. Infrared Stimulated Luminescence Age Data.....	54
Appendix B. Seismicity in and near the Granite Falls 7.5-minute Quadrangle.....	56
Appendix C. U-Pb Zircon Geochronology	58
Methods	58
Sample 15-26H—Rhyolite of Hansen Lake (Unit Evr).....	58
Sample 15-40W#1—Dike of unit Eian.....	58
Sample 15-28AF—Volcaniclastic Metasandstone in the Western Mélange Belt	59
Appendix D. Geochemical Data	62
Appendix E. Isotope Geochemistry	63

FIGURES

Figure 1. Simplified regional tectonic map of the central Puget Lowland and Cascade Range foothills.....	2
Figure 2. Liquefaction features in unconsolidated recessional outwash sand and gravelly sand (unit Qgos) in the Menzel Lake gravel pit.	6
Figure 3. Schematic north-south cross section across the Pilchuck River anticline	11
Figure 4. East–northeast-looking block diagrams showing the development of the Explorer Falls basin.....	13
Figure 5. Contact relations of unit Eian.	18
Figure 6. Meter-scale, dacitic porphyritic dikes (unit Eian) intruding faulted Western mélange belt metasedimentary rocks (unit tz) in the Iron Mountain quarry.	18
Figure 7. Schematic map-view representation of the ‘transtensional pull apart basin’ model of the Eocene intrusive rocks of the Granite Falls stock	19
Figure 8. Structural block diagram showing the Sultan River and Lake Chaplain thrusts bounding the Lake Chaplain nappe	20
Figure 9. Stereonet of foliation and bedding in the Western mélange belt.....	21
Figure 10A. Vanadium (V) vs. Scandium (Sc) provenance diagram	26
Figure 10B. Lanthanum/Lutetium (La/Lu) vs. Lead/ Ytterbium (Pb/Yb) diagram.....	26
Figure 10C. Roser and Korsch discriminant function diagram	27
Figure 10D. Total alkali versus silica diagram	27
Figure 10E. MORB-normalized spider diagram.....	29
Figure 10F. Average REE contents of Eocene igneous units.....	29
Figure 10G. Comparison of high field strength element ratios.....	29
Figure 10H. Sr-Nd isotopic compositions.	29
Figure 11. Aeromagnetic anomaly and isostatic gravity map	30
Figure 12. Geophysical cross section model	32
Figure 13. Slickenlines on a steeply-dipping fault exposed in the rock quarry directly north of the Carpenter Creek fault.....	42
Figure 14. Regional neotectonic context of the Granite Falls Quadrangle.....	45
Figure B2. Earthquake focal mechanism ternary diagram.	56
Figure B1. Earthquake epicenters in and around the Granite Falls, Lake Roesiger, and Lake Chaplain 7.5-minute quadrangles	57
Figure C1. Concordia diagram for sample 15-26H.....	59
Figure C2. Concordia diagram for sample 15-40W#1	59
Figure C3. Probability density plot for all WMB metasandstone samples.	61
Figure C4. Probability density plot for sample 15-28AF.....	61

TABLES

Table 1.	Sedimentary provenances for Quaternary deposits.....	4
Table A1.	Infrared stimulated luminescence ages (IRSL)	53
Table C1.	Regional detrital zircon age information	59
Table E1.	Nd and Sr isotopic data.....	61
Table E2.	Pb isotopic data.....	62

MAP SHEET

Geologic Map of the Granite Falls 7.5-minute Quadrangle, Snohomish County, Washington

Geologic Map of the Granite Falls 7.5-minute Quadrangle, Snohomish County, Washington

by Joe D. Dragovich^{1, 10}, Skyler P. Mavor¹, Megan L. Anderson², Shannon A. Mahan³, James H. MacDonald, Jr.⁴, Jeffery H. Tepper⁵, Daniel T. Smith⁶, Bruce A. Stoker⁷, Curtis J. Koger⁸, Recep Cakir¹, S. Andrew DuFrane⁸, Spenser P. Scott¹, and Benjamin P. Justman³

¹ Washington Division of Geology and Earth Resources
MS 47007
Olympia, WA 98504-7007

² Colorado College
Department of Geology
14 E Cache La Poudre St
Colorado Springs, CO 80903

³ U.S. Geological Survey
Box 25046, MS 974
Denver Federal Center
Denver, CO 80225-5046

⁴ Florida Gulf Coast University
Department of Marine and Ecological Science
Fort Myers, FL 33965

⁵ University of Puget Sound
Geology Department
Tacoma, WA 98416-1048

⁶ King County Department of Natural Resources and Parks,
Water and Land Resource Division
201 S Jackson St
Seattle, WA 98104

⁷ Earth Systems
19729 207th Ave SE
Monroe, WA 98272

⁸ Associated Earth Sciences, Inc.
911 5th Ave, Suite 100
Kirkland, WA 98033

⁹ University of Alberta
Department of Earth and Atmospheric Sciences
1-26 Earth Sciences Building
Edmonton, Alberta,
Canada T6G 2E3

¹⁰ Associated Earth Sciences, Inc.
1552 Commerce Street, Suite 102
Tacoma, WA 98402

INTRODUCTION

The Granite Falls 7.5-minute quadrangle contains the city of Granite Falls, Washington. This map is the tenth in a series of geologic maps along the eastern margin of the Puget Lowland. Each map represents a year-long effort to document surficial and bedrock geology and geologic structures in the lower Snoqualmie, Skykomish, and Pilchuck River basins of King and Snohomish Counties. This effort has particular relevance to the understanding of geologic hazards facing the greater Seattle/Everett area, because it documents that this densely populated region is also seismically active.

Major active or potentially active faults in and near the quadrangle include the Southern Whidbey Island fault zone (SWIF), Cherry Creek fault zone (CCFZ), Monroe fault (MF), Pilchuck fault zone (PF), Woods Creek fault zone (WCFZ), and the Granite Falls fault zone (GFFZ). Active or potentially active structures include the Monroe anticline (MA), Monroe syncline (MS), Explorer Falls basin (EFB) and the Lake Bosworth basin (BLB)(Fig. 1). The map area is north of the Rattlesnake Mountain fault zone and the SWIF—fault zones that cut late Pleistocene strata in King and Snohomish Counties. The active CCFZ is conjugate to the SWIF and was responsible for the shallow 1996 Duvall earthquake (M5.4). Both of these structures are responding to north–south crustal compression across the Puget Lowland (Wells and others, 1998). The EFB is a graben that was initially mapped in the Lake Chaplain quadrangle southeast of the map area and extends into the Lake Roesiger quadrangle south of the Granite Falls quadrangle.

The map sheet presents the geologic map, two cross sections, and a correlation diagram. Appendix A contains infrared stimulated luminescence (IRSL) age information for

Quaternary deposits. Appendices B and C provide earthquake and U-Pb zircon age data, respectively. Appendix D provides geochemical data for sand and rock samples. Appendix E presents isotope geochemistry for rock samples. Our Data Supplement provides earthquake, U-Pb zircon, whole-rock geochemical data as well as a full sample inventory for the study in a separate Excel spreadsheet.

The Granite Falls quadrangle abuts the Lake Chaplain and Lake Roesiger quadrangles (Dragovich and others, 2014a, 2015), and this report continues that mapping northward. To reduce the number of references to these studies we will simply use the terms “Monroe quadrangle”, “Lake Chaplain quadrangle”, and “Lake Roesiger quadrangle”. Mapping in the Granite Falls quadrangle has resulted in new insights into the geology of the adjacent quadrangles.

To enhance our mapping, we compiled several types of geologic analyses including prior geologic mapping of Booth (1989), Minard (1985a,b), Danner (1957) and Tabor and others (2002), and surface and subsurface information provided by geotechnical companies. We follow the nomenclature of Newcomb (1952), Booth (1989, 1990) and Thorson (1989) for many glacial features and add a few informal names. Our fault, fold, and geomorphic feature nomenclature, such as for the Granite Falls fault zone (GFFZ) and the various glacial recessional complexes, is informal.

METHODS

We use the Udden-Wentworth scale (Pettijohn, 1957) to classify unconsolidated sediments, Dickinson’s (1970) terminology for

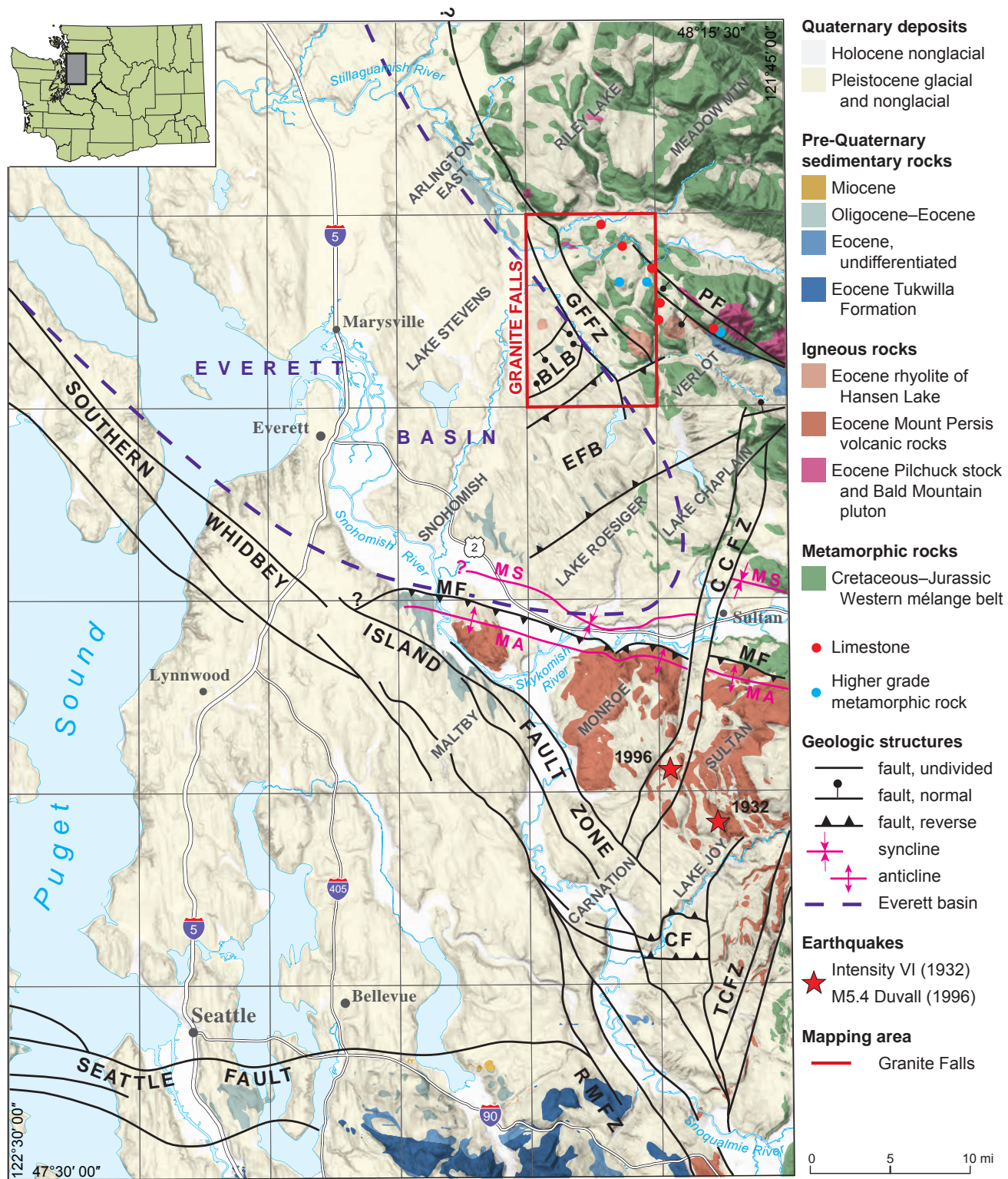


Figure 1. Simplified regional tectonic map of the central Puget Lowland and Cascade Range foothills showing the Granite Falls 7.5-minute quadrangle (red rectangle). We extend the Explorer Falls basin (EFB) from the Lake Chaplain quadrangle (Dragovich and others, 2014a) and Lake Roesiger quadrangle (Dragovich and others, 2015) into the Granite Falls quadrangle and add the Bosworth Lake Basin (BLB). The EFB is bound by the Three Lakes Hill fault on the south and the Carpenter Creek fault on the north. We also show the Pilchuck River fault (PF) of Tabor and others (2002) east of the map area. The PF and EFB might be related Eocene extensional structures that preserve Paleogene to Pleistocene basin sediments in the Pilchuck River valley. The broad Granite Falls fault zone (GFFZ) bounds the Everett basin in the Granite Falls quadrangle. The GFFZ is likely the southwestern extension of the Lake McMurray fault zone of Dragovich and DeOme (2006) and is similar to the Lake Chaplain fault of Cheney (1987). See Dragovich and others, (2011a, 2012, 2013, 2014a, 2015) for previous mapping of the Monroe syncline (MS), Monroe fault (MF) and the Monroe anticline (MA) as well as the Cherry Creek fault zone (CCFZ). The Tokul Creek fault zone (TCFZ) is similar to the CCFZ; they are likely left-lateral conjugates of the southern Whidbey Island fault zone (SWIF). The Rattlesnake Mountain fault zone (RMFZ) is likely a southern continuation of the SWIF. The Seattle fault and the SWIF are significantly simplified from Dragovich and others (2002) and Sherrod and others (2008).

sandstones, and Le Maître and others' (2002) and Frost and others' (2001) terminology for igneous rocks. Clinopyroxenes are collectively described as 'augite' but may include other petrographically similar varieties. We use the time scales of the U.S. Geological Survey Geologic Names Committee (2010) and Wolfe and others (1998). Description of weathering rinds on basaltic clasts follows the methodology of Colman and Pierce (1981). We used the landslide classification system of Varnes (1978a,b). Quaternary sand deposit provenance is defined by compositional data derived from sand modal estimation data, petrographic observations, and sand geochemistry, as well as field data and observations (Table 1). Thin-section modal estimation data on sand-size fractions helped differentiate several glacial and nonglacial units. An important compositional discriminator for Quaternary strata studied for this report is the ternary system composed of monocristalline quartz (Qm_x); quartz-mica tectonite, polycristalline quartz, and chert (Qp_x); and potassium feldspar (PF_x). The normalized $Qm_xQp_xPF_x$ data provided herein were obtained from petrographic examination of 30 sand samples from the Granite Falls quadrangle, as well as from Dragovich (2007) and Dragovich and others (2009b, 2010a,b, 2012, 2013, 2014a, 2015). Elsewhere, percentages for individual mineral or lithic grains are not normalized and represent their abundance within the total clast population. See *Geochemistry* for a presentation and discussion of major and trace element compositions of the Western mélangé belt (WMB), Eocene igneous rocks, and Quaternary sand deposit samples.

DESCRIPTION OF MAP UNITS

Quaternary Sedimentary Deposits

HOLOCENE NONGLACIAL DEPOSITS

Qp Peat—Loose or soft peat, muck, and organic silt and clay, with local diatomite and thin beds of Mazama ash (Rigg, 1958). Peat is present in abandoned river channels where it is interstratified with alluvial deposits (for example, in the South Fork Stillaguamish River valley). Peat is also found in upland depressions and kettles overlying low-permeability glacial deposits such as till or ice-contact deposits. Low-energy silt, sand and peat deposits dominate Carpenter and Worthy Creek Holocene valley fill. Most peat was mapped using lidar, USGS topographic maps, and Booth (1990). Rigg and Richardson (1938), Hansen (1947), and Rigg (1958) cored peat in sec. 18, T30N R7E, near the eastern border of the town of Granite Falls; they documented an 8.2-m-thick sequence of sphagnum and fibrous and sedimentary peat interbedded with pumicite overlying lake mud. See Rigg (1958) for a description of other peat deposits near the study area.

Qa Alluvium—Sand, silt, gravelly sand, and sandy pebble gravel; locally includes peat and organic sediments and (or) cobble gravel; clasts subrounded to rounded; some subangular to angular clasts in Canyon Creek, Worthy Creek, and Carpenter Creek alluvium;

loose; well stratified and sorted; planar-bedded sand, and detrital wood are common; sand is typically light olive gray to light brownish gray. Pilchuck River sand (~74% SiO_2) contains metasedimentary lithic grains of mostly meta-argillite, metasandstone, metachert and phyllite (~50%), monocristalline quartz (~15–22%), polycristalline quartz (~10–22%), plagioclase (~8–20%), some granitic lithic grains (~2–5%), volcanic/greenstone lithic grains (3–5%), hornblende (~4–5%), potassium feldspar (~4–8%) and mica grains (~5%), and a trace of both pyroxene and serpentinite grains. South Fork Stillaguamish River sand (~74% SiO_2) is dominated by local mélangé belt metasedimentary clasts (~35%) and contains significant monocristalline quartz (~15%), polycristalline quartz (~12%), plagioclase (~10%), and volcanic lithic and greenstone grains (~10%). It also includes some hornblende (~3%), granitic lithic grains (~5%), and potassium feldspar (~2%), as well as mica, serpentinite, pyroxene and sedimentary lithic grains (~8%). This combination of minerals and lithic grains (and their relative proportions) for the South Fork Stillaguamish and Pilchuck Rivers represents sediment eroded from the central Cascade Range to the east and has a Pilchuck provenance (PP provenance; Table 1). Some of the metasedimentary lithic grains may be from the feldspathic sandstone of Tabor and others (2002) in the Pilchuck River valley to the east (Fig. 1). There is less mica in modern channel sands than in the PP facies sands (for example, unit Qcph) due to the dominance of exposed overbank sand facies in the ancient successions. Canyon Creek sand (~72% SiO_2) is mostly subangular to subrounded grains of phyllite, meta-argillite, metasandstone, metachert (70–80%) with monocristalline quartz (~10%), polycristalline quartz (~10%), and plagioclase (~5%), as well as greenstone lithic grains and minor pyroxene, potassium feldspar, and volcanic lithic grains. The abundance of phyllitic and metachert lithic clasts is consistent with sources in the higher grade local mélangé exposed in the Canyon Creek basin to the northeast. Carpenter Creek alluvium contains reworked Pleistocene sediment partly as a result of glacial to sub-glacial or proglacial erosion of these unconsolidated deposits during Vashon ice recession. Our field examination of the Carpenter Creek alluvium indicates that it is dominated by sand, silt, clay, and peat and is similar to the mica-rich, locally derived Woods Creek alluvium in the Lake Roesiger quadrangle.

Qls Landslide deposits (Holocene to latest Pleistocene) Diamicton or boulder gravel with minor sand or gravel beds; locally modified by stream processes; loose or soft; typically poorly sorted and unstratified; clasts are angular to subangular where derived from bedrock but mostly rounded where the origin is Quaternary deposits. Mapped landslides include lateral spreads, slump earthflows, debris slumps, larger

Table 1. Sedimentary provenances for Quaternary deposits in the Granite Falls, Lake Roesiger, Lake Chaplain, Sultan, Lake Joy, Monroe, Carnation, North Bend, Fall City, and Snoqualmie quadrangles (Dragovich, 2007; Dragovich and others, 2009a,b,c, 2010a,b, 2011a,b, 2012, 2013, 2014a, 2015, this study). The top-most row of the table explains the presentation of information for each provenance type. Geologic units from the Granite Falls quadrangle are black, those in adjacent quadrangles are gray. Provenance is assigned using composition from sand point-count data, petrographic observations, geochemistry, field data, and detrital zircon ages. Nonglacial Pleistocene fluvial units are similar to those of modern (Holocene) rivers of the same provenance. EFB, Explorer Falls basin; RMFZ, Rattlesnake Mountain fault zone; SWIF, southern Whidbey Island fault zone. SP, Snoqualmie or Skykomish River provenance; PP, Pilchuck River provenance; LP, local provenance; PG, Puget Group provenance; NP, northern or continental glacial provenance.

Provenance name	Dominant lithology	Other relevant information
Lithofacies type		
River type or name		
Geologic units	Flow direction	
SP provenance	Abundant monocrySTALLINE quartz, K-spar, and plagioclase, with minor but distinct granitic lithic grains, biotite, pyroxene, and hornblende.	The major bedrock sources for SP sediments are Tertiary intrusive rocks such as the widely exposed Snoqualmie, Index, and Grotto batholiths. Ancient (Pleistocene) and modern Skykomish River and Snoqualmie River alluvial facies are similar in composition. The Monroe synclinal basin hosts a substantial thickness of these deposits. These major river valleys appear to be structurally controlled by faults such as the RMFZ–SWIF and (or) Monroe fault. See PP provenance for the occurrence of Whidbey Formation and Hamm Creek unit deposits of Cascade Range lithofacies in the Granite Falls area.
Cascade Range lithofacies		
Snoqualmie and Skykomish rivers	Regional-scale modern and ancient rivers; generally flow west from the Cascade Range.	
Qa (Snoqualmie and Skykomish Rivers), QCo, QCws, QCh, QCpf, QCph		
PP provenance	MonocrySTALLINE quartz, K-spar, and plagioclase, with lesser but distinct metasedimentary lithic grains, biotite, pyroxene, and hornblende.	Ancient Pilchuck River alluvium is generally more weathered than correlative SP deposits to the south, but they are compositionally similar. In detail, these deposits have more detritus from the Western mélange belt, particularly metasedimentary detritus, as documented by detrital zircon ages (Dragovich and others, 2014a, 2015). Thick deposits of ancient Pilchuck River sediment (unit QCph) occur in the Pleistocene Explorer Falls basin; PP-provenance sediment fills the valley axis and LP-provenance (unit QCph) alluvial fan deposits occur along the basin margin. In the Granite Falls quadrangle, Whidbey and Hamm Creek PP strata are exposed in the northernmost part of the EFB on the northern limb of the Pilchuck anticline, as well as in the newly named Bosworth Lake basin.
Cascade Range lithofacies		
Pilchuck River	Regional-scale modern and ancient Pilchuck River; generally flows west from the Cascade Range.	
Qa, QCh, QCph, QCwpv		
LP provenance	Lithic grains are common and include volcanic, meta-argillite, and metasandstone detritus primarily derived from the volcanic rocks of Mount Persis and the Western mélange belt (WMB). Serpentinite (to 10%) occurs in unit QCph along the northernmost part of the EFB, indicating derivation of sediment from north of the Carpenter Creek fault.	Ancient Tolt River alluvium and alluvial fan deposits are similar to modern Tolt River alluvium. Ancient Tolt River alluvium interfingers with ancient Snoqualmie River alluvium. Ancient Youngs–Elwell Creek alluvium interfingers with ancient Skykomish River alluvium (unit QCo). (See Dragovich and others, dates.) Ancient alluvium (unit QCph) dominated by metasedimentary clasts of the WMB distinctly interfinger with PP Pleistocene alluvium (unit QCph) in the Explorer Falls basin. In the Granite Falls quadrangle we map LP of the Hamm Creek unit along the northern limb of the Pilchuck anticline. Unit Qa along Canyon Creek has a composition, thus provenance, more consistent with LP than PP due to the Holocene erosion of this river system into predominantly into mélange belt lithologies. In many areas LP Pleistocene alluvial and alluvial facies develop across potentially active fault scarps and thus have important potential neotectonic implications.
Western mélange belt and (or) Mount Persis lithofacies		
Local rivers and streams	Low-order rivers and local streams that generally flow west in the foothills of the Cascade Range. Includes the modern and ancient Tolt River, Sultan River, and Youngs–Elwell Creek and Canyon Creek valleys.	
Qa (Tolt River, Youngs–Elwell Creek, and Sultan River), QCoI, QCChmp, QChI, QCphI		
PG provenance	Abundant lithic grains of andesite and recycled arkosic (feldspathic) sandstone and siltstone clasts from the Tukwila, Renton, and Tiger Mountain Formations.	These deposits are similar to the locally derived LP deposits, but differ because their source regions have distinctive and unique lithologies that provide paleogeographic information about ancient sediment dispersal systems. Fluvial PG sediments likely interfinger with fluvial SP sediments southwest of the map area near Carnation.
Puget Group lithofacies		
Local rivers and streams	Local rivers and streams that flow north and northwest into the lowlands.	
QCwp		
NP provenance	Polymict lithic clast types—including high-grade metamorphic clasts—and a high polycrystalline/ monocrySTALLINE quartz ratio; less K-spar compared to Cascade Range sources. Locally mixed with Cascade Range lithofacies.	See Booth (1990) for further discussion of the provenance and depositional environments of NP glacial deposits. These sediments are locally mixed with some sediments of eastern and northeastern Cascade Range provenance (particularly some Vashon Stade recessional deposits transported by ice-marginal meltwater), particularly in some proglacial lake settings proximal to the Cascade Range. Continental glacial deposits distinguished from nonglacial sediments by higher polycrystalline quartz content and the variable or polymictic composition of the sands.
Northern lithofacies		
Continental glaciers	Deposited by continental glaciers that advanced from the north. Flow directions vary based on local glacial conditions and topography.	
Qglr, Qgos, Qgod, Qgof, Qgic, Qgik, Qgog, Qglv, Qgav, Qglv, Qgtp, Qgop, Qglp, Qgdd, Qgtd, Qgdpd		

debris flow deposits, and areas of thick colluvium and talus. This unit may include chaotic or stratified slump blocks or debris-flow aprons that originated in unstable Vashon recessional deposits perched on hillslopes. Some landslides may have initiated during late Pleistocene deglaciation. We show only the most prominent landslide complexes in the study area, for example, the geomorphically distinct landslides in the South Fork Stillaguamish River, Pilchuck River, and Canyon Creek gorges in the eastern part of the map area. In the southern part of the quadrangle, groundwater flow through highly weathered and clay-rich Pleistocene sediments has resulted in both deep-seated and shallow landslides.

Qaf Alluvial fan deposits (Holocene to latest Pleistocene)—Diamicton, gravel, boulder gravel, and sand; loose; poorly to moderately sorted; moderately stratified to massive; locally contains locally voluminous debris flow deposits. Fan-shaped morphology results where streams emerge from confining valleys. Unit Qaf was distinguished from unit Qls by location and morphology on lidar imagery and (or) aerial photographs. Some fans may have begun as fan deltas that graded to local proglacial lakes.

PLEISTOCENE GLACIAL AND NONGLACIAL DEPOSITS

Vashon Stade of the Fraser Glaciation

During the most recent glaciation, continental ice of the Puget lobe advanced south from British Columbia across the Puget Lowland and across the foothills of the Cascade Range, up major west-draining river valleys, covered the map area, and terminated along the Cascade Range 9 to 13 mi east of this quadrangle (Booth, 1990). Glacial ice and meltwater deposited glacial drift and carved the southern Puget Lowland into a complex geomorphology that provides insight into late Pleistocene glacial processes. Vashon deposits are typically fresh or slightly weathered; basalt clasts have thin (commonly <1.0 mm) or no weathering rinds.

Vashon Recessional Deposits

Deglaciation of the Puget lobe ice sheet began ~14,000 yr BP along the Cascade foothills directly east of the map area, and the map area was ice free by ~13,500 yr BP (Porter and Swanson, 1998; Dragovich and others, 2014a). The lobe's ice front receded northwest across the map area, leaving widespread deposits that are horizontally and vertically complex due to facies changes generated by dynamic glacial depositional environments. A series of ice-marginal lakes and connecting glaciofluvial channels formed in the wake of the retreating ice lobe. The geometry, inset relations, and elevations of the recessional deposits reflect successive lowering of base level as valleys became ice-free and spillways migrated west and north. Younger inset or terraced recessional deposits grade to these new spillways (Knoll, 1967; Booth, 1990; Porter and Swanson, 1998; Dragovich and others, 2014a, 2015). Sand in these recessional deposits is rich in polycrystalline quartz

and generally compositionally distinct from the Pleistocene Cascade Range provenance (Table 1). However, some early Vashon recessional sands have a Cascade provenance; their sources were meltwater streams emanating from the Cascades and that flowed into ice-dammed lakes in the Pilchuck, South Fork Stillaguamish, and Canyon Creek valleys. Also, local glacial reworking of older unconsolidated deposits in the Explorer Falls and Bosworth Lake basins produced recessional sand deposits containing Quaternary detritus that has a partial Cascade Range provenance. See *Vashon Recessional Lake and Delta Formation* for further discussion.

Qglr Recessional glaciolacustrine deposits—Silt, clayey or sandy silt, and silty sand, typically with scattered dropstones; local lenses or beds of sand or gravel; loose or soft; massive or laminated to thinly bedded; locally displays varve-like rhythmites. Upward-fining sequences record waning lake sedimentation in small proglacial lakes. Upward-coarsening sequences may begin as glacial-lake deposits (units Qglr and Qgos) and grade into overlying deltaic (unit Qgod) or fluvial (unit Qgof) deposits as outwash prograded into glacial Lake Skykomish or smaller ice-marginal glacial lake environments. Sediments of glacial Lake Pilchuck were deposited at various elevations in the eastern part of the map area and record a westward-receding ice margin and episodic but gradual lowering of lake levels from ~900–940 ft in the Mountain Loop Highway ice-contact complex in the northeastern corner of the map area to ~460 ft elevation of the Granite Falls Delta Complex in the northwestern part of the quadrangle. See *Vashon Recessional Lake and Delta Formation* for further discussion. In the Pilchuck River valley in the northeast corner of the map area, Booth (1989, 1990) mapped recessional glaciolacustrine deposits. Our mapping confirms these recessional deposits and includes both recessional sand deposits (unit Qgos) and advance lake deposits (unit Qglv). Broecker and others (1956) reported an uncalibrated radiocarbon date of 11,900 yr BP from peat overlying soft blue clay (unit Qglr) in the Lake Joy quadrangle; that indicates the broader area was ice free before that time.

Qgos Outwash sand—Sand and pebbly sand with some interbeds of silty sand, silt, or gravel; sand is typically gray to brownish gray and weathers light brownish gray; loose or soft; unstratified to weakly stratified; locally planar-bedded, laminated, or, rarely, crossbedded. Sands in the Menzel Lake Pit (significant site 10D) show widespread sand dikes (Fig. 2). Sand contains monocrystalline quartz (~15–20%), polycrystalline quartz (~20–28%), plagioclase (~15%), mica (~1–5%), and minor hornblende/pyroxene (~3%), and local minor potassium feldspar (~0–3%). Lithic grains (~30–35%) are comprised of metamorphic grains and fewer sedimentary, volcanic, and granitic grains. The overall sand composition and fining trends indicate substantial subglacial and englacial to proglacial

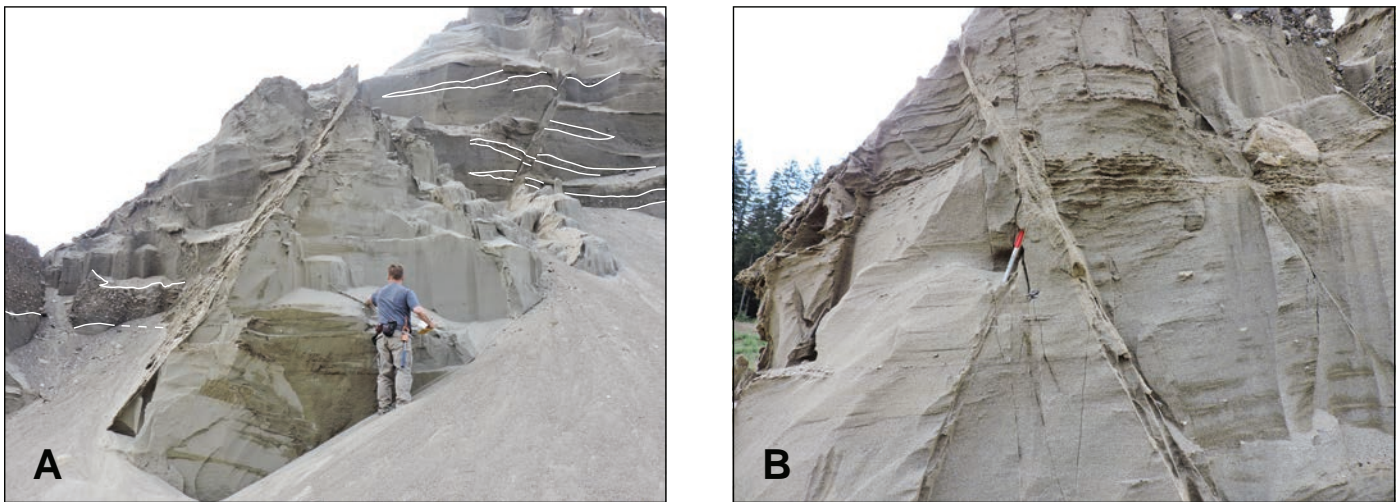


Figure 2. Liquefaction features in unconsolidated recessional outwash sand and gravelly sand (unit Qgos) in the Menzel Lake gravel pit. This deformation is interpreted as a post-glaciation liquefaction event or events producing thin sand dikes and extensional displacement features that probably result from lateral spreading of these loose deposits. A) Displacement along a steeply dipping surface showing offset locally as high ~2 m likely the result of slumping during lateral spreading (white lines added along strata for emphasis). B) Detail of conjugate fault surfaces offsetting sub-horizontal bedding. Extensional offset along ‘fault-like’ discontinuities combined with the orientation of the displacement planes with sloping free faces in the Menzel Lake ice-contact complex suggest lateral spreading.

recessional deposition that has a partial Cascade Range provenance. The fairly high percentage of polycrystalline quartz is consistent with a strong northern glacial provenance. Unit Qgos is interbedded with recessional lake deposits (unit Qglr), fluvial outwash deposits (unit Qgof), and deltaic or kame-delta deposits (unit Qgod). Vertical and horizontal fining trends indicate mostly shallow-water glaciolacustrine deposition along delta fronts or sandy lake facies adjacent to silty glaciolacustrine deposits (unit Qglr). In some places, sandy deposits may be higher energy lake facies that represent former shorelines or sandy turbidites in finer grained lake sediments. Most of the lateral and vertical fining trends—from gravel to sand to silt across these complexes—are best explained by simple progradation of a delta into a glacial lake environment proximal to the ice front. Local examples of this are the Mountain Loop Highway ice-contact complex and the Menzel Lake delta complex; in these areas, lake sand (unit Qgos) and near-ice deposits (unit Qgic) coarsen upward into sand and gravel (unit Qgod or Qgof) and fine downward or laterally into silty lake deposits (unit Qglr). Local differences in the proximity of outwash and ice-front deposits complicate this interpretation. Delta front and lake sands in the Granite Falls delta complex in and west of the City of Granite Falls are associated with the last episode of glaciolacustrine deposition in the map area. These sands correlate with the Stillaguamish Sand Member of the Vashon Drift of Newcomb (1952), Minard (1985a,b), and Tabor (2002). Minard (1985b) noted:

“At least 15 m of the unit is exposed in a pit along the south side of the South Fork of the Stillaguamish River, but the unit may be as much as 30 m thick. The

large volume of material was deposited by combined southward flow of the South Fork of the Stillaguamish and Pilchuck Rivers when ice blocked the South Fork at Arlington, forming glacial Lake Stillaguamish and diverting drainage south through the Pilchuck River valley”.

Qgod Deltaic outwash and kame deltas—Sandy cobble gravel, gravel, and pebbly sand; sand is typically dark blue-gray to light gray and weathers yellowish brown or brownish gray; loose; moderately to well sorted and well stratified in thin to very thick beds. Deltas have high-amplitude planar foreset beds that graded to temporary ice-dammed lake levels; examples are at significant sites 10P, 17F, 42X in the Canyon Creek delta complex, near Worthy Creek, and near the Mountain Loop Highway ice-contact complex. Deltas and delta complexes in the map area include the Worthy Creek, Canyon Creek, Granite Falls, Menzel Lake, and Carpenter Creek complexes. Deltas are also present in the Mountain Loop Highway and Pilchuck River ice-contact complexes. Delta-front gravel consistently grades to more distal delta front sand (unit Qgos) and glacial-lake silt (unit Qglr) in most areas. The delta complexes are graded to various levels of glacial Lakes Pilchuck and Stillaguamish and mostly accumulated adjacent to ice-contact complexes or have pitted outwash plains or other evidence for ice-proximal deposition. These deposits have a northern source provenance (NP provenance; Table 1). See *Vashon Recessional Lake and Delta Formation* for further discussion.

- Qgof Fluvial outwash deposits**—Cobble and boulder gravel, gravel, pebbly sand, and interbeds of sand and (or) rare silt; sand is gray-brown and weathers olive-yellow; loose; moderately to well stratified and commonly contains medium to very thick subhorizontal beds that have local bar or ripple crossbedding, imbricated gravel, scour structures, and (or) rip-up clasts. Most fluvial outwash—such as the Menzel Lake delta—grades laterally into ice-contact complexes and suggests near-ice origin. This unit generally lacks ice-contact sedimentary structures and other geomorphic and stratigraphic evidence for nearby ice, but some unit Qgof outwash grades laterally into pitted outwash plains that suggest isolated kettle lakes. For example, fluvial outwash east of the Mountain Loop Highway contact complex is mildly pitted and resembles kame complexes in the map area (also see unit Qgik). In several areas unit Qgof is topset beds of deltas (unit Qgod). Many Vashon outwash recessional deposits in the map area are preserved in remnant fluvial terraces formed as a result of fluvial meltwater incision into recessional outwash or older deposits as the glacial lake base levels dropped during deglaciation. For example, multiple prominent terrace levels above the South Fork Stillaguamish River are graded to falling lake levels. Lidar imagery indicates that as many as 10 terraces occur above the south fork and record incision during recession. The timing and elevation of local controlling outlet lakes, deltas, and connecting channels are also discussed by Thorson (1989), Booth (1989, 1990), and Dragovich and others (2011a, 2013, 2014a, 2015) and in the section titled Vashon Recessional Lake and Delta Formation.
- Qgic Ice-contact deposits, undivided**—Cobble to boulder gravel and gravel, locally containing diamicton, silty pebble gravel, sand, pebbly sand, and silt; loose or soft; moderately stratified; medium to very thickly bedded with varied sorting; abrupt grain-size changes common. Primary structures include oversteepened and contorted bedding and other ice-shear features, all of which produce varied dips. Diamicton was deposited in melt-out, debris flow, and dropstone-rich lacustrine environments, among others. The surface of the deposit is typically hummocky and contains kettle depressions. Ice-contact deposits are common in the map area and generally define north-south to north-northeast- to south-southwest-trending belts of discontinuous complexes. Some of the prominent examples are the Mountain Loop Highway and Pilchuck River ice-contact complexes. The Mountain Loop Highway complex includes glaciolacustrine, glaciofluvial, and deltaic outwash locally forming kames and hummocky dead-ice facies. Dead-ice deposits grade into recessional outwash fluvial and deltaic deposits (units Qgof and Qgod) of the Menzel Lake and Carpenter Creek deltaic complexes and associated glacial lake deposits probably deposited in glacial Lake Pilchuck (units Qglr and Qgos). Eskers are evident on lidar in the Carpenter Creek ice-contact deposits; see significant site 23H in the south-central part of the map area. These deposits indicate subglacial drainage southeast towards the ice margin. Ice-contact deposits and related kames form four discontinuous north-northeast-trending belts; this implies that the ice margin progressively waned or stagnated along highland areas during ice recession. These belts correlate to recessional intervals 3 to 5 of Booth (1989). Similar ice-contact belts are mapped in the Lake Roesiger, Lake Chaplain, and Sultan quadrangles, where these deposits are progressively younger to the west or northwest. Some small, isolated ice-contact deposits were likely deposited adjacent to local ice tongues that were stable just long enough for debris to accumulate. See Booth (1989, 1990) or Knoll (1967) for a discussion of the temporal and spatial relations of deglaciation and Booth (1984, 1986, 1990) for a subglacial depositional model and a discussion of the geomorphology of proglacial, englacial, and subglacial features mapped in the Granite Falls 15-minute quadrangle. Also see *Vashon Recessional Lake and Delta Formation* in the discussion. Unit Qgic is locally divided into:
- Qgik Kames**—Cobble and boulder gravel, gravel, sand, pebbly sand, and rare lenses of diamicton (mostly flow or melt-out till from buried sediment-laden ice blocks); sand is typically dark yellowish gray to gray; loose; moderately to well stratified, medium to very thickly bedded, and commonly contains rip-up clasts of till or silt, cut-and-fill structures, and (or) localized oversteepened or slumped bedding. This unit includes both fluvial and local deltaic kame deposits. We mapped kames where sedimentary structures, geomorphology, and (or) geologic setting imply lateral ice buttressing. The Mountain Loop Highway ice-contact complex contains both ice-contact diamicton and fluvial gravels (unit Qgik) that form a distinct inset terrace at 900–940 ft elevation. Lower elevation portions of this complex, along the easternmost edge of the quadrangle, form an inset kame terrace composed of deltaic deposits that grade southward into lake deposits. In other areas, receding or wasting ice impinged upon highlands, leaving small isolated kame deposits. Some fluvial-deltaic deposits grade laterally into or overlie kame deltas (unit Qgod) and (or) proglacial-lake deposits (units Qgos and Qglr), forming upward-coarsening sequences.
- Qgog Outwash gravel deposits, undivided**—Boulder-pebble gravel to pebbly sand; loose; massive to crudely bedded; mostly ice-contact deposits, including kame

outwash, but may include any of the gravelly Vashon recessional facies or gravelly glacial lake beach facies. This unit is poorly exposed, hence depositional environment is not defined.

Vashon Advance Proglacial and Subglacial Deposits

Throughout the map area, drumlins and flutes show that ice of the Puget lobe advanced from west-northwest to east-southeast; the curvature of the fluting shows an increasingly easterly track up the Pilchuck River valley. Ice advance over this part of the lowland occurred about 14,500 radiocarbon years ago and blocked Pleistocene rivers, creating extensive temporary lakes across much of the map area (Mackin, 1941; Booth, 1989, 1990). Most advance outwash consists of proglacial fluvial-deltaic deposits; kame, other ice-contact, or subglacial ice-tunnel sediments that were deposited between advancing ice and restricting highlands. Facies relations among river and delta deposits (unit Qgav) and lake deposits (unit Qglv), as well as their thickness and widespread distribution, indicate that one or more large proglacial lakes progressively occupied significant portions of the region during ice advance (Knoll, 1967; Dragovich and others, 2007, 2009a,c, 2010b, 2011a, 2012, 2013, 2014a, 2015).

Several fluvial-deltaic complexes mantle the pre-Vashon Stade topography. Deltas prograded into paleovalleys, particularly along the east-southeastern portion of the map area. As in the Sultan and Lake Chaplain quadrangles, a complex series of deposits formed in front of the advancing ice. Regionally, bedding in advance outwash and lake deposits has a general southeast dip that reflects either: (1) glaciofluvial or deltaic deposition of foreset beds on the lee side of fluvial bars that slope away from the advancing ice, or (2) steep gradient, high-energy braided stream channel deposits (Dragovich and others, 2015). These subtle dips probably do not indicate significant tectonic tilting in most of the quadrangle. In contrast older Pleistocene ('ancient') alluvial nonglacial (overbank) deposits—unit Qcph, for example—that were originally subhorizontal were subsequently tilted.

Advance outwash is polycrystalline-quartz-rich, contains a variety of lithic sedimentary, igneous, and metamorphic grain types (unnormalized ~50–70%), and has an average ternary composition of ~Qm₄₀Qp₅₄PF₆. Cascade Range provenance sediments, in contrast, contain significant polycrystalline quartz and less monocrystalline quartz, plagioclase, and little or no hornblende, potassium feldspar, or mica (0–4%) (Table 1). Regional petrographic and geochemical analyses of polymict advance outwash sand (65–71% SiO₂) indicate a complex provenance involving local and northern sources, particularly where advance outwash has scoured and incorporated the underlying strata (Dragovich and others, 2014).

Qgtv Lodgment till—Unstratified mixture of clay, silt, sand, and gravel (diamicton), and rare lenses of sand and gravel; grayish blue to very dark gray, locally slightly weathered to mottled yellow-brown; larger clasts are supported in a matrix of sand and silt; unsorted; dense; accreted at the base of the Vashon-age ice sheet and typically displays a subhorizontal

shear fabric. Clasts are both locally derived and northern sourced and rounded to subangular. Angular clasts are present where this unit directly overlies bedrock. Till is generally 1.0 to ~20 m thick and is unconformable on advance deposits, older Quaternary deposits, and bedrock. An outcrop of glacial diamicton along the Pilchuck River at significant site 201B is likely Vashon-age till and has a sub-vertical, north-east-striking shear fabric that might be tectonic and related to nearby strands of the Granite Falls fault zone. This fault is locally injected by steeply dipping clastic dikes. We observed older till only rarely in the map area. A probable alpine till containing clasts derived largely from the mélangé belt rocks occurs at significant site 17X directly south of the South Fork Stillaguamish River near the eastern boundary of the study area.

Qgav Advance outwash deposits—Sand and pebble gravel, sand and cobble gravel, and local silt; dense; sandy beds are dark green-gray, weathering to yellowish brown, light-yellowish brown, or pale brown; typically well sorted; mostly thinly to very thickly bedded with local silt interbeds, rip-up clasts, deltaic and bar foresets, and cut-and fill-structures; locally contains detritus reworked from underlying Quaternary units, such as units Qch and Qcph. Advance outwash is intricately interlayered with, conformably overlies, or may locally underlie glacial-lake deposits (unit Qglv). Unit Qgav is most commonly overlain by Vashon lodgment till (unit Qgtv) along a sharp contact. Composite sections of fluvial-deltaic advance outwash and glacial-lake deposits are thick where deltas prograded into restricted proglacial lakes during ice advance. Radiocarbon dates reported for unit Qgav from studies south or west of the map area are 14,450 to 14,560 yr BP (17,313–17,426 cal yr BP) (Porter and Swanson, 1998; Associated Earth Sciences, Inc., 2003; Dragovich and others, 2007, 2014a). OSL and IRSL ages of 14.1 ± 0.59 ka and 16.4 ± 0.64 ka respectively and a radiocarbon age of 14,900 ± 50 yr BP (17,985–18,250 cal yr BP) are from this unit directly west of the Sultan River in the Lake Chaplain quadrangle southeast of the map area.

Qglv Advance glaciolacustrine (lake) deposits—Silt, clayey silt, pebbly silt, and diamicton, locally with very thin to thick beds of sand or pebbly sand; stiff to hard, or dense to very dense; stratification and sorting varied, but commonly massive or thinly bedded, laminated, or varved; typically contains scattered dropstones and beds or lenses of massive till-like diamicton that may be iceberg melt-out till or flow till. Some exposures are mostly diamicton with thin, wispy interbeds of silt or laminated silt and sand. Outcrops with contorted or folded bedding as a result of ice-shear are sparse in the Lake Roesiger and Granite Falls areas compared to the Sultan and Lake Chaplain quadrangles. At significant site 30H, along

the Pilchuck River in the western part of the map area, chaotically folded advance lake laminated silt contains open to tight folds probably due to ice shear. Advance lake deposits are widely exposed in the quadrangle, forming deposits that are locally as much as 40 m thick (Cross Sections A and B). These deposits represent a large proglacial lake or lakes dammed between the east-southeasterly advance of the Puget lobe and the Cascade foothills; the unit is widespread across the quadrangle. Unit **Qga_v** regionally overlies unit **Qgl_v** as a result of progradation of fluvial and deltaic outwash over proglacial lake deposits, but there are local exceptions where this order is reversed. In places, the two units are complexly interbedded or display inset relations. Some of the more complexly layered advance outwash and lake sections may be the result of partial draining of proglacial lakes and (or) changes to the outwash channels or depocenters. Unit **Qgl_v** may correspond to the transitional beds of Booth (1989, 1990) mapped outside this quadrangle and correlates with the Lawton Clay mapped elsewhere in the Puget Lowland. See Pessl and others (1989) and Minard (1985a,b) for a regional description of the 'transitional beds'.

Pre-Fraser Glacial and Nonglacial Deposits

QCpf **Pre-Fraser continental nonglacial deposits, ancient Pilchuck River facies, undivided (Pleistocene)**—Sand, silt, clay with local organic matter and peat, and lesser sand and gravel deposited prior to the Fraser glaciation; sands typically weathered to a yellow-brown-gray; dense; laminated to very thickly bedded and mostly well stratified; contains charcoal, logs, sticks, disseminated organic matter, trough-and-ripple crossbedding, and graded beds; liquefaction features (sand dikes, flames, and distorted bedding) observed in most outcrops. Unit **QCpf** at significant site 43A is distinctly tilted, liquefied, and possibly faulted; these sediments may correlate with the Whidbey Formation sediments mapped north and east of this site in the northern part of Explorer Falls basin. Unit **QCpf** south of the Pilchuck River in the northwestern part of the map area is sand and silt deposits with sparse gravel beds and abundant wood. (See borings B1 and B2 on the western part of Cross Section A) These nonglacial deposits are below Vashon glacial deposits and are of unknown age (Associated Earth Sciences, Inc., 1994). We also tentatively map isolated locally derived nonglacial detritus in the northeast part of the map area directly southwest of the Pilchuck River fault as unit **QCpf** on the basis of the nonglacial composition, density, and moderate to strong weathering. These deposits are lithic rich: 40 to 50 percent WMB-derived meta-argillite, phyllite, metasandstone, and metachert grains suggest these deposits are locally derived. However, the modest polycrystalline quartz (~15%), percent monocrystalline quartz (~15%), plagioclase (~10%) and some potassium feldspar and hornblende

(~2–4%) content suggest a transitional ancient PP provenance (Table 1). Similar to modern Pilchuck River deposits, stratigraphic style and the dominance of sands and silts in unit **QCpf** suggest deposition as thick fining-upward gravel-sand-silt sequences. This is typical of meandering river systems, where thick successions of thinly bedded sand and silt likely represent overbank deposits similar to the other PP units, including modern Pilchuck River alluvium. These nonglacial PP sediments are poorly exposed and offer no age information. Unit **QCpf** deposits are likely correlative with the Whidbey Formation (unit **QCwpv**), the Hamm Creek unit of Troost and others (2005)(unit **Qch**), or the pre-Hamm Creek unit deposits of the Explorer Falls or Bosworth Lake basins. For more regional information, see unit **QCpf** in the Lake Chaplain, Lake Roesiger, Sultan, and Monroe quadrangles, as well as unit **QCpf** of Booth (1990).

QCwpv **Whidbey Formation, Pilchuck Valley facies (Pleistocene)**—Sand, silt, clayey silt, and silty sand with less pebbly sand, clay, gravel, and (or) organic sediment including peat; lenses of pebble gravel observed; dense or hard; well sorted and stratified; mostly laminated to thickly bedded sand and silt with thin beds or laminae of clay locally; commonly planar bedded; contain charcoal, disseminated organic matter, trough-and-ripple crossbedding, graded beds in places. Sand contains abundant monocrystalline quartz (20–22%), polycrystalline quartz (15–25%), and plagioclase (10–15%) and minor but significant potassium feldspar (5–8%), hornblende (2–5%), and some mica (2–20%), and accessory augite, epidote, and opaque minerals. These sand beds are moderately lithic rich (~15–30%); the varied lithic fraction is dominated by metasedimentary (13–22%) and granitic grains (~5%); also present are some sedimentary and volcanic grains, as in other PP-provenance deposits (units **Qa**, **Qch**, and **QCph**). Geochemically, these deposits were derived from sources that were transitional between Pilchuck (PP) and local metamorphic (LP) sources (Table 1)(see *Geochemistry*, below). Microscopically, sand is less weathered than early to mid-Pleistocene alluvium (unit **QCph**) in the Bosworth Lake and Explorer Falls basins. The Whidbey Formation is mapped in two areas of the quadrangle. The northern exposures represent ancient Pilchuck alluvium exposed along Canyon Creek. Unlike the modern Canyon Creek alluvium that contains abundant mélange belt metasedimentary grains (70–80%), this ancient alluvium contains clasts more consistent with the broader Pilchuck River valley source area. (See PP in Table 1 and unit **Qa**). The southern exposures are typical PP alluvium with a strong mélange belt and granitic provincial signature. The Whidbey Formation here appears to be ancient alluvium inset against the Hamm Creek and pre-Hamm Creek PP alluvium as a result of growth folding along the Pilchuck River anticline south of the

Carpenter Creek fault and in the northernmost part of the Explorer Falls basin (see *Explorer Falls basin* below). Previous studies reported 13 IRSL and OSL ages from the Whidbey Formation in quadrangles to the south and southeast that range from ~75 to 143 ka and several infinite radiocarbon ages (Dragovich and others, 2009a,c, 2011a,b, 2012, 2014a,b, 2015). We obtained two new ages for the Whidbey Formation unit Q_{CWPV} : an 83.9 ± 5.15 ka age at site 34D along Canyon Creek, and a 117 ± 19 ka age at site 33D (Appendix A). We correlate these deposits with the Whidbey Formation (75,000–130,000 yr BP) on the basis of age, composition, and stratigraphic position. For additional information on the Whidbey Formation south to southeast of this quadrangle, see references above, Dragovich and others (2010a,b), and Capps and others (1973).

Q_{ch} Hamm Creek unit, Pilchuck Valley facies (Pleistocene)—Sand, silt, and silty sands, and lesser pebbly sand, clay, organic sediments containing disseminated organic materials (wood, charcoal, and plant fossils), and sparse lenses or beds of gravel; dense or hard; sands are weathered to a distinctive bright orange-brown; dense or hard; well sorted and stratified; mostly occurs as laminated to thinly bedded sands and silts, locally with crossbedding or graded beds; rare folded or chaotic bedding from soft-sediment deformation or tectonic liquefaction. Sands are lithic poor and contain abundant monocrystalline quartz (~20–25%), mica (~10–30%), plagioclase (~10–20%), polycrystalline quartz (~5–15%), hornblende (~0–10%), potassium feldspar (~3–6%), lithic clasts (~10–22%) and locally a few pyroxene grains. Lithic clasts are dominantly of metasedimentary origin with some granitic volcanic, and greenstone/greenschist clast types. Much of the detrital mica likely represents metasedimentary grains derived from mélangé in the Pilchuck River valley or Tertiary intrusive rock sources. Minor but distinct tourmaline detrital grains occur in most samples in the Bosworth Lake basin and are likely derived from Eocene igneous contact complexes to the northeast or east (see unit E_{lan} in Cross Sections A and B). Sands contain significant monocrystalline quartz and mica, as do other ancient (units Q_{CWPV} and Q_{Cph}) and modern (unit Q_a) PP sands. Unit Q_{Ch} sand geochemistry suggests the unit was predominantly derived from sources that were transitional between eastern (PP) and local metamorphic (LP) sources (Table 1)(see *Geochemistry* below).

Although much work remains, the Hamm Creek unit (unit Q_{Ch}) is exposed along the northern part of the Pilchuck River anticline, where the unit is inferred to be inset against older pre-Hamm Creek strata; the Whidbey Formation (unit Q_{CWPV}) probably overlies unit Q_{Ch} as a result of deposition during growth folding along the northern part of the Explorer Falls basin in the late Pleistocene (Fig. 3). In this model,

Pleistocene nonglacial fluvial strata derived from the Cascades and representing ancient Pilchuck River alluvium is structurally trapped in the northern part of the Explorer Falls basin over time.

The Hamm Creek strata in the Bosworth Lake basin are inferred to overlie pre-Hamm Creek strata filling a thick Quaternary basin with PP strata (Cross Section B). Well records (for example: W105, W203, and W204) indicate at least ~125 m of clay, sand, and organic material we interpret as composite PP strata of both units Q_{Ch} and Q_{Cph} . Both the Explorer Falls and Bosworth Lake basins are inferred to be Pleistocene extensional basins. See *Bosworth Lake Basin and Northeast-trending Pleistocene Transensional Basins—Possible Regional Tectonic Implications* for further information. We obtained two IRSL ages for the Hamm Creek unit from the northern part of the Explorer Falls basin: 237 ± 33.6 ka at age site 33A, and 263 ± 40.6 ka at age site 33B. We also obtained two new IRSL ages for this unit in the Bosworth Lake basin: 170 ± 15 ka at age site 33E, and 218 ± 29.5 ka at age site 34B. We correlate these nonglacial strata with the Hamm Creek unit of Troost and others (2005) on the basis of age, nonglacial sedimentary character and weathering. For example, petrography indicates that the sand in this unit mostly lacks the oxide and cryptocrystalline brown weathering products commonly observed in unit Q_{Cph} . Troost and others (2005) mapped the Hamm Creek unit in southwest Seattle, Redondo, and in Snohomish County. They indicate that the unit was deposited during marine isotope interglacial stage 7, from 188 to 243 ka (Morrison, 1991), although more recent pollen record data of Roucoux and others (2008) show that MIS 7 lasted from 186 to 245 ka, consistent with our dates, stratigraphy, and composition for the Hamm Creek unit in this map area. Robinson and others (2002) outline the temporal problems with MIS 7 and suggest this interglacial might have ended ~178 ka. Appendix A contains our IRSL age information and other observations for samples 33E and 33B.

Q_{chl} Hamm Creek nonglacial deposits, locally derived facies (Pleistocene)—Pebbly sand, sand, with lesser gravel, cobble gravel, and rare silt; locally contains organic sediments; dense or hard; thinly to thickly bedded commonly with lenticular interbeds; rare low-angle foreset beds; well sorted; angular to subrounded; distinctive dark bluish gray, weathers grayish brown. These deposits contain 50–60 percent WMB-derived meta-argillite, phyllite, metasandstone, metachert grains and some greenstone (~10%). These clasts locally form distinctive dark-colored lithic sand layers. The deposits also contain ~10 percent monocrystalline quartz, ~14 percent polycrystalline quartz, and ~8 percent plagioclase. Unlike unit Q_{Ch} , these locally derived sediments mostly lack distinct Cascade Range detritus such as potassium feldspar, mica, pyroxene, and granitic lithic

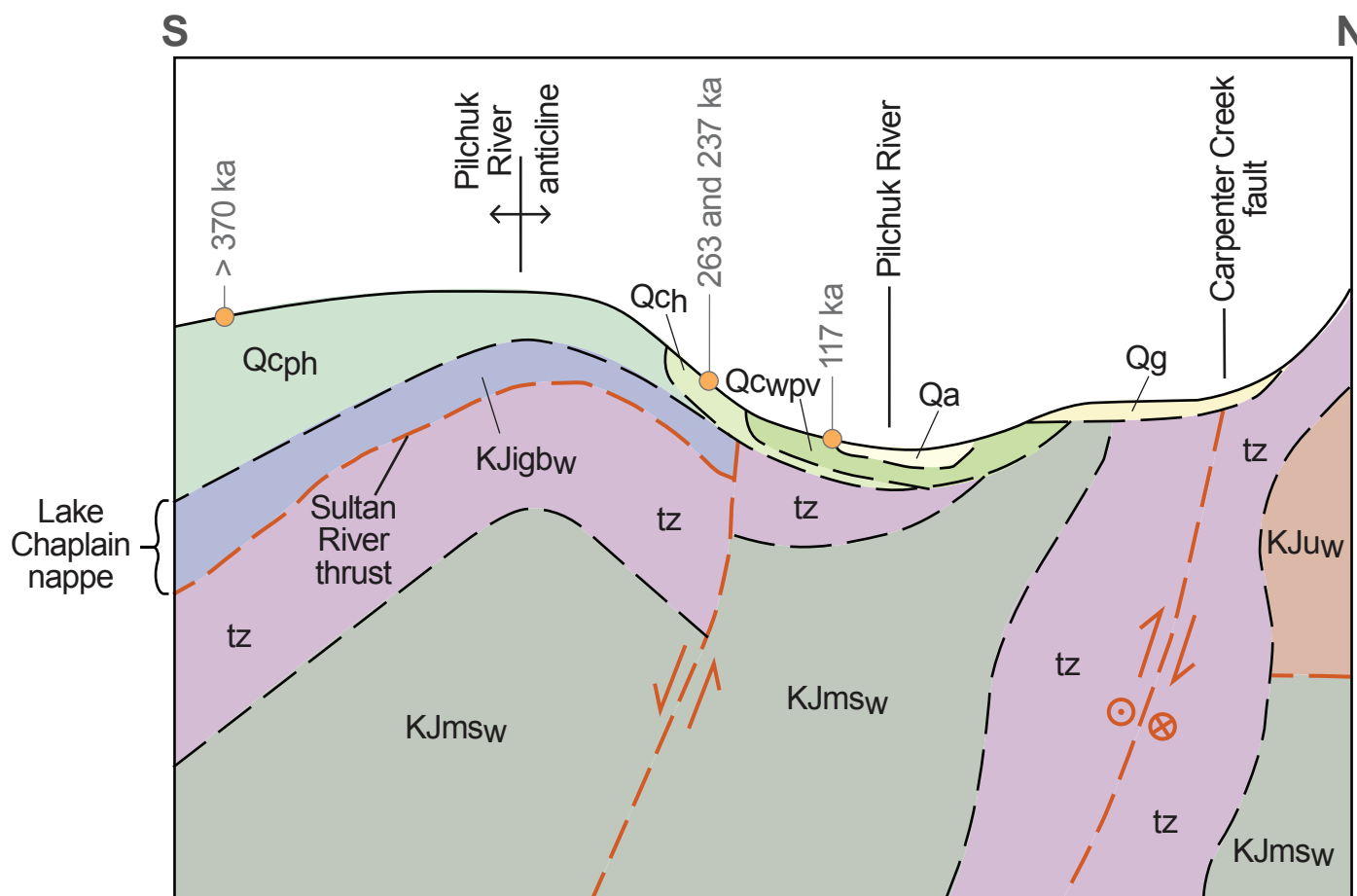


Figure 3. Schematic north-south cross section across the Pilchuck River anticline in the southernmost part of the map area. We interpret this anticline as a growth fold developed as a result of compression along the Carpenter Creek fault (CCF). The Carpenter Creek earthquake cluster is related to active compression across the CCF as a result of oblique reverse slip along this structure. Development of the anticline appears to have trapped the Pilchuck River between the CCF and the growing fold resulting in an inset relationship between three units from the Pilchuck River provenance— Q_{cwpv} , Q_{ch} and Q_{cph} (Table 1). We suspect that this growth folding occurred before deposition of the Hamm Creek formation but after deposition of Q_{cph} . Unit Q_{cph} deposition occurred during the Early to Middle Pleistocene transensional development of the Explorer Falls and Bosworth Lake basins and deposition of thick Cascade provenance fluvial deposits; later north-south compression occurred during the Late Pleistocene. For clarity, Vashon glacial units have been simplified to an undivided unit Q_g , and unit Q_{ch} is included as unit Q_{ch} .

grains (0–2%) (Table 1). Like unit Q_{ch} , outcrop and thin-section observations indicate that the weathering of the deposits is overall moderate and generally more intense than in the nearby Whidbey Formation sands but less than the older unit Q_{cph} deposits mapped directly south of these deposits. These sediments were deposited in alluvial fans along the northern margin of the EFB and are interbedded with fluvial Cascade Range-provenance sediments of unit Q_{ch} along the northern limb of the Pilchuck River anticline (see Explorer Falls Basin for further information). We obtained new IRSL ages of 237 ± 33.6 ka at age site 33A, and 263 ± 40.6 ka at age site 33B in nearby interbedded unit Q_{ch} deposits, consistent with the weathering characteristics and other age constraints for this unit.

Q_{cph} **Pre-Hamm Creek nonglacial deposits (Pleistocene)**—Pebble gravel, gravelly sand, pebbly sand, sand, silty sand, and silt, local cobble gravel and clay; sand is typically yellowish brown to pale brown but in places grey to blue grey, and weathers

to orange; oxidized, and strongly weathered; thin to very thickly bedded; well stratified; rip-up clasts, cross bedding, graded beds, leaves, twigs, charcoal, logs, or disseminated organic matter are common; liquefaction features such as flame structures are found in a few outcrops. Gravel clasts are generally WMB metasedimentary rock and vein quartz; clasts of metagabbro, greenstone, granite, and volcanics are less common. Petrographic inspection of several sand samples revealed abundant angular to subangular monocrystalline quartz (20–40%), conspicuous biotite and white mica (15–25%), potassium feldspar (2–10%), plagioclase (15–25%), and minor but significant hornblende (3–10%) and phyllite, metasandstone, meta-argillite, metachert, and foliated quartz-mica aggregate lithic grains (10–30%). Most samples have minor, distinct granitic lithic grains, and some sand contains minor pyroxene, garnet, epidote, greenstone, and greenschist grains. Sand (67–76% SiO_2) has a strong metamorphic to granitic provenance from local WMB basement and Tertiary plutonic rocks (Table 1). The abundant mica is likely from the Tertiary plutonic

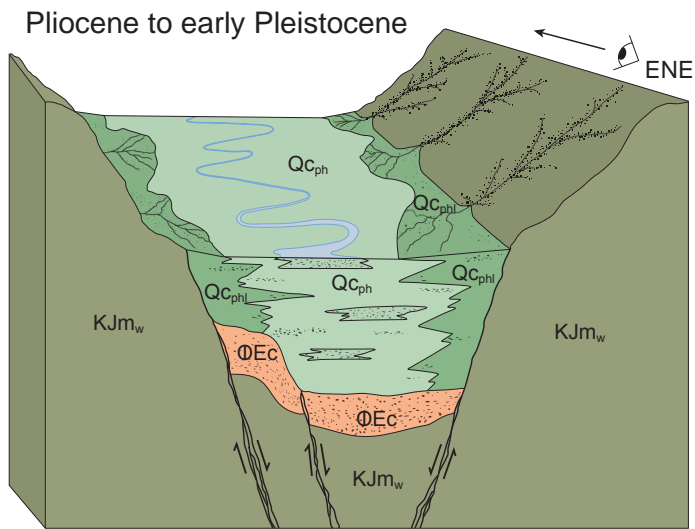
or foliated WMB rocks such as phyllite or meta-argillite. Polycrystalline quartz is a conspicuous minor constituent (to 15% locally) and is most likely derived from metachert and (or) vein quartz that is common to the northeast to east in the eastern and Western mélangé belts of Tabor and others (1993, 2002). Overall, unit Q_{Cph} sediments were derived from the Cascade Range via the Pleistocene Pilchuck valley, paleogeography broadly similar to the modern river valley. Deposits with a Pilchuck River provenance (PP; Table 1) contain more mélangé belt detritus than the Holocene and Pleistocene Skykomish River deposits (SP; Table 1) mapped south of the quadrangle, but they are otherwise broadly similar. However, SP deposits have a more granitic provenance consistent with the Cascade source areas for the Skykomish River. Weathering rinds on basaltic clasts are 0.2 to 5.0 mm thick (average of 2.5 mm); clay and other microcrystalline or cryptocrystalline weathering products were observed petrographically in the sand samples. The high loss on ignition (LOI)(~2.5–5.5%) and chemical index of alteration (CIA)(~62–66) of the geochemical samples in this unit and unit Q_{Cphl} are likely the result of moderate to intense weathering of the sand grains (Appendix D)(Dragovich and others, 2015, this study).

Well logs indicate a thick package of nonglacial sediment in the southwestern corner of the quadrangle. Detailed lithologic logs from water wells such as W46, W87, W153 and W197 indicate at least 90 m and potentially >140 m of sand, silt, clay, and organic material we interpret as nonglacial fluvial deposits. Several wells (W93, W240) indicate that unit Q_{Cph} in places overlies a sandstone with interbedded coal that we interpret as unit ØE_C (Cross Section B). Units Q_{Cph} and Q_{Cphl} are mapped in the Explorer Falls basin (EFB)(Dragovich and others, 2014a). Pleistocene Pilchuck alluvium occupies the more axial parts of this now-inverted basin and stratigraphically inter-tongues with locally derived Pleistocene alluvium (unit Q_{Cphl}) along the northern and southern edges of the basin (Fig. 4). In the southeasternmost part of the map area the Whidbey Formation and Hamm Creek unit are inset against the pre-Hamm Creek deposits on the northern limb of the Pilchuck River anticline perhaps due to Pleistocene growth folding. Dragovich and others (2015) document that the distribution of outcrops, internal deformation, kinematics of bounding faults, and the thickness of basin sediments (up to 215–245 m in the Lake Roesiger quadrangle) all suggest that the EFB has been locally inverted. Dragovich and others (2014a) suggest that the west tilt of the basin in the Lake Chaplain quadrangle is a result of uplift of the Cascade Range. Unit Q_{Cph} also is inferred to underlie the Hamm Creek unit in the Bosworth Lake basin along the west central part of the map area (Cross Section B).

The amount and style of deformation and deep and persistent weathering suggest that unit Q_{Cph} entirely predates the Hamm Creek nonglacial interval of Troost and others (2005), about 178 to 245 ka, and was deposited prior the MIS 7 of Morrison (1991). Dragovich and others (2015) obtained an IRSL age of >370 ka along the boundary between the Lake Roesiger and Granite Falls quadrangles (see age site 14–33A) and near the Pilchuck River anticline. They also obtained an IRSL ages of >455 ka, >540 ka at age site 14–35A from the northern top of Three Lakes Hill. See Dragovich and others (2014a) for further OSL/IRSL age information as well as detrital zircon ages from the EFB directly south of the Granite Falls quadrangle. The detrital zircon information confirms that the sand has a PP provenance (Table 1).

Q_{Cphl} Pre-Hamm Creek nonglacial deposits, locally derived (Pleistocene)—Pebbly sand, sand, sandy pebble gravel, less gravel, cobble to boulder gravel, and rare silt; locally contains peat, logs or organic sediments; dense or hard; thinly to thickly bedded, commonly with lenticular interbeds; sparse low-angle foreset beds; well sorted; angular to subrounded; distinctive dark bluish gray, weathers grayish brown. These deposits are lithic rich, 50–90 percent WMB-derived meta-argillite, phyllite, metasandstone, and metachert gains and locally as much as 10 percent WMB greenstone, and metagabbro with serpentinite grains (see unit KJ_{Uw}). In the southeastern part of the EFB, these ‘black sands’ contain as much as 95 percent metasedimentary clasts that locally form very distinctive dark-colored lithic sand deposits. The deposits also contain 5 to 15 percent monocrystalline and polycrystalline quartz and plagioclase with very little potassium feldspar (0–5%) and hornblende (0–2%). Unlike unit Q_{Cph}, these locally derived sediments mostly lack distinct Cascade Range detritus such as potassium feldspar, mica, pyroxene and granitic lithic grains (0–2%)(Table 1). Outcrop and petrographic observations show that these sediments are more weathered than the younger Whidbey Formation and Hamm Creek unit nonglacial sediments. Like unit Q_{Cph}, these sediments have conspicuous 2- to 6-mm-thick weathering rinds on basalt and basaltic greenstone gravel clasts and abundant brown sand- and silt-sized cryptocrystalline weathering products observed microscopically. Weathering is also recorded geochemically by the high LOI (3.5–5.6%) and CIA (55–66%)(Appendix D). These sediments were deposited in alluvial fans along the north and south margins of the EFB and unconformably overlie fluvial Cascade Range-provenance sediments of unit Q_{Cph} mapped along the basin axis in the Lake Chaplain, Lake Roesiger and current map areas (Fig. 4). The contact between the nonglacial geologic units are generally inferred on the basis of weathering characteristics, structure and geochronology. An IRSL age of 455 ±65 ka from the southern edge of the

A – Explorer Falls basin formation



B – Explorer Falls basin inversion

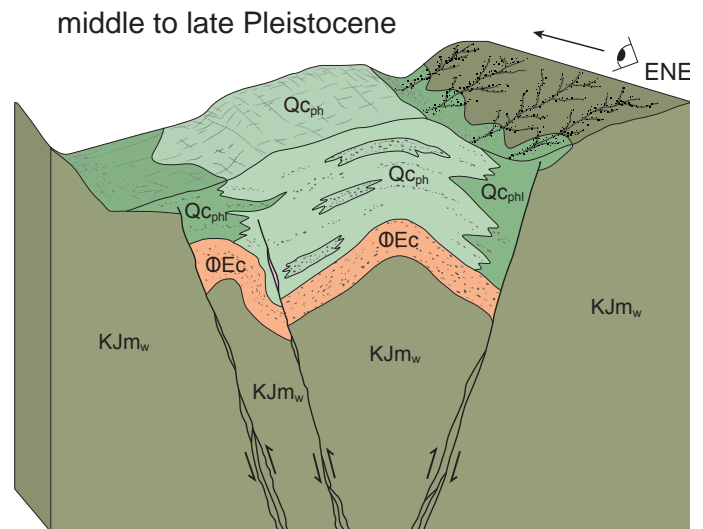


Figure 4. East–northeast-looking block diagrams showing the development of the Explorer Falls basin (EFB) reprinted from Dragovich and others (2015). The northern main fault is the Carpenter Creek fault mapped in the southeastern part of the Granite Falls quadrangle; the southern fault represents the Three Lakes Hill fault mapped to the south of the quadrangle. Although the rocks of Bulson Creek (unit OE_c) likely were deposited in the proto-EFB during the Eocene–Oligocene extension, here we show the Quaternary development of the basin. The diagram’s location is east of the Everett basin and schematically represents the EFB within the Lake Roesiger and Granite Falls quadrangles. Around Lake Roesiger rocks of Bulson Creek are preserved between Cretaceous and Quaternary units; however, to the east in the Lake Chaplain quadrangle Dragovich and others (2014a) show that uplift and tilting of the EFB has exposed older early Eocene Chuckanut Formation equivalent Eocene fluvial deposits containing arkose in the lowermost part of the EFB. A) The EFB graben in the Pliocene to early Pleistocene contained marginal alluvial fans (unit Qc_{ph})—with distinct locally-derived WMB detritus—that interfinger with axial Cascade Range provenance alluvium of the Pilchuck River (unit Qc_{phl}). The homogeneous composition of the marginal facies suggests prolonged erosion of the WMB uplands. B) Inversion of the EFB occurs due to rejuvenation of the basin-bounding Carpenter Creek and Three Lake Hill faults as reverse faults. Basin inversion leads to intrabasinal deformation, including folding, tilting, and local uplift. As shown schematically in Figure 3, new mapping and geochronology documents younger Pleistocene fluvial deposits correlated with the Hamm and Whidbey Formations that occur on the northern limb of the Pilchuck River anticline. Age and other information across this possible growth fold suggests that EFB transtension ended before deposition of the Hamm Creek formation. As we illustrate in Figure 14, the extensional development of the EFB may be due to subduction of the Juan De Fuca plate.

EFB in the Lake Roesiger quadrangle, the weathering characteristics, and other age constraints for unit Qc_{ph} all indicate a middle to early Pleistocene age for this unit.

Qgnpf Pre-Fraser glacial and nonglacial deposits (Pleistocene to Pliocene?)(cross sections only)—Dense to very dense gravel, boulder gravel, sand, silt, clay, and diamicton; locally contains peat or organic sediments. This unit is shown in cross section where pre-Fraser deposits may include older glacial material. Knoll (1967), Booth (1990), and Dragovich and others (2007, 2009a,b,c, 2010a,b, 2012, 2015) describe outcrops of old and undivided glacial and nonglacial deposits elsewhere in the Pilchuck River, Woods Creek, Snoqualmie, and Skykomish valleys.

Tertiary Volcanic, Intrusive, and Sedimentary Rocks

OE_c Rocks of Bulson Creek, continental facies (Oligocene to Eocene)—Lithic to lithofeldspathic sandstone, conglomerate, pebbly sandstone, with lesser siltstone, and (or) coal, minor claystone; rare metachert pebble conglomerate; locally tuffaceous; light yellowish brown to light olive brown. Sandstone

is generally moderately to well sorted, mostly sub-angular to subrounded grains. Siltstone grains are mostly angular to subangular. Unit is well stratified and thinly to very thickly bedded with local foresets, troughs, or scoured beds. Fossil leaves, twigs, and logs are common (Danner, 1957). In the map area, unit OE_c is lithic rich with metasedimentary, granitic, and volcanic lithic clasts and contains fewer monocrystalline quartz, plagioclase, and lithic sand grains; clast compositions suggest a local Cascade provenance dominated by Tertiary igneous and local mélangé belt detritus. Conglomerate pebble and cobble clasts on average are composed of volcanic (~28%), metasedimentary (~21%), tuff/metatuff (~12%), metachert (~11%), sedimentary (~10%), granitic (~8%), greenstone (~5%), vein quartz (~3%), and schist (~2%) rock types. In the Lake Roesiger quadrangle, Dragovich and others (2014a) map lithic sandstones along the periphery of the Explorer Falls basin that contain abundant metasedimentary rock fragments (meta-argillite, metasandstone, phyllite, and metachert) (~60–80%), other lithic grains, including greenstone, metagabbro, volcanic, and a few granitic grains, with less plagioclase, polycrystalline quartz, and monocrystalline quartz.

Surface mapping and subsurface data, along with geophysical modeling, indicate that the thickness of unit ΦE_C is highly varied throughout the map area. Overall, the unit thickens westward from just a few meters in patches along the Granite Falls fault zone to greater than 1,000 m in the southwestern part of the quadrangle near the Everett basin (Cross Section B). This substantial thickening was also observed across the Woods Creek fault zone in the Lake Roesiger quadrangle where high-quality logs from oil and gas wells from the eastern part of the Everett basin recorded >940 m of sandstone, shale, carbonaceous shale, coal, and conglomerate with some detectable oil and gas (McFarland, 1981). Unit ΦE_C also appears to thicken into the Explorer Falls and Bosworth Lake basins west of the Granite Falls fault zone along the western part of the map area. Also, the rocks of Bulson Creek thicken dramatically west of the Granite Falls fault zone, which demarks the eastern extent of the Everett basin. A 1-m-thick unit ΦE_C basal conglomerate is exposed along the South Fork Stillaguamish River directly east of Granite Falls where flattened coalified logs and conglomerate dominated by sub-rounded granodiorite (unit E_{gd}) cobbles and boulders unconformably overlie the unit E_{ian} contact complex. Unit ΦE_C is thus younger than the intrusive complex. The high percentage of volcanic and granitic clasts combined with the moderate induration indicates the fluvial rocks of Bulson Creek are younger than the Eocene intrusive rocks (~44–50 Ma) of the Pilchuck River valley. This erosional remnant of a high-energy fluvial deposit may reflect structural control of ΦE_C deposition along the northeast-trending extensional ‘pull-apart basin’ associated with the Granite Falls fault zone. In the Lake Roesiger quadrangle, unit ΦE_C appears to represent local alluvial fans along the margins of the EFB (Dragovich and others, 2015). Similar to the rocks of Bulson Creek to the north (Marcus, 1991), unit ΦE_C prograded westward into nearshore and deeper marine depositional environments of unit ΦE_n along the westernmost part of the quadrangle. As a result, unit ΦE_C likely interfingers at depth with unit ΦE_n of Dragovich and others (2002b) along the western margin of the quadrangle. On the basis of composition, stratigraphy, and structure, we correlate these rocks with the Bulson Creek unit of Marcus (1991) and Lovseth (1975). See Danner (1957), Minard (1981), Tabor and others (1993), and Whetten and others (1988) for further information about other potential correlatives for unit ΦE_C .

ΦE_n **Rocks of Bulson Creek, nearshore to marine facies of Lovseth (1975)(Oligocene to Eocene)**—Shale, siltstone, sandstone, and mostly pebble conglomerate along the South Fork Stillaguamish River in the northwestern part of the map area; dark gray and olive gray to reddish brown and tan; massive and thick to thin bedded, shaley; varies from moderately well indurated to loose and crumbly. Minard (1985a) noted that

siderite concretions as much as 1 m in diameter are common in the sandstone. Minard (1985a,b) reported quartz, quartzite or metachert, and volcanic rock pebbles and a varied suite of sand grains including quartz, feldspar, mica, phyllite, and pyroxene grains in the sandstone. Unit ΦE_n includes the Riverside Formation of Danner (1957). We follow Whetten and others (1988) and correlate this unit with the rocks of Bulson Creek of Lovseth (1975). Although this facies of the rocks of Bulson Creek is very poorly exposed in the map area (Tabor and others, 2002), water well logs west of Granite Falls indicate that a thick fine-grained sedimentary unit is probably widespread. Danner (1957) reported that marine beds of this formation generally grade upward into coarse-grained clastic rocks of continental facies—we suspect this is due to deltaic progradation of the continental facies over the shallow marine facies. We infer that these marine deposits of unit ΦE_n interfinger with the fluvial deltaic deposits of unit ΦE_C along the westernmost part of the map area and that they have a composite thickness of about 750 m, consistent with our geophysical modeling (Cross Section B). Danner (1957) suggested these sedimentary rocks were unconformably deposited on volcanic rocks of unit E_{vr} (his Pilchuck Bend Formation), but he did not describe outcrop evidence to that effect. Weaver (1912, 1937, 1942) assigned a middle Oligocene age to this unit on the basis of fossil mussels and supported by interpretations from Newcomb (1952) of a “probable Oligocene or Eocene age” at U.W. location 129 of Weaver (1912, p. 59; 1942, p. 103) on the west bank of the Stillaguamish River northwest of the town of Granite Falls (central western part of sec. 11, T30N R6E). See Danner (1957) and Tabor and others (2002) for additional information about the age. See unit ΦE_C for additional information on correlatives of the rocks of Bulson Creek.

E_{vr} **Rhyolite of Hansen Lake (Eocene)**—Glassy to devitrified, metaluminous to peraluminous medium-K calc-alkaline biotite ash-flow tuff, lapilli tuff, lapillistone, tuff breccia and flows; fragmental tuff and breccia deposits typically dominated by lithic fragments; tuff and breccia commonly multi-colored from greyish green to brownish orange. Flows are grey to dark grey on fresh faces. Geochemically analyzed samples are dacitic, however, field and thin-section observations suggest this complex probably varies from andesite to rhyolite. We were unable to locate the highly altered mafic tuff and breccia reported by Tabor and others (2002) northwest of Bosworth Lake. Danner (1957) reported pieces of carbonized wood at one site. Tuff and lapilli tuffs typically contain microlitic felsite clasts (locally including pumice) in a varied glassy matrix (20–30%) containing plagioclase microlites. Clast outlines suggest some tuffaceous rocks were originally welded. Blocky plagioclase phenocrysts are probably mostly andesine (5–10%), and small quartz phenocrysts (2–3%) are common.

Metasandstone lithic fragments in some tuff beds were likely derived from the mélangé belt basement during intrusion or extrusion. Felsic lapilli grains compose as much as 60 percent of some rocks and are probably dacite or dacitic pumice in most samples. Flows typically contain small microphenocrysts to large blades of plagioclase (to 4 mm long) with microphenocrysts of quartz and small grains of subhedral fine potassium feldspar. Glass (~50%) is typically replaced by fine, clear, green chlorite and sugary epidote and contains disseminated quartz and potassium feldspar in some samples; chlorite, epidote, and calcite replacement of minerals is local. No mafic minerals were noted, but scarce grains that might be altered biotite or other mafic minerals were noted in a few thin-sections. Tabor (2002) reported that the Hansen Lake rhyolite east of the map area is commonly perlitic and contains sanidine, plagioclase, quartz, and garnet phenocrysts. We only rarely observed garnet in outcrop and were unable to confirm garnet petrographically. Tuffs locally contain numerous fragments of semi-vesicular to pumiceous dacite. Tabor and others (2002, p. 28) summarized early work on the Hansen Lake rhyolite east of the Granite Falls quadrangle:

“Danner (1957, p. 484–492) included rhyolite cropping out north of the Pilchuck River [east of the map area] in what he referred to as the Hansen Mountain Group. He and Wiebe (1963, p. 16–19) describe these unusual garnet-bearing rhyolite flows and tuffs. Campbell (1991, p. 114–116) gives major and trace element data. Wiebe (1963, p. 36–39; 1968, p. 691) thought that the rhyolite mapped east of the Granite Falls quadrangle was genetically related to the Mount Pilchuck stock based on the petrologic similarity and especially on the garnets common in both the intrusive and extrusive rocks.”

Tabor and others (2002) included the more geographically restricted Pilchuck Bend formation of Danner (1957) in their Hansen Lake rhyolite, a correlation generally supported by our mapping, geochemistry, and geochronology. They also considered their unit Evr to be younger than the early Eocene feldspathic sandstone and conglomerate exposed east of the map area (Fig. 1) and correlative with the lower part of Chuckanut Formation. We obtained a U-Pb single-zircon age of 42.92 ± 0.45 Ma for the columnar felsic flow exposed along the Pilchuck River at age site 26H (Appendix C). The new date and geochemical and isotopic information indicate that the Evr in the map area is an extrusive equivalent of the 44–45 Ma Granite Falls stock intrusive assemblage locally exposed northeast of the rhyolite bodies. Tabor and others (2002, table 2) reported a

biotite K-Ar age of ~53 Ma, and sanidine K-Ar age of ~46 Ma for rhyolite east of the map area; they suggested a compromise age of ~49 Ma, given that the Mount Pilchuck stock was thought to represent the same magma as the rhyolite of Hanson Lake east of the Granite Falls quadrangle. Unit Evr in the study area is probably overall a younger extrusive center than the Hansen Lake rhyolite extrusive center to the east, and thus the igneous ‘Hansen Lake complex’ likely youngs to the west due to a progressive shift in volcanism, or represents two centers with different ages (~49 and 43 Ma). We envision mostly volcanic domes for the original depositional environment of these extrusive rocks. Columnar jointing is well developed at the thick continuous flow at age site 26H; the flow dips ~60° northeast (this study; Danner, 1957). On Cross Section A we infer that unit Evr is 120–180 m thick. U-Pb age, isotopic, and geochemical information indicate that unit Evr is the extrusive equivalent of the Granite Falls stock and that these volcanic deposits were probably fed by dikes of unit Eian which are geochemically very similar to the stock. As discussed in *Regional and Local Eocene Tectonics and Magmatism*, intrusion and extrusion are likely structurally controlled, and thus we suspect that this igneous complex formed along or within one of the northeast-trending Eocene extensional basins common to the region.

Eigd Granite Falls stock, main-phase intrusive complex (Eocene)—Metaluminous, light- to dark-grey hypidiomorphic medium-K calc-alkaline hornblende granodiorite. Locally grades to minor quartz gabbro near the contact complexes along the margins of the main phase intrusions. Dominantly medium grained to slightly porphyritic, but varies from coarse to fine grained, particularly along and near border phase unit Eian dikes. See unit Eian below for further description of the contact complexes associated with the Granite Falls stock intrusive complex. The stock is dominantly massive, particularly in the interior of the stock, although we locally observed a weak igneous flow fabric along, and locally sub-parallel to, the margins of the stock near the contact complex bodies. The margins of the intrusive bodies are also weakly to strongly cataclastically deformed; phanerites near the contact complexes display a spaced fracture cleavage. Cataclastic fault fabrics and zones are more numerous and generally thicker near borders of the intrusive complex. Granodiorite typically contains phenocrysts of subhedral to euhedral plagioclase (30–46%; as much as 6 mm across) with interstitial quartz (10–35%) and potassium feldspar (10–20%), partially chloritized hornblende (5–20%), disseminated opaque minerals (0–5%), and rare biotite in a few samples. Plagioclase phenocrysts display oscillatory zoning; microprobe analysis indicates plagioclase is andesine (Glenn Thompson, Florida Gulf Coast Univ., written commun., 2016). Potassium feldspar and quartz are

typically subhedral to anhedral and interstitial to the blocky plagioclase. Sericite and epidote as replacement products are locally noted; chlorite alteration (2–9%), including partially to wholly chloritized hornblende, is common. We could not petrographically confirm probable garnet (~1%) noted in the field at one outcrop. Danner (1957) reported minor amounts of orthoclase, small euhedral crystals of zircon, and graphic intergrowths of quartz and feldspars. Tabor and others (2002) noted that the pluton locally contains hypersthene and small amounts of elbaite (tourmaline). We observed elbaite both in the Eian dikes of the complex and as a common detrital trace mineral in the Pleistocene nonglacial deposits of the Bosworth Lake basin. The main phase granodiorite grades to quartz gabbro or a gabbro mafic border phase near the contact complexes in some areas along Canyon Creek and the South Fork Stillaguamish River. These rocks have a higher color index and contain subhedral to euhedral and radiating blocky plagioclase phenocrysts (~55%; up to 4 mm), mostly subhedral hornblende phenocrysts (~20%) with interstitial quartz (~10%), and apatite and opaque minerals (~5%). Slightly corroded biotite blades (~10%) occur as glomeropheres with other mafic minerals. The unit typically contains potassium feldspar (~10%), some of which may be secondary. The Granite Falls stock is in the northern part of the Granite Falls quadrangle. Whetten and others (1988) and Tabor and others (2002) mapped a small satellite body of the stock directly northwest of the map area. The main phase and contact complexes of the intrusive complex are inferred to underlie much of the northern part of the map area (Cross Section A). Kaiser (1934) described a tunnel “driven 850 feet [260m] through granodiorite before contacting the older rocks” at the abandoned Yankee Boy mine (significant site YBM). Everywhere it was observed, the Granite Falls stock contact complex (unit Eian) is in fault or tectonic contact with the WMB country rock. Contact relations including the strong thermal metamorphism of the country rock, as well as the correlation of unit Evr extrusive complex with the intrusive complex, indicate epizonal or shallow intrusion of the body during regional Eocene transtension (see *Regional and Local Eocene Tectonics and Magmatism*). Using the amphibole geothermometer of Ridolfi and others (2010), preliminary microprobe analyses of seven magnesio-hornblendes indicate a crystallization temperature of $823 \pm 10^\circ \text{C}$ (Thompson, written commun., 2016). Tabor and others (2002, p. 28) indicated that:

“...granodiorite lacks peraluminous indicator minerals like the nearby Mount Pilchuck stock and Bald Mountain pluton and is chemically metaluminous (Campbell, 1991, p. 59–66). Thermal metamorphism is notable around the stock at distances of 2 km or more

from the exposed contact, suggesting a low-dipping contact or a swarm of such bodies in the area. The stock contains a distinctive blue-green tourmaline (elbaite), which is also present in the Mount Pilchuck stock and is prevalent in the thermal aureole, particularly notable in hornfelsed mafic tuffs and graywacke at the large quarry at Iron Mountain near Granite Falls.”

A preliminary U-Pb single zircon age for the Granite Falls stock of $45.30 \pm 0.11 \text{ Ma}$ (Michael Eddy, MIT; written commun., 2016) is similar to the K-Ar hornblende age of $44.4 \pm 1.4 \text{ Ma}$ reported by Yeats and Engels (1971) at age site USGS_23. These ages are also similar to our new $43.95 \pm 0.44 \text{ Ma}$ age for a dacite dike of the complex (see unit Eian). This information indicates that the complex is ~44–45 Ma, the same age as the ~44 Ma Evr unit. The combined datasets suggest the Granite Falls stock is the plutonic source of the western Hansen Lake Rhyolite exposures. Although we discuss this more fully with unit Eian and in *Regional and Local Eocene Tectonics and Magmatism*, we attribute the intrusive/extrusive complex to regional and local Eocene transtensional structures.

Eian Granite Falls stock, contact complex and dikes (Eocene)—Contact complex bounding the Granite Falls stock main phase containing metaluminous to peraluminous medium- to high-K calc-alkaline dacite and rhyolite dikes with lesser andesite; locally includes fine- to medium-grained gabbro and minor granodiorite. Also includes solitary dikes and dike complexes intruding fault zones away from the main stock and thicker contact complexes bounding the main stock. The contact complexes associated with the stock are dominated by numerous aphanitic dikes but also contain phaneritic dikes of varied composition. Aphanitic dikes are very dark grey to black with conchoidal fracture; gabbros are generally dark to very dark gray; porphyritic dikes range from light grey to grey. Dikes vary from massive, fine-grained featureless bodies to porphyritic bodies to cataclastically deformed bodies that have a distinct fracture cleavage. Individual dikes in the complex range from about 1 to 20 meters thick and many are cut by meter-scale faults that parallel the overall trend of the intrusive complex. Some phanerite bodies and dikes in the complex contain a weak flow or shear fabric that also generally parallels the trend of the dike complex. We observed that the dikes of the contact complexes intrude faults and that the dikes are locally faulted along the same trends, suggesting overall syn-tectonic intrusion of the bodies.

Andesite dikes and pods in the complex typically contain abundant blades of subhedral to euhedral plagioclase (~25–40%; as much as 2 mm long) in a chloritic glass matrix (~20%) along with scattered opaque

minerals (~5%). Most dikes contain as much as 35 percent augite microphenocrysts or as much as 12 percent hornblende, and some andesite dikes contain quartz grains (~0–5%) and (or) accessory potassium feldspar, epidote, sphene, or tourmaline. Tabor and others (2002) also reported minor elbaite (tourmaline) in the Granite Falls stock; we also observed this mineral petrographically in several of the dikes. Some andesite dikes contain biotite and actinolite, possibly a result of contact metamorphism by the generally later main phase granodiorite stock.

Dacitic to rhyolitic dikes in the contact complexes or fault zones vary in texture and composition. Most dikes contain blocky subhedral to euhedral plagioclase (~20–60%; as long as 8 mm) in chloritized glass (~20–50%) and microporphyritic plagioclase locally with interstitial anhedral quartz grains (~0–10%), scattered opaque minerals (as much as ~5%) and minor hornblende (~0–1%) locally. In most rocks the matrix is a clear and partially recrystallized polygonal matrix of quartz (~28–30%) with chocolate brown fine-grained biotite (~15–25%), plagioclase (~15–20%), and potassium feldspar (~0–15%), along with disseminated opaque minerals (to ~10%). We saw subhedral to anhedral quartz and plagioclase microphenocrysts locally in these felsic rocks. Hornblende (~0–3%) in a few of the dikes is typically mostly chloritized or replaced by biotite; potassium feldspar noted in some of these dikes might be partially to wholly secondary. Secondary calcite and epidote is also present in some of the dacite to rhyolite dikes.

Lenses and pods of hypidiomorphic granular granodiorite in the complex are similar in hand sample to unit E₁g₁d and contain subhedral to euhedral plagioclase phenocrysts (~50%; as much as 2 mm long) and lesser interstitial quartz (~12%) and potassium feldspar (~10%) and opaque minerals (~8%). Pervasive replacement of the primary mineral species hornblende (~15%) and probable augite (~5%) by chlorite and calcite is common. A few isolated granodiorite bodies in the contact complex were observed to intrude the dikes of the complex, although intrusion of dikes into granodiorite is also observed, and thus syn-intrusive relations can generally be inferred. Gabbro dikes contain subhedral to euhedral plagioclase phenocrysts (~56%; up to 5 mm), subhedral hornblende phenocrysts (~30%), and opaque minerals (~6%), as well as much secondary chlorite after hornblende (~8%).

We mapped Eocene contact complexes around the Granite Falls stock, as well as dike complexes and individual dikes intruding fault zones. We infer that the dikes and dike complexes are common in the subsurface across much of the northern part of the map area (Cross Section A) and locally prevalent in the Iron Mountain, Granite Falls and Carpenter Creek fault zones. The contact relations between the granodiorite intrusions of the Granite Falls stock main

phase and the contact complex dikes are important in deciphering Eocene intrusive and tectonic history of the area. Although relative age relations of the various dikes are difficult to decipher, most contact and geochronologic relations are consistent with the main phase granodiorite stock and satellite bodies being slightly older than the contact complex dikes. In several localities (for example, U-Pb site 40W), unit E₁an outcrops as 50-cm- to 3-m-wide dikes that intrude metasedimentary rocks of the Western mélangé belt. These dikes have a porphyritic texture bordered by a chilled margin along the edges of the intrusion (Figs. 5 and 6). Major element, trace element, and isotope geochemistry of unit E₁an suggest existence of two geochemically distinct populations that appear to have formed from different sources. One chemically distinct set of dikes is compositionally akin to the Granite Falls stock and is likely a chilled version of the stock and satellite bodies of the stock. (See *Geochemistry* and Appendices D and E for further information.) The Eocene igneous complex in the study area is tightly dated between 43 and 45 Ma. We obtained a U-Pb single zircon age of 43.95 ± 0.44 Ma for a dacite/rhyolite porphyry dike at age site 40W; this dike distinctly intrudes steeply northeast dipping metasedimentary rocks of the Western mélangé belt and cataclasite of the broad east-northeast-trending Iron Mountain fault zone (Fig. 6). This age is similar to that of the 44–45 Ma Granite Falls stock and of the 43 Ma Hanson Lake rhyolite and likely reflects intrusion during regional transtension as illustrated in Figure 7. See *Regional and Local Eocene Tectonics and Magmatism* for a full discussion of our proposed ‘pull-apart basin’ model for the Eocene intrusive rocks in the quadrangle.

Mesozoic Low- to Medium-Grade Metamorphic Rocks of the Western Mélangé Belt

The metamorphic basement in the map area is the Western mélangé belt (WMB), a low- to medium-grade sequence of highly disrupted oceanic and arc rocks mapped widely in the region (Frizzel and others, 1987; Tabor and others, 1993, 2002). Tabor and others (1993, 2000) indicate that meta-argillite forms the mélangé matrix and encloses tectonic bodies, such as metagabbro knockers. These findings are confirmed by our quadrangle mapping south of the Granite Falls quadrangle. However, very thick sequences of less-deformed strata are locally and regionally well exposed. For example, stratigraphic coherent WMB strata is common in the eastern part of the map area. In these areas meta-argillite forms thin to thick interbeds within metasandstone, or well-stratified metasedimentary rocks are interbedded with metavolcanic rocks (Dragovich and others, 2013, 2014a, 2015). Although the WMB is a regional structural amalgamation of various tectonic environments, the stratigraphic style, including partial Bouma sequences, indicate that most WMB metasedimentary rocks originated as Cretaceous to Jurassic arc volcanic sediments and near-arc

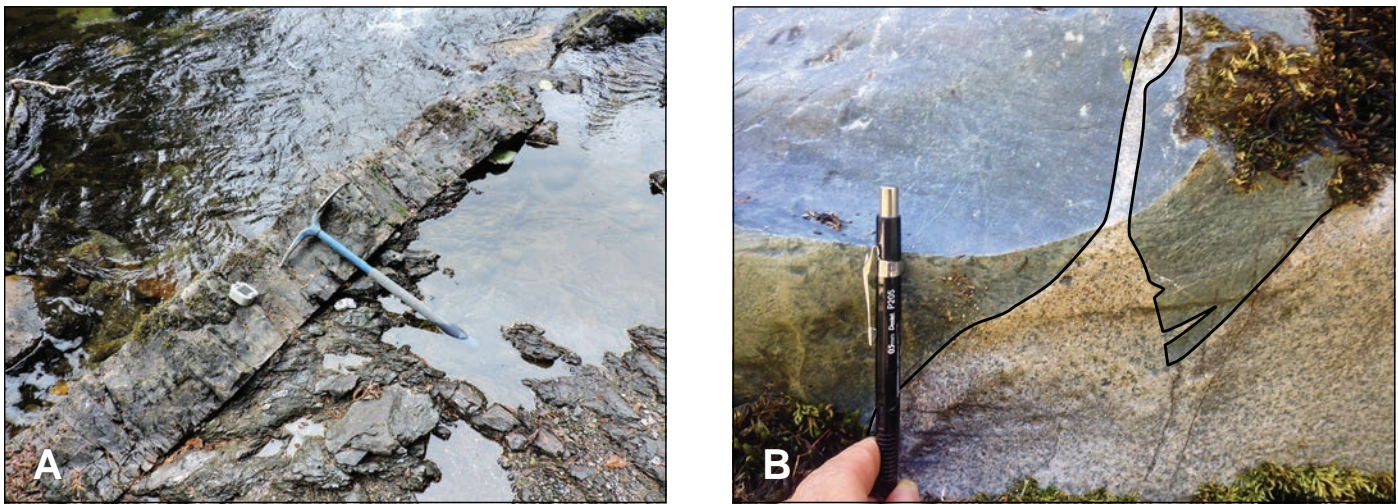


Figure 5. Contact relations of unit Eian. A) Porphyritic dike (unit Eian) cross cutting sheared meta-argillite in the Western mélangé belt (unit KJmsw). This exposure is in the Pilchuck River in the southeastern portion of the quadrangle and is one of a family of dikes mapped along the Pilchuck River directly south of the Carpenter Creek fault (CCF) and within the northernmost part of the Explorer Falls basin. These Eocene dikes trend east-northeast and are interpreted to be related to Eocene extension. B) Well exposed intrusive relationship between the Granite Falls Stock main phase granodiorite and contact complex (dark rock bounded by black line) under the Mountain Loop Highway Bridge; this outcrop is part of a series of exceptional rock exposures in the South Fork Stillaguamish River and directly upstream from the Granite Falls fish ladder. Granodiorite of the Granite Falls Stock (unit Eigd) is seen to intrude aphanitic country rock of unit Eian. However, because we also observed dikes intruding the stock we broadly envision a comagmatic history for these ~44–45 Ma intrusive bodies. We also postulate a syn-tectonic intrusive history during regional Eocene transtension for these igneous bodies because the dikes in the contact complex intrude faults and then are again faulted locally with faults bounding Eocene igneous bodies in and around the map area.

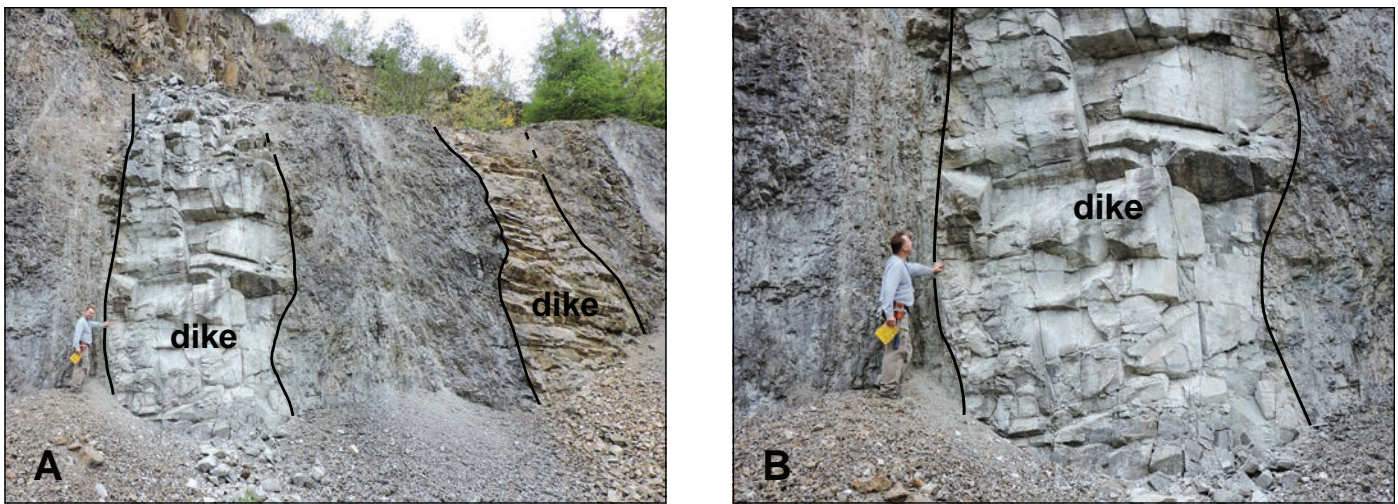


Figure 6. Meter-scale, dacitic porphyritic dikes (unit Eian) intruding faulted Western mélangé belt metasedimentary rocks (unit tz) in the Iron Mountain quarry. The most prominent dike (sample 15-40W#1), gave a U-Pb date of 43.95 ± 0.44 Ma (Appendix C). Geochronologic constraints (this study; Eddy, personal comm.; Yeats and Engles, 1971), geochemistry, along with field relations, suggest that diking generally accompanied intrusion of the 44 Ma Granite Falls Stock during regional transtension. Trace element and isotopic geochemistry of dikes suggest they were likely generated from the same melt source as the nearby Granite Falls Stock.

turbidites deposited in an accretionary wedge close to volcanic centers (Jett, 1986; Frizzel and others, 1987; Jett and Heller, 1988; Dragovich and others, 2014a; MacDonald and others, 2014). Locally, distinct volcanic arc flows are interbedded with volcanic-provenance metasedimentary strata and may be shallow-water forearc deposits. Regularly stratified and folded, moderately distal to distal turbidites and interbedded metatuffs are folded around the Worthy Creek syncline and nearby areas in the east-central part of the map area east of the Granite Falls fault zone (GFFZ). These rocks are regularly stratified, systematically folded across a broad area, probably as a result of accretionary tectonics. Feldspathic metasedimentary rocks

(‘meta-arkose’) in unit KJmsw originated as turbidites eroded from a two-mica granitic source, perhaps following exhumation and erosion of the arc’s plutonic root or from other extra-regional late Cretaceous-age sources (Sauer and others, 2014; Dragovich and others, 2014a,b, 2015). This meta-arkose occurs only at a structurally low position below the Lake Chaplain nappe in the WMB and below the Sultan River thrust in the southernmost part of the map area (Fig. 8).

A moderate to strong syn-metamorphic foliation is sub-parallel to bedding and likely resulted from the shearing of turbidites in an accretionary prism. The disruption of beds, crude foliation, and (or) pervasive cataclasis is apparent in

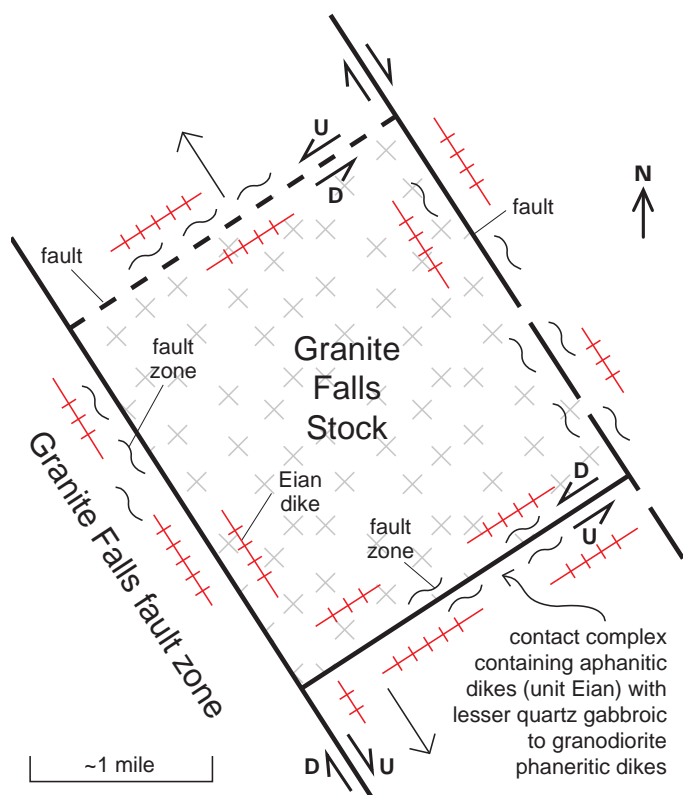


Figure 7. Schematic map-view representation of the 'transtensional pull apart basin' model of the Eocene intrusive rocks of the Granite Falls stock (unit Eigd). The stock intruded and thermally metamorphosed aphanitic rocks of unit Eian in the contact complexes (Fig. 3). Cross-cutting faulted and intrusive age relationships indicate both a syn-tectonic and co-magmatic intrusive history for the contact complex and stock intrusive bodies. The best exposures of the Eigd/Eian contact are found in the South Fork Stillaguamish River and Canyon Creek (for example, significant site 13L).

many outcrops (Frizzell and others, 1987). This primary foliation generally dips steeply to the northeast and suggests that the foliation was broadly synchronous with progressive deformation during the first accretionary shear deformation across the belt (Fig. 9; Dragovich and others, 2014a). Variation in foliation orientation is related to post-metamorphism folding and fault-block rotation. Although internal deformation and tectonic mixing of lithologies is minimal in some areas, large overturned folds locally record significant regional shortening (for example, near the Sultan River southeast of the map area). We name the Worthy Creek and Chitwood Lake synclines for two major structures that fold the primary WMB foliation in the eastern part of the map area.

Rocks of the WMB in the map area are predominantly metamorphosed to prehnite-pumpellyite facies; the metamorphic grade generally increases northeastward to greenschist facies, consistent with mapping southwest to northeast of the map area (Dragovich and others, 2014a; Tabor and others, 1993, 2002). Rocks of the Lake Chaplain nappe in the study area grade up to amphibolite facies. Mapping and structural analyses in the Granite Falls quadrangle suggest that tectonic bodies of marble and quartz muscovite schist are structurally dispersed along a folded thrust fault that likely separates low-grade metasedimentary rocks from phyllite in a structurally high position within the WMB. A belt of ultramafic rocks

within and west of the GFFZ may be the lowermost portion of the Eastern mélangé belt of Tabor and others (2002). (See *Mesozoic to Tertiary Tectonics of the Western Mélangé Belt*.)

Tabor and others (1993) assigned earliest Cretaceous and Late Jurassic ages to the Western mélangé belt on the basis of sheared and deformed "*Buchia concentria*" and "*Aucella sp. (Buchia sp.)*" along the Sultan River in the adjacent Lake Chaplain quadrangle. The age of these bivalves is restricted to the Tithonian (Late Jurassic) (Danner, 1957). Danner (1957) reported that a collection of *Aucellus*, possible *Terebellina* tubes, and radiolarian fossils suggest an Early Cretaceous to Late Jurassic depositional age for the phyllitic metasedimentary rocks in the same area. Tabor and others (1993, 2000) and Frizzell and others (1987) reported Kimmeridgian to Valanginian (157–134 Ma) radiolarian ages from metachert beds south of the map area.

Work in nearby quadrangles indicates that the WMB metasedimentary rocks contain Late Jurassic to Early Cretaceous fossils that are most consistent with an age range of ~134 to 157 Ma (Danner, 1957; Tabor and others, 1993, 2000) and with our new 166 Ma detrital zircon age for a volcanoclastic metasandstone in the map area. Limiting depositional ages from detrital zircon studies in the WMB arkosic metasedimentary rocks indicate that these deposits are younger than previously accepted and at least locally Late Cretaceous (~74 Ma) in age in a structurally low position below the Lake Chaplain nappe (Dragovich and others, 2009a,b, 2014a; Brown, 2012; Sauer and others, 2014). The young age for this facies is consistent with exhumation of the volcanic arc and a transition to younger intrusive igneous provenances in the sediments of the accretionary prism.

KJm_w Western mélangé belt of Frizzell and others (1987), undivided (Cretaceous to Jurassic)(cross sections only)—Meta-argillite, metasandstone, greenstone, metachert, with less metadiabase, metagabbro, metatonalite (metatrandhjemite), slate, (banded) amphibolite and hornblendite, and phyllite, with minor marble, metaquartz-diorite, and rare ultramafic rocks observed regionally (Fuller, 1925; Danner, 1957; Tabor and others, 1993, 2002; Dragovich and others, 2007, 2009a,b,c, 2010a,b, 2011a,b, 2012, 2013, 2014a, 2015). Although meta-argillite is easily eroded and does not form prominent outcrops in many areas, its voluminous presence as detritus in units Qcphl and Qchl suggests that erodible metasedimentary rocks—including meta-argillite—are likely common beneath Quaternary cover and were more extensively exposed during long Pleistocene interglacial periods.

KJmv_w Metavolcanic rocks—Greenstone derived from metamorphosed basaltic to andesitic tuff, tuff breccia, and lapilli tuff with basaltic to dacitic volcanic flows (48–70% SiO₂) common in and near the study area; regionally, the tuffs are calc-alkaline and predominantly intermediate in composition; basalt flows and rare volcanic breccia observed regionally; greenstone is greenish gray to dark greenish black. Tabor and others (2000) described boudins of metamorphosed

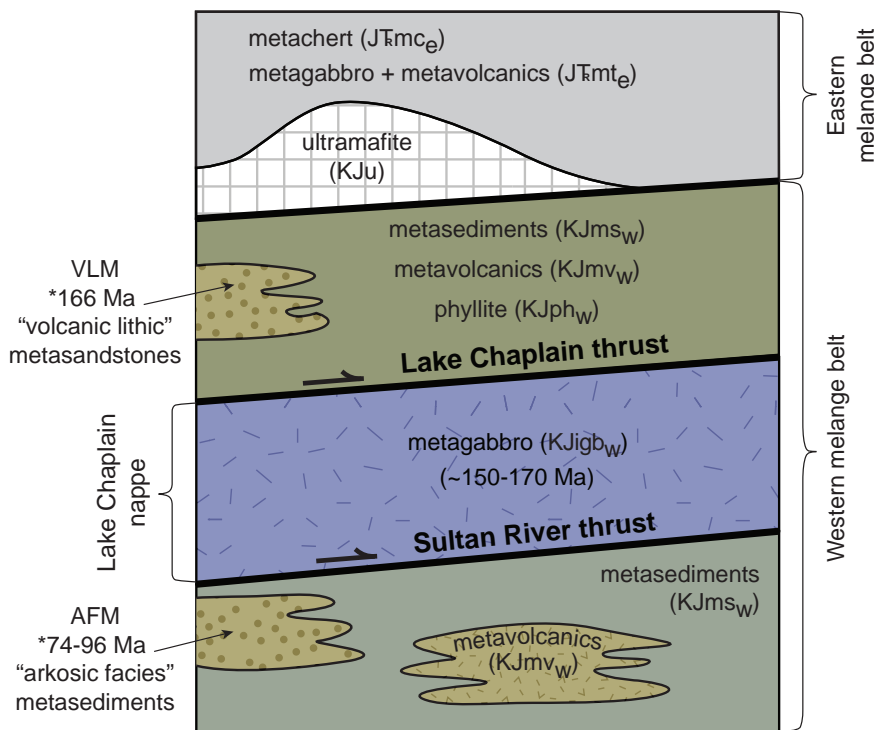


Figure 8. Structural block diagram showing the Sultan River and Lake Chaplain thrusts bounding the Lake Chaplain nappe (LCN) of Dragovich and others (2014a, 2015). Southwest of the map area low-grade metasedimentary and metavolcanic rocks (i.e., units KJms_W and KJmv_W) underlie and overlie the LCN in the Sultan River area where Dragovich and others (2014a) named the Sultan River and Lake Chaplain thrusts. The LCN contains disrupted arc metagabbroic rocks (unit KJigb_W) in the Lake Chaplain, Lake Roesiger and Granite Falls quadrangles. The LCN and the Sultan River thrust are exposed in the southeastern corner of the Granite Falls quadrangle south of the Carpenter Creek fault. North of the Carpenter Creek fault, where we obtained 166 Ma maximum detrital age for volcanoclastic metasandstone, higher structural levels for the WMB are exposed above the LCN. Regional and local detrital zircon age information (Appendix C, Fig. C3 and Table C1) for WMB metasandstones demonstrates that they are generally stratigraphically younger down section, consistent with an accretionary thrust stacking model. Although we preserve the loose correlation of the widespread ultramafic bodies in the Granite Falls quadrangle with the WMB, we suggest that these alpine ultramafic serpentinites perhaps represent the lowest part of the Eastern mélangé belt and demarcate the thrust contact between the belts defined by Tabor and others (2002) and Tabor (1994).

quartz-porphyry dikes in faintly foliated greenstone south of the study area. Although most greenstones in the map area are pyroclastic, some of the thicker greenstone bodies are probable flows. Regionally metamorphosed flows are mostly massive to moderately foliated metabasaltic andesite, locally with amygdaloids, pillow textures, and eutaxitic flow structures (Dragovich and others, 2009a,b,c, 2013, 2014a, 2015). Amygdaloidal metadacitic greenstone flows, characteristic of island arcs (MacDonald and others, 2014), are fairly abundant in the Lake Chaplain quadrangle and contain microlitic and eutaxitic plagioclase phenocrysts, along with a few large plagioclase phenocrysts, in a homogeneous clear matrix containing interstitial quartz. As also observed in the Lake Chaplain quadrangle, metatuffaceous and tuff breccia interbeds within the WMB phyllite (unit KJph_W) are higher grade actinolite-bearing greenschist. We observed widespread very thin to very thick metatuffs interbedded within metasedimentary rocks in the quadrangle. These tuffs contain significant augite surrounded by interstitial plagioclase, chlorite, opaque minerals, and a few euhedral plagioclase phenocrysts and are similar to dacitic to rhyolitic crystal-vitric 'apple green' metatuffs (56–77% SiO₂) in adjacent quadrangles (Dragovich and others, 2009a,b,c, 2014a, 2015, this study). Metamorphosed basaltic to andesitic flows studied regionally typically contain plagioclase microlites in a light green chloritized or saussuritized matrix. Greenstone occurs as widespread metatuff interbeds in the metasedimentary rocks and as more localized flows. Most of the vitric tuffs are completely recrystallized granoblastic greenschist that lacks relict grains and contains some interstitial chlorite

and opaque minerals; a few contain relict subhedral to euhedral crystals of quartz and plagioclase (≤ 3 mm) in a recrystallized clear quartzose matrix (40–50%) that also has large embayed relict volcanic quartz grains (≤ 2 mm) locally. Crystal lithic and crystal vitric to crystal metatuffaceous beds in the Granite Falls quadrangle generally contain plagioclase (~30–60%), quartzose grains (to ~30%) commonly in a chloritized glass matrix (~15–35%). Some samples contain abundant augite crystals (to ~40%), microlitic volcanic lithic clasts (to 35%), and accessory sphene (~5%). Metamorphic minerals in the greenstone include epidote, prehnite, calcite, and pumpellyite. Rare volcanic breccia contains felsic pumice clasts and volcanic quartz grains in a clear quartzo-feldspathic glass matrix. Faulted, thick greenstone flows are well exposed in a rock quarry at significant site 9M directly north of the Carpenter Creek fault. These flows are broadly andesitic in composition and contain abundant radiating plagioclase blades (~40%) along with quartz in veins and grains (~20%) in a metamorphosed chloritized matrix (~20%) containing distinct calcite, prehnite (~12%), and opaque minerals (~8%). Southeast of the map area, a very thick mafic mugearitic (basaltic trachyandesite) flow interbedded with metachert has an alkali oceanic-island basalt (OIB) provenance (Dragovich and others, 2013). A near-arc accretionary prism setting is supported by the Jurassic (166 Ma) age population of our newly dated WMB volcanoclastic metasandstone. A near-arc depositional environment for the WMB accretionary prism is indicated by the common arc-related metatuff interbeds in the metasedimentary rocks and

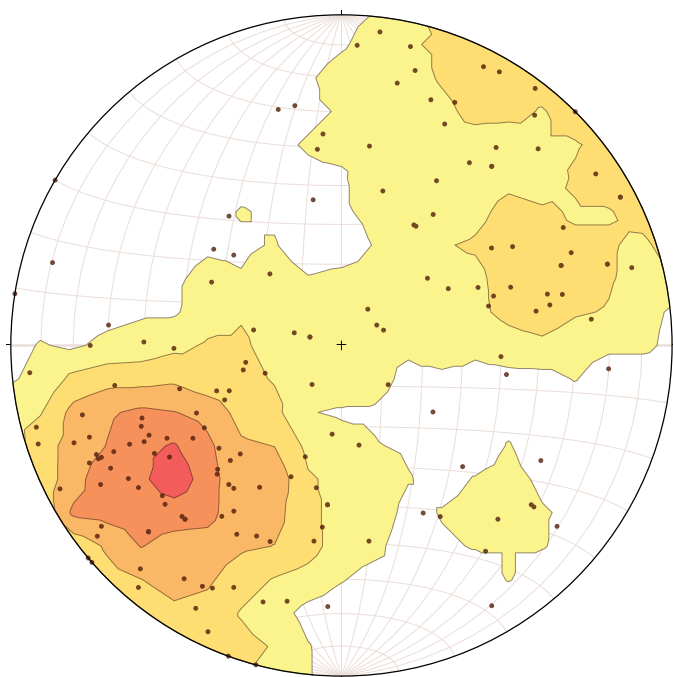


Figure 9. Stereonet of poles to foliation and bedding in the Western mélangé belt (WMB). Bedding is generally transposed parallel to the S1 foliation in the WMB. A dominant northeast-dipping population and a subsidiary southwest dipping population reflect the mapped NW–SE tracing upright folds resulting from a D2 folding. Rare S2 axial planar cleavage is also observed in metasedimentary rocks in the Granite Falls quadrangle. The orientation of WMB bedding and foliation in the Granite Falls quadrangle is similar to the orientation of the S1 foliation and bedding observed in the nearby Lake Chaplain quadrangle (Dragovich and others, 2014a). Measurement scatter is thought to reflect brittle deformation along mapped and small-scale late Mesozoic to early Cenozoic faults, but could also suggest non-cylindrical folding during the D2 event.

evolved arc-related flows across the belt. See *Mesozoic to Tertiary Tectonics of the Western Mélangé Belt*.

KJmsw Metasedimentary rocks—Marine feldspathic to feldspatholithic subquartzose metasandstone, silty metasandstone, meta-argillite, metatuff, tuffaceous metasandstone, and chert pebble metaconglomerate; lesser metachert and marble as discontinuous pods; typically greenish gray, dark or bluish gray, or gray-green; weathers brown; meta-argillite is typically black or greenish blue-black to dark gray. Relict sand grains in metasandstone and meta-argillite are subrounded to angular; graded bedding and load casts are locally preserved. Moderately sorted pebble metaconglomerate contain subrounded metachert, argillite, metasandstone and metatuff clasts and rare cobbles. Unit KJmsw is moderately foliated and partially recrystallized to the prehnite-pumpellyite facies. A synkinematic metamorphic fabric is defined by subparallel white mica, chlorite, and relict clasts. Metamorphic minerals are white mica, epidote or clinozoisite, chlorite ± pumpellyite, and prehnite. We divided metasandstone in the Lake Roesiger, Lake Chaplain, and current quadrangle into two distinct groups: feldspathic metasandstone, similar to the arkosic petrofacies of Tabor and others (1993) and Jett

and Heller (1988), and feldspatholithic to lithofeldspathic metasandstone, generally similar to the lithic petrofacies of Jett and Heller (1988). Our new geochemical, petrographic, stratigraphic, and detrital-zircon data presented in this document further support this general subdivision.

The feldspathic metasandstone (63–73% SiO₂) contains angular to subangular relict grains of monocrystalline quartz (30–50%), plagioclase (25–30%), and potassium feldspar (3–20%), and minor polycrystalline quartz (0–10%), significant detrital biotite and muscovite, and few opaque minerals. These rocks locally contain some volcanic or granitic lithic grains, but they are generally lithic poor and likely derived from felsic two-mica granites. The general angularity of the grains suggests ‘first cycle’ sediments or sediments that generally were not substantially reworked and were derived from a homogeneous, perhaps nearby, intrusive source. The arkosic petrofacies is rare in the study area and observed only at significant site 14–36N along the southern boundary of the quadrangle. The arkosic petrofacies occurs at a structurally low level, below the Lake Chaplain nappe (Fig. 8). The restriction of exposures of this arkosic petrofacies to only south of the Carpenter Creek fault suggests this is a significant structural boundary in the map area. The feldspatholithic to lithofeldspathic metasandstone in the quadrangle generally contains monocrystalline quartz (15–35%), plagioclase (25–40%), less polycrystalline quartz (0–20%), augite (0–8%), and very little or no relict potassium feldspar (0–5%). It also locally contains mica (0–7%), sedimentary lithic grains (0–5%), and rare hornblende or metamorphic lithic grains (0–1%). Volcanic lithic grains (5–35%) commonly have a felty or microlitic texture, indicative of andesitic to dacitic volcanism in the adjacent arc (Jett and Heller, 1988). Metasandstone includes some poorly sorted metasandstone (‘wacke’) that is compositionally and texturally immature, consistent with rapid sedimentation near a volcanic arc. Meta-argillite and fine-grained argillaceous metasandstones have a similar composition and mostly contain angular monocrystalline quartz (~30–50%), plagioclase (~20–40%), and volcanic lithic grains (~10–20%), locally with some detrital augite grains in an argillaceous matrix. A volcanoclastic pebble metaconglomerate is mostly mafic vesicular volcanic clasts to felsic microlitic volcanic clasts (~75%), sedimentary clasts (~8%), and quartz and plagioclase (~15%); augite occurs as both free crystals and phenocrysts in some metaconglomerate volcanic pebbles (~2%). Tuffaceous feldspatholithic metasandstone contains significant relict quartz and plagioclase and likely originated as reworked crystal-vitric tuffs. Interbeds of vitric and crystal-vitric metatuff contain relict plagioclase and quartz phenocrysts, locally with pyroxene, in a light green, semi-transparent chloritic matrix. These widespread

metatuffs record a major pyroclastic contribution to the WMB, which also contains arc gabbro, volcanoclastic rocks, and some localized volcanic flows (see unit KJmv_w). Metachert is dominantly composed of recrystallized polygonal quartz that contains relict recrystallized radiolarian fossils (up to 60%) and locally has thin interbeds of meta-argillite. The chert bands vary from undeformed to strongly deformed; en echelon or cross-cutting quartz veins are common. The two most prominent occurrences of metachert are at significant sites 14G and 204F. Marble occurs mostly as dark-gray to white coarsely crystalline carbonate-rich small to moderate-size pods that are mostly massive but locally interbedded with bioclastic layers. At age site 15L we located fusulinid fossils that Danner (1966, p. 320) described as:

“...large fusulinid tests composed mostly of the genus *Yabeina* but containing also *Schwagerina* and *Codonofusiella*. Fragments of calcareous algae are also common. This quarry is the site of the first Permian fossil locality discovered in western Washington and contains the youngest marine Permian fauna known in the United States.”

Additionally, Danner (1966) noted Permian fossils at our age site 7F in the Shumway quarry and described limestone similar to that at the Granite Falls quarry (significant site 17V, this study). Tabor and others (2002, p. 25) wrote:

“Sparse fossils in the Western mélangé belt, including radiolarians in chert and megafossils in argillite, indicate that, with the exception of limestone, most of its components and its matrix are Mesozoic (Late Jurassic to earliest Cretaceous) in age. The limestone blocks are Permian in age, and a few chert blocks are Early Jurassic. The linearity of limestone outcrops east of Granite Falls, also parallel to the regional structural grain, suggest that the limestone originally had stratigraphic continuity prior to strong deformation. Because the limestone ages are older than the host clastic rocks, we assume that the limestones were emplaced as olistostromes, perhaps along one stratigraphic horizon.”

Structural, stratigraphic, and metamorphic information from this study suggests that the marble, along with quartz muscovite schist bodies (unit KJph_w), are structurally emplaced and may denote a regional thrust fault and (or) deformed major accretionary structural surface in the WMB. (See *Metamorphic*

Grade, Stratigraphy, and Structural Stacking of the WMB.)

Previous work in nearby quadrangles has resulted in maximum depositional ages in arkosic metasediments of ~74 Ma (Dragovich and others, 2014a), ~87 Ma (Brown, 2012), and ~96 Ma (Dragovich and others, 2009a,b)(Fig. C3; Table C1). The ~74 Ma age is significantly younger than previous estimates for the WMB by Brown (2012); it shows the arkosic petrofacies is locally as young as latest Cretaceous and, thus, accretionary mélangé belt formation and sedimentation continued into at least the latest Cretaceous. The composition and age of the arkosic petrofacies suggest a two-mica granitic source such as the Idaho Batholith. The youngest population age (~74 Ma) is also consistent with unroofing of the volcanic arc and exhumation of older intrusive igneous rocks. Near Lake Roesiger, Dragovich and others (2015) obtained a maximum depositional age for a sandy volcanoclastic meta-argillite of ~110 Ma (Fig. C3; Table C1). We obtained a youngest U-Pb age distribution of ~166 Ma for a volcanic feldspatholithic metasediment at age site 15–28AF (Figs. C3, C4, and Data Supplement). The ~166 Ma depositional age for volcanoclastic metasediment deposits is within the published 150–170 Ma U-Pb age range for the WMB metagabbro and metatonalite intrusive rocks (Tabor and others, 2000).

The age information suggests an arc proximal to an accretionary prism or structural mixing of multiple arcs in an accretionary setting from ~110 Ma to 170 Ma. Tabor and others (1993, p. 14) summarized WMB fossil age information as follows:

“A *Buchia* from matrix argillite and graywacke beds (table 1, no. 1F-3F) appears to be restricted to the Tithonian (Danner, 1957, p. 410), and more definitive radiolarian samples indicate ages from Kimmeridgian to Valanginian (Frizzell and others, 1987) that, in numerical age, range from 156 to 131 Ma based on the time scale of Harland and others (1982).”

We can broaden the age range for the volcanic lithic petrofacies and related metaigneous rocks to ~110–170 Ma (Fig. C3; Table C1). The uniformity of the detrital zircon ages and the general lack of exotic zircons for sample 15–28AF may indicate that much of the older WMB accretionary prism was adjacent to a simple volcanic island arc or arcs distant and (or) shielded from the craton. See unit KJms_w and *Mesozoic to Tertiary Tectonics of the Western Mélangé Belt* below.

KJph_w **Phyllite**—Phyllite, phyllitic metasediment, meta-argillite, slate, and minor semischist rock types,

including local foliated metatuffaceous greenschist interbeds; dark bluish gray, weathers to bluish gray; moderately to well-stratified; thin to very thickly bedded; sequences of phyllite have well-developed schistosity that is transposed parallel to bedding. The metamorphic fabric is defined by subparallel chlorite or white mica, relict grains, and quartzose metamorphic segregations. Unit KJph_w includes feldspathic to feldspatholithic metasandstones, meta-argillite, and metasilstones similar to the lithic petrofacies in unit KJms_w described above. Phyllite typically contains relict subrounded to angular grains of monoclinic quartz, plagioclase, and locally abundant volcanic lithic clasts. The volcanic petrography of the relict sand grains and the presence of foliated metatuff beds in the phyllite suggest a recrystallized volcanoclastic protolith for most of the metasandstones. These metaclastic rocks are most similar to the lithic petrofacies of Jett and Heller (1988), yet some are more quartz-feldspathic metasedimentary rocks that were probably derived from a crystal-vitric tuffaceous source. Quartz muscovite schist bodies at significant sites 35K and 203Z are included in unit KJph_w and interpreted as exotic, fault bounded, tectonic bodies. These recrystallized rocks contain polygonal quartz (~65%), muscovite (~20–35%), and in places veins of calcite (to 15%). In both areas the muscovite is distinctly crenulated and forms a deformed schistose fabric. These high-grade rocks are proximal to the Worthy Creek fault and the unnamed fault northeast of that area; they likely correlate with a similar tectonic body described by Weibe (1963) along strike east of the area. We suspect these exotic bodies, along with the marble bodies, might delineate a folded regional thrust or thrusts. See *Mesozoic to Tertiary Tectonics of the Western Mélange Belt*. Metamorphic minerals in phyllite include sericite, chlorite, albite, calcite, and sodic plagioclase. Prehnite is common in matrix veins, and actinolite is seen in a few compositionally immature metasedimentary rocks. The phyllite unit is mapped mainly in the northeastern part of the map area, where it is interbedded with greenschist (unit KJsh_w). Overall, these minerals are consistent with a greenschist metamorphic facies. There is a general increase in metamorphic grade northeast across the WMB (Tabor and others, 1993). This increase is interrupted by local grade increases created by thrusting and reverse faulting that juxtaposes low- and medium-grade rocks (Dragovich and others, 2014a). The general northeast increase in grade is conspicuously broken in the map area where an uplifted block of higher grade phyllite is bounded by lower grade metasedimentary rocks across high-angle faults (Cross Section B). The island-arc setting for the metamorphosed intrusive rocks, tuffs, and flows holds for most of the mélangé belt protoliths, including most of the phyllitic rocks.

KJigbw Metagabbro—Metagabbro, quartz metagabbro and minor metadiabase dikes and rare zones of felsic pegmatite; greenish gray; medium to coarse grained; hypidiomorphic granular massive to slightly foliated; locally schistose or gneissose locally with a flaser gneissic fabric. Metagabbro (44–59% SiO₂; Dragovich and others, 2015) generally contains actinolized hornblende (5–30%) and plagioclase (45–65%) along with opaque minerals including magnetite (2–5%). Tabor and others (1993) report rare hypersthene and clinopyroxene relicts in metagabbro. Metamorphosed quartz gabbro is common in the map area and has 10 to 15 percent quartz. A medium- to fine-grained andesitic metadiabase dike intruding metagabbro in the southeast corner of the map is composed of polygonal plagioclase (~30%), quartz (~30%), chlorite and chloritized biotite (~25%), and opaque minerals (~15%). In the adjacent Lake Chaplain quadrangle metadiabase dikes similarly intrude metagabbro, and there are large outcrops of metatrandhjemite. Regionally, metatrandhjemite/metatonalite, feldspathic hornblendite, amphibolite, quartz amphibolite and gneissic amphibolite, and rare metaquartz diorite are spatially or genetically associated with metagabbro (Dragovich and others, 2009c, 2014a, 2015). Metamorphic minerals include hornblende, actinolite, prehnite, pumpellyite, chlorite, epidote, sphene, and calcite. Metagabbroic rocks are faulted against metasedimentary and metavolcanic rocks and are tectonic fragments within the mélangé belt (Tabor and others, 1993; Dragovich and others, 2013). Metagabbro and metatrandhjemite in the Lake Chaplain and Lake Roesiger areas are confined to a thrust sheet termed the Lake Chaplain nappe (Fig. 8). Dragovich and others (2014a) mapped the lower thrust to this nappe as the Sultan River thrust. This nappe and thrust are in the southeastern portion of the map area directly south of the Carpenter Creek fault, where thick tectonized metasedimentary rocks and metagabbro bound the folded Sultan River thrust. Retrogressive, protomylonitic to cataclastic shear zones occur in unit tz and metagabbro above the Sultan River thrust in the southeast part of the map area (see *Mesozoic to Tertiary Tectonics of the Western Mélange Belt* for further information). Tabor and others (1993) reported that metagabbro west of the Sultan River and directly southeast of the quadrangle has a hornblende K-Ar age of 118 ± 7.7 Ma; they also reported regional U-Th-Pb zircon ages of 150 to 170 Ma for metagabbro and metatonalite. This indicates that the plutonic rocks are similar in age to the enclosing metasedimentary rocks that we document to have a maximum depositional age of ~166 Ma.

KJuw Ultramafic rocks—Serpentinite with rare serpentinized peridotite or pyroxenite; dark greenish gray to greenish black and weathers to pale green,

dark reddish yellow, brownish yellow, or very pale orange. Ultramafic rocks range from massive with spaced fracture planes to locally intensely fractured to strongly foliated with S-C mylonite fabrics observed along a few of the Granite Falls fault zone (GFFZ) strands; most fracture or foliation surfaces are slickensided. Serpentinite consist of serpentine-group minerals (67–90%) and opaque minerals (9–20%); it locally contains tremolite (0–8%), partially to completely serpentinized pyroxene (0–5%), talc (0–5%), and calcite or magnesite (0–5%). Unit KJuwI, or listwänites, are metasomatized ultramafic rocks rich in silica and carbonate minerals as described below. Mapping and subsurface stratigraphic and geophysical analyses indicate that the ultramafic bodies align along the northwest structural grain of the GFFZ in the map area and appear to form multiple, lozenge-shaped bodies in cross section (Cross Sections A and B). We interpret these disseminated tectonic bodies in the GFFZ transition to a more coherent alpine ultramafic body west of the fault zone and under the eastern edge of the Everett basin where we use measured geophysical (particularly magnetic susceptibility) properties along with geophysical anomalies (Figs. 11 and 12) to estimate the body to be close to 3,000 m thick. Additionally, the ultramafic bodies in the GFFZ are truncated by the east-northeast-trending Carpenter Creek fault zone where southside up reverse motion on this fault has juxtaposed the structurally high portion of the WMB against the structurally lower part of the Lake Chaplain nappe south of the fault (Fig. 3). We consider the gradational contacts between moderately serpentinized pyroxenite pods and layers and surrounding thick serpentinite as the result of partial retrograde metamorphism and hydration of primary mantle rocks. Outcroppings of ultramafic and related silica-carbonate rocks (below) are widespread in the GFFZ and likely represent a structurally dismembered ultramafic body or bodies that originally represented a large and more coherent alpine ultramafic body. A strong aeromagnetic anomaly coincides with the distribution of ultramafic rocks along the Boyd Lake fault. (See Cross Section A and *Isostatic Gravity and Aeromagnetic Analyses* for further information.) These ultramafic bodies are in fault contact with WMB basement rocks across the GFFZ and are intruded by Tertiary igneous rocks such as unit Eian. The rocks of Bulson Creek unconformably overlie the ultramafic basement. Ultramafic rocks are rare throughout the WMB as a whole (Frizzell and others, 1987). Although we correlate the ultramafic with the WMB, as do Tabor and others (2002), the ultramafic mapped at depth to the east is a slightly tilted coherent tabular body that may be the result of thrusting of the Eastern mélangé belt over the WMB and thus may demark the structurally lowest part of the eastern mélangé belt (EMB). (See *Mesozoic to Tertiary Tectonics of the Western Mélangé Belt.*)

Although a Cretaceous age for the ultramafic bodies cannot be discounted, the ultramafic bodies represent the dismembered portion of an ophiolitic portion of the EMB or WMB that are typically constrained to be broadly Jurassic regionally (Dragovich and others, 2002b).

KJuwI Listwänite, silica-carbonate rocks—Silica-carbonate mineralization products (listwänites); locally contain pods of incompletely altered serpentinite and intense secondarily brecciated silica-carbonate rock; original serpentinite mesh textures or relict pyroxene grains locally preserved. Diagnostic weathered colors range from orange to brownish orange or brownish yellow; fresh faces are buff to orange with pale green speckles. Brecciated silica-carbonate rock typically contains fragments (1–5 cm) in a siliceous gray matrix. Silica-carbonate rocks commonly display compositionally banded veins or replacement bands of micro- or macrocrystalline quartz, microcrystalline magnesite, fibrous chalcidony, and (or) macrocrystalline dolomite or sulfide minerals. Structural control of this unit in the GFFZ has produced a moderate to strong northwest-trending banding, fracture, or foliation. Dominant hydrothermal minerals include microcrystalline quartz (20–45%) and carbonates (5–65%). Magnetite occurs as an accessory mineral (to 10%); various oxides are also typically present (0–15%). Carbonate minerals in listwänite include magnesite, calcite and (or) dolomite and quartz is commonly texturally opaline with carbonate minerals and quartz forming granular aggregates and vein swarms. Hansen and others (2005) document that “serpentine + olivine + brucite reacted with CO₂ to form serpentine + magnesite, then magnesite + talc, and finally magnesite + quartz” consistent with our general observations. Listwänites and ultramafic rocks are only exposed within the GFFZ in the Granite Falls quadrangle. The eastern contact of this belt is coincident with the easternmost fault strands of the GFFZ. For example, the easternmost occurrence of unit KJuwI (near the Wayside mine at significant site WM) is within the Boyd Lake fault, the easternmost strand of the GFFZ. Because of their resistance to weathering, listwänite bodies locally form ridges; the result is topographic inversion of these initially faulted and erodible ultramafic rocks. This is best observed near Menzel Lake, where unit KJuwI forms prominent NNW-trending whaleback ridges. Danner (1957, p. 368) described silica-carbonate rock near Menzel Lake as forming a (north-northwest trending) elongate ridge. In the Granite Falls quadrangle, listwänite bodies occur near faults or within unit tz of the GFFZ, indicating structurally controlled metasomatism. This structural control of listwänite formation via percolation of the CO₂-rich fluids through faults and fractures was documented by Hansen and others (2005) and Dragovich and others (2002a). The ultramafic rock protolith of

listwänite is inferred to be Mesozoic in age. Following Hancock (1928), we suspect that fluids responsible for the carbonation of serpentinized ultramafic rocks are largely related to nearby Eocene magmatism, and that these metasomatic fluids followed GFFZ faults as preferential pathways.

Holocene to Mesozoic Tectonic Zones

tz **Tectonic zone**—Cataclasite, fault breccia, clay-rich fault gouge, protomylonite, and moderately to strongly slickenlined, fractured, and veined rocks in fault zones; green and yellow to orange to variously colored, and mottled. Widespread calcite and quartz veins are prominent within most mapped tectonic zones, particularly along thrust and reverse faults (Dragovich and others, 2014a, 2015, this study). Unit tz is mapped in distinct areas of brittle or brittle–ductile deformation along two types of faults: (1) high-angle faults with Tertiary and younger deformation, such as the Granite Falls, Carpenter Creek, and Iron Mountain fault zones, and (2) Cretaceous–Jurassic WMB thrust faults—such as thick zones of unit tz above and below the Sultan River thrust in the southeastern corner of the map area. Bedrock exposures in mine or quarry faces or along logging road cutbanks within the high-angle fault zones reveal >1,000-m-thick, continuous to semi-continuous zones of shear. This shear is manifested by discrete faults, highly fractured and slickensided rocks, and generally disrupted rocks. Shear fabric along high-angle faults in this unit varies from brittle gouge to chloritized protomylonite. In many of these areas, bedding and other planar features are transposed into high-angle strike-slip to oblique slip fault zones. These very thick tectonic zones probably indicate long-lived major fault zones. We map the Sultan River thrust in the southeastern corner of the map area around significant site 38L, where a thick zone of unit tz WMB metasedimentary rocks with strong penetrative and shallowly dipping fabric underlies the thrust. The thrust is also overlain by strongly tectonized metagabbro displaying a strong, planar, gently dipping protomylonitic thrust shear fabric that grades upward to the sheared ridge-capping metagabbroic klippen. Deformed metagabbro in the Sultan River thrust is fractured and contains a retrograde mineral assemblage; thrust fabrics exhibit a retrogressive sub-planar shear fabric that is partially defined by secondary chlorite. This foliation—containing sutured quartz, and plagioclase—indicates semi-ductile shear at least locally. The relation between regional metamorphism and shear fabrics indicates a late- to post-metamorphic thrusting in the WMB. Zones of hydrothermal alteration were noted along some faults, but we did not depict these as separate map units. Common alteration minerals include chlorite and calcite but locally include opal or secondary quartz, zeolite, white mica, biotite, and (or) clay. Alteration mineral assemblages

are principally propylitic but may include phyllic and potassic assemblages. Potassium feldspar with sulfide mineralization is also locally conspicuous in the Granite Falls and Iron Mountain fault zones; historically economic mineralization occurs at the Wayside and Yankee Boy mines (significant sites WM and YBM); Hancock (1928) and Kaiser (1934) wrote that mineralization is structurally controlled and that ore formation is hypogenic, resulting from intrusion of the Eocene Granite Falls stock or related dikes. We did not map Quaternary tectonic deformation zones in the Granite Falls quadrangle. We have documented areas of liquefaction and probably faulted and tilted Quaternary sediment within the GFFZ. For further information, see *Neotectonism in the Map Area*.

GEOCHEMISTRY

We use major and trace-element geochemistry to study the composition, provenance, petrogenesis, original tectonic setting, and depositional environment of rock units in and around the Granite Falls quadrangle. We obtained major and trace-element data for nine Quaternary sands and 26 rock samples, plus trace-element data for an additional three rock samples and Nd-Sr isotope data for nine rock samples. See Appendix D for analytical methods and Data Supplement for geochemical data.

Quaternary Sand Deposits

A large geochemical dataset for Quaternary sands (n=145) has been compiled from our previously published mapping studies, covering eight quadrangles south and east of the current study area (Dragovich and others, 2007a,b, 2008a,b, 2010a,b, 2011a,b, 2012, 2013, 2014a,b, 2015, this study). These sand samples include ancient and modern nonglacial alluvium and various glacial deposits representing various sedimentary provenances (Table 1). We are able to discriminate modern and ancient alluvial sands that have a local provenance (LP) from samples that have a granitic Cascade provenance (SP) on the basis of their Sc and V concentrations (Fig. 10A)(Dragovich and others, 2010a,b, 2011a,b). In addition, we can distinguish glacial (NP) from nonglacial sediments using trace-element ratios (Fig. 10B)(Dragovich and others, 2010a,b, 2011a,b, 2014a, 2015).

Modern and ancient Pilchuck (PP) and Stillaguamish alluvial sediments (units Qa, Qcph, Qch, and Qcwpv) plot together on several geochemical diagrams (Figs. 10A, 10B, 10C; Dragovich and others, 2015). These units have moderate Sc and V values and plot in the field defined by previous PP samples (Fig. 10B)(Dragovich and others, 2015). Modern and ancient alluvium plot transitionally between intermediate and mafic igneous provenances on Figure 10C. The high Pb/Yb ratios of the modern and ancient Pilchuck and Stillaguamish alluvium (Fig. 10B) suggest a granitic provenance (McLennan and others, 1990; McDonough and Sun, 1995). However, the high chondrite normalized La/Lu ratios of the modern and ancient Pilchuck and Stillaguamish alluvium is more consistent with LP alluvium that contains abundant Western mélange belt (WMB) clasts (Fig. 10B). Petrographically, modern and

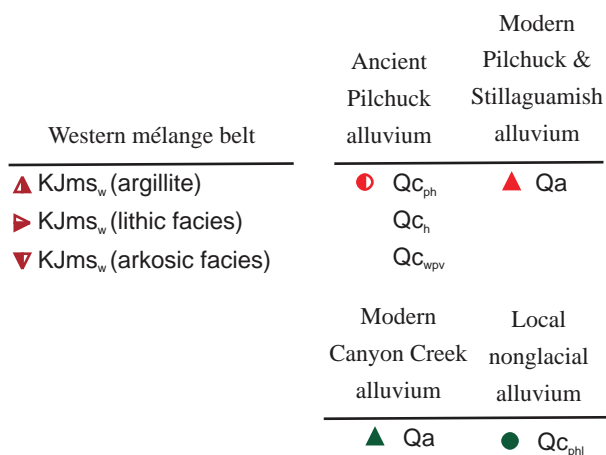
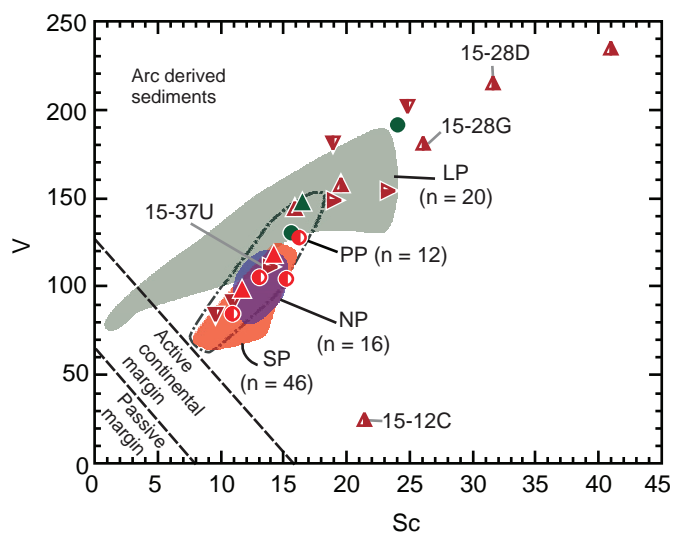


Figure 10A. Vanadium (V) vs. Scandium (Sc) provenance diagram of Bhatia and Crook (1986) for Quaternary sand samples and metasediments of the WMB. LP, local provenance; NP, northern provenance deposited during continental glaciations; PP, Pilchuck River provenance; SP, Skykomish and Snoqualmie Rivers provenance; n, number of samples. Colored fields for NP, SP, and LP are from Dragovich and others (2007, 2009a,b, 2010a,b, 2011a,b, 2013, 2014a). Unlabeled WMB data are from Dragovich and others (2015). See Table 1 for more provenance information.

ancient Pilchuck and Stillaguamish alluvium contains both abundant metasedimentary detritus that we interpret as having a WMB provenance and granitic detritus that was most likely similar to that from SP sources (Data Supplement; Table 1). The transitional LP–SP geochemical affinities of the modern and ancient Pilchuck and Stillaguamish alluvium from the Granite Falls quadrangle (Figs. 10A and 10B) supports this petrographic interpretation (Dragovich and others, 2007a,b, 2009a,b, 2010a,b, 2011a,b, 2012, 2013, 2014a, 2015).

The modern Canyon Creek (unit Qa) and ancient local alluvium from the Granite Falls quadrangle (unit Qc_{phl}) have abundant metasedimentary detritus that we believe is largely derived from the WMB. (See LP facies in Table 1.) These samples plot together on our geochemical diagrams (Figs. 10A–H). Both have high Sc (15–25 ppm) and V (129–191 ppm) (Fig. 10A) and plot in the field defined by LP from previous studies. Sample 15–34A also has high MgO (5.36 wt. %), Ni (~304

Figure La_Lu_Pb_Yb

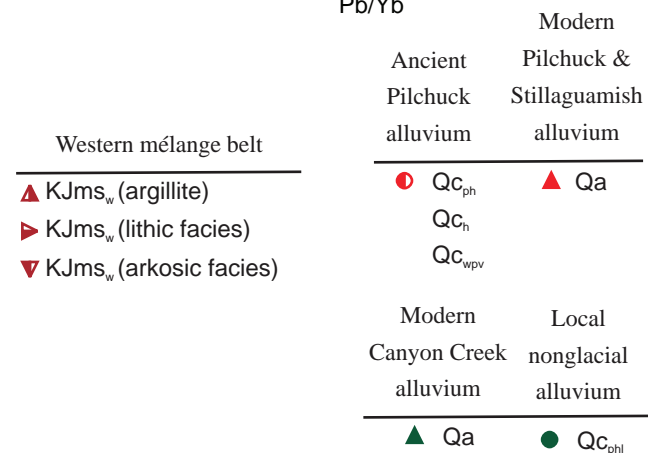
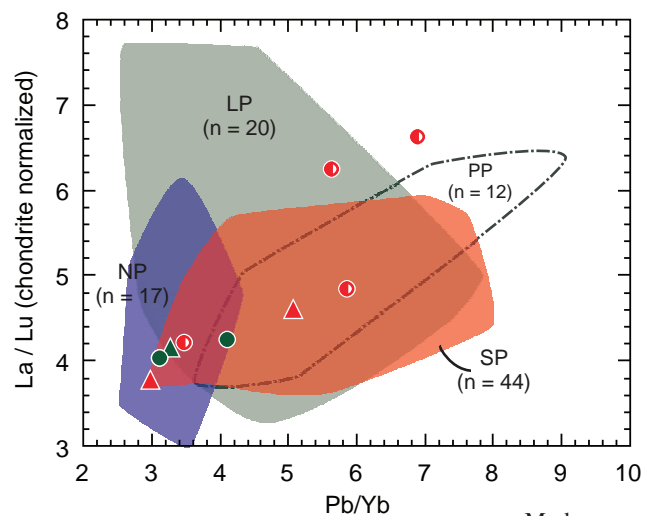


Figure 10B. Chondrite-normalized Lanthanum/Lutetium (La/Lu) vs. Lead/Ytterbium (Pb/Yb) diagram for Quaternary sand samples in this study. Chondrite normalization values are from McDonough and Sun (1995). Provenance field names (LP, NP, PP, and SP) are the same as Figure 8B and in Table 1. Colored fields for NP, SP, and LP are from Dragovich and others (2007, 2010a,b, 2011a,b, 2013, 2014a, 2015). See Table 1 for more provenance information. n, number of samples.

ppm), Cr (~540 ppm), TiO₂ (0.8 wt. %), and FeO* (7.88 wt. %) content (Data Supplement), probably because of the many included ultramafic clasts. Local alluvium samples plot in the mafic igneous provenance field on Figure 10C. This is generally true for LP reported in previous studies (Dragovich and others, 2010a,b, 2011a,b, 2014a, 2015). The modern and ancient local alluvium from this study are plotting in the overlap field for SP and LP sands defined in previous studies (Dragovich and others, 2007a,b, 2009a,b, 2010a,b, 2011a,b, 2012, 2013, 2014a,b, 2015) probably because of minor contributions of PP-type clasts. The meta-igneous and metasedimentary rocks from the WMB have geochemical affinities like the modern and ancient local alluvium (Vance and others, 1980; Tabor, 1994; Dragovich and others, 2014a; MacDonald and others, 2014). LP sands plot near WMB metasedimentary rocks on Figures 10A and 10C. The geochemistry supports the petrography in that the WMB provided the majority of the detritus for the Canyon Creek and Qc_h, and Qc_{phl} alluvium. The local

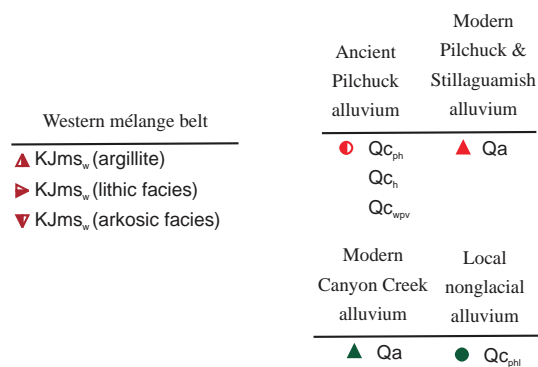
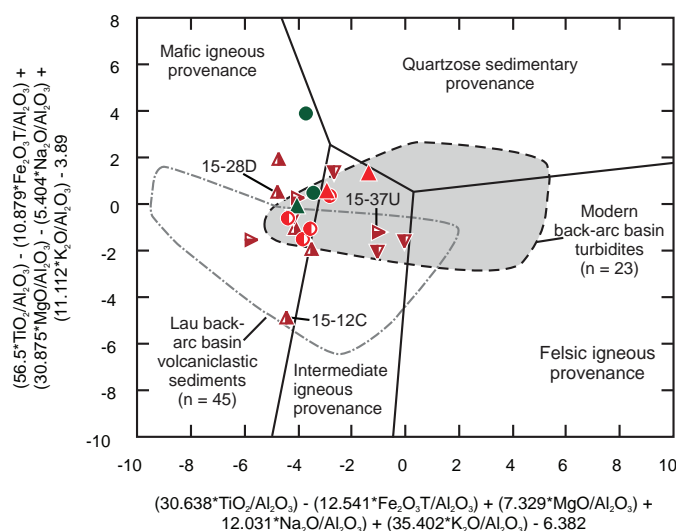


Figure 10C. Roser and Korsch discriminant function diagram for Quaternary samples and metasediments of the WMB (Roser and Korsch, 1988). Data from Dragovich and others (2014a, 2015) and this study. Note that the modern and ancient local and Pilchuck River provenance samples plot primarily in the mafic and intermediate igneous provenance field, consistent with their petrography (Table 1). Unlabeled WMB data are from Dragovich and others (2015). n, number of samples.

alluvium sands can be distinguished from Pilchuck facies alluvium in this and adjacent quadrangles by their higher S, V, and TiO₂ values, more mafic provenance, and lower SiO₂ values (Figs. 10A, 10C; Data Supplement).

Eocene Igneous Rocks

We measured major and trace elements in representative samples of the Granite Falls stock (unit Eigd; n=4), lava flows of the Hansen Lake Rhyolite (unit Evr; n=2), and Eocene dikes from several locations (unit Eian; n=8). Isotopic analyses of Sr-Nd (n=9) and Pb (n=3) were performed on some of these units and, for comparison, on two samples of Western mélange belt argillite (unit KJms_w) and two samples of Eocene plutons from the adjoining Verlot quadrangle to the east. As a group, the Granite Falls quadrangle Eocene rocks (Fig. 10D, Data Supplement) are chemically diverse (e.g., 55–72 wt.% SiO₂, 5.4–0.7 wt.% MgO). They classify as calc-alkaline on AFM (Irvine and Baragar, 1971) and FeO^T/MgO vs SiO₂ (Miyashiro, 1974) diagrams and display volcanic arc affinities on spidergrams (Fig. 10E, Data Supplement) and other tectonic discrimination plots.

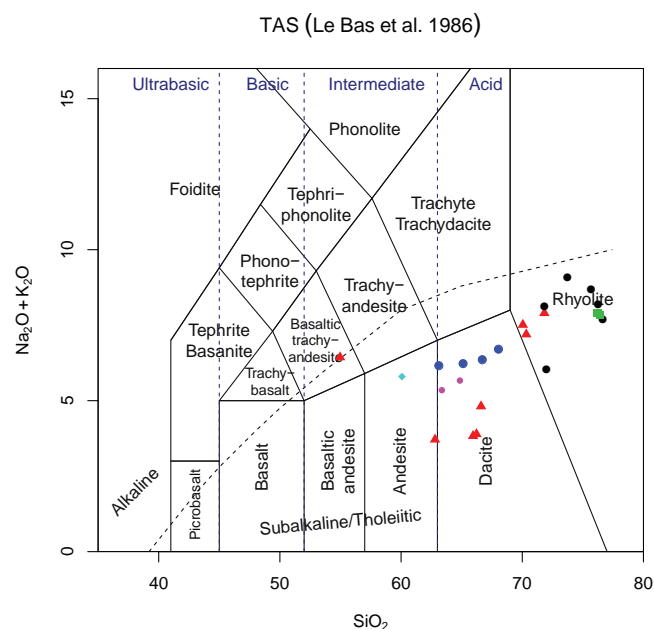


Figure 10D. Total alkali versus silica diagram (LeBas and others, 1986) illustrating the diversity of igneous rocks from the Granite Falls Quadrangle. Major element data for the Bald Mountain pluton (black circles) and Mount Pilchuck stock (green squares) are from Campbell (1991). Eian (triangles), Eigd (blue circles), Evr (pink circles), KJm_w (diamond).

Samples of the Granite Falls stock show limited chemical variation (63–68 wt.% SiO₂, 1.7–2.1 wt.% MgO), and there is no evidence that the border phase identified in the field (sample 22J) is more mafic than the rest of the stock. All stock samples are metaluminous (ASI = 0.80–0.98) and display modest LREE enrichment (La/Ybn=4.7–8.4) and moderate negative Eu anomalies (Eu/Eu*=0.65–71), except sample 4E, which appears to have accumulated feldspar (Eu/Eu*=1.12)(Fig. 10F, Data Supplement). Extrusive rocks of unit Evr classify as medium-K calc-alkaline dacites and are chemically similar to the stock. These dacites are slightly less evolved than the stock (e.g., higher average MgO, lower average SiO₂ and K₂O) and one garnet-bearing rock, sample 30G, is weakly peraluminous (ASI=1.07), but many trace element characteristics of the two units are very similar, including REE patterns (Fig. 10F, Data Supplement) and immobile trace element abundances (Fig. 10G, Data Supplement). Isotopic data (Table E1) provide further evidence that units Eigd and Evr are genetically related: the units share similar initial ⁸⁷Sr/⁸⁶Sr and εNd values that are distinctly less radiogenic than those of the other Eocene units, particularly the Mount Pilchuck and Bald Mountain plutons (Fig. 10H). Isotopic traits of these two plutons (⁸⁷Sr/⁸⁶Sr_i = 0.7065–7075, εNd(t) = -0.4 to +0.7) point to derivation from a metasedimentary source, as previously inferred for the Mount Pilchuck stock from the peraluminous mineralogy, chemistry, and high initial ⁸⁷Sr/⁸⁶Sr values (Campbell, 1991; Tabor and others, 2002). The identity of this source is unknown, but Nd isotopic data yield an early Paleozoic or late Proterozoic depleted mantle model age (Table E1). In contrast, the Granite Falls stock (unit Eigd) and associated lavas (unit Evr) were likely derived from a mafic to-intermediate source that has arc chemical affinities. Based on Sr-Nd isotopic similarities,

the WMB volcanoclastic metasandstone (for example, sample 15–210DF; see discussion below), which has arc affinities, could be representative of the source for units Eigd and Evr, but WMB argillite (samples 15–210G, 15–210B) could not. The arkosic petrofacies of the WMB (unit KJms_W) may be representative of the metasedimentary rocks at depth that melted to produce the S-type granites east of the map area. This inference is consistent with the aluminous character of these mica-rich metasedimentary rocks and with the low structural level inferred for this petrofacies regionally, which may place it at depth beneath the Mount Pilchuck and Bald Mountain area. The depth to this petrofacies is unknown, but present information suggests this structural element lies below the present erosional level of Pilchuck Valley north of the Carpenter Creek fault.

The Eocene dikes (unit Eian) are the most chemically diverse unit in the map area (55–72 wt.% SiO₂, 5.4–0.7 wt.% MgO, molar Mg/Mg+Fe = 0.49–0.29) and can be divided into a less-enriched group (LEG) and a more-enriched group (MEG). LEG samples tend to be more primitive, having lower concentrations of SiO₂ and high field strength elements [HFSE], and higher compatible elements (e.g., MgO, Sc, V). They are also metaluminous (ASI = 0.8–1.0). Conversely, the MEG samples are more evolved, with higher SiO₂ and La/Ybn values, and generally peraluminous (ASI = 1.0–1.8). There is no indication of a correlation of dike chemistry with either sample location or age; both LEG and MEG occur among ‘early’ dikes that show evidence of contact metamorphism and among ‘late’ dikes that do not. Large differences in HFSE abundances (Fig. 10G) and REE patterns (Fig. 10F) are difficult to model by fractionation processes and strongly suggest the LEG and MEG were derived from different sources. Trace-element data for MEG dikes are very similar to those of the Granite Falls stock (Figs. 10F, 10G), suggesting that these dikes could have been feeders for the pluton. The presence of enclaves and synplutonic dikes within the pluton further supports this possibility. Sr-Nd isotopic data for one LEG sample (Fig. 10H) are significantly more crust-like than the data for unit Eigd or Evr samples and may reflect crustal contamination. It is unknown whether this sample is representative of unit Eian in general.

Western Mélange Belt

We analyzed six WMB samples for this study (Data Supplement): two metasandstones, three meta-argillites, one metatuff, and one metaquartz gabbro; these add to the WMB dataset from our previous mapping studies (Dragovich and others, 2009a,b, 2013, 2014a, 2015). The WMB has undergone prehnite-pumpellyite to amphibolite-facies metamorphism and many elements can be mobile under these conditions (e.g., K and Ca; Cann, 1970; Pearce, 1996, 2014). Therefore, we make petrologic interpretations using only elements considered to be immobile up to and including amphibolite-facies metamorphism (Pearce, 1996, 2014).

The metasandstones and meta-argillites have high V (26–236 ppm) and Sc (9–41 ppm) and plot in the oceanic arc-derived sediments field on Figure 10A. They also plot in the mafic or intermediate igneous provenance field on the discriminant function diagram of Roser and Korsch (1988). They

predominantly plot in the fields defined as modern back-arc basin volcanoclastic sediments (Fig. 10C). These metasedimentary rocks have low La (3.7–31.0 ppm), Ce (9.1–55.7 ppm), Hf (1.1–4.7 ppm), Th (0.2–9.2 ppm), and Zr (39.2–182.2 ppm) (Data Supplement), which suggests that recycled or cratonic detritus was not a major depositional component (Bhatia and Crook, 1986; McLennan and others, 1990). High Sc and V, and low Ce, La, and Th, suggest a mafic to intermediate volcanic arc source (Bhatia and Crook, 1986; Roser and Korsch, 1988; McLennan and others, 1990). The metasandstone samples from the WMB have been separated petrographically into the arkosic and lithic petrofacies of Jett and Heller (1988). Although detrital zircon age populations for the arkosic metasandstone include older cratonic sources (Brown, 2012; Dragovich and others, 2014a; Sauer and others, 2014), our new detrital zircon age information for a volcanic lithic metasandstone in the map area contains very little or no cratonic or pre-Jurassic detritus, consistent with the trace-element data (sample 15–210DF, Fig. C3, Table C1). The arkosic petrofacies samples from the Lake Chaplain and Lake Roesiger quadrangles have lower Sc and V, and higher Th and Zr than other WMB metasedimentary samples (Fig. 10A). This arkosic petrofacies plots in the intermediate igneous provenance field on Figure 10C. This geochemistry and petrographic analysis (Dragovich and others, 2014a; Jett and Heller, 1988), suggests that these arkosic samples came from a continental arc source that had received detritus from the North American craton (Bhatia and Crook, 1986; Roser and Korsch, 1988; McLennan and others, 1990). This is supported by positive εNd values reported by Sauer and others (2014) for an arkosic petrofacies metasandstone in the Lake Chaplain quadrangle. The depleted Nd isotopes reported here, along with the geochemistry, new detrital U-Pb ages (Table C1), and petrography of the lithic petrofacies of the WMB, are consistent with deposition in a back-arc basin or forearc setting that received detritus from an intermediate to mafic arc source (Bhatia and Crook, 1986; Roser and Korsch, 1988; McLennan and others, 1990).

A metatuff and metaquartz gabbro were also analyzed for this study. The metatuff was originally a fine-grained tuffaceous sandstone with very thin tuffaceous interbeds. The high SiO₂ content of the metaquartz gabbro (64.8 wt. %); may be the result of low-grade metamorphism, but the rock name is based on petrography, not geochemistry. The metatuff and metaquartz gabbro have calc-alkaline affinities on AFM, FeO^T/MgO vs SiO₂, and Th/Yb vs Nb/Yb plots (Pearce, 1996, 2014). MORB-normalized trace-element ratios for these samples (not shown) suggest derivation from an enriched MORB source that underwent subduction enrichment. This is consistent with metatuff sample data from previous studies; however, metagabbro samples from previous studies had a more depleted source (Dragovich and others, 2009a,b, 2013, 2014a, 2015). We also analyzed a serpentinite (sample 15–10B, Data Supplement) collected from a lenticular ultramafic body within the Granite Falls fault zone. Loss on ignition for this sample is very high (13.78), causing the major element totals to be low (Data Supplement), but Deschamps and others (2013) suggest that serpentinitization does not significantly modify the geochemical signature of the ultramafic protolith. This

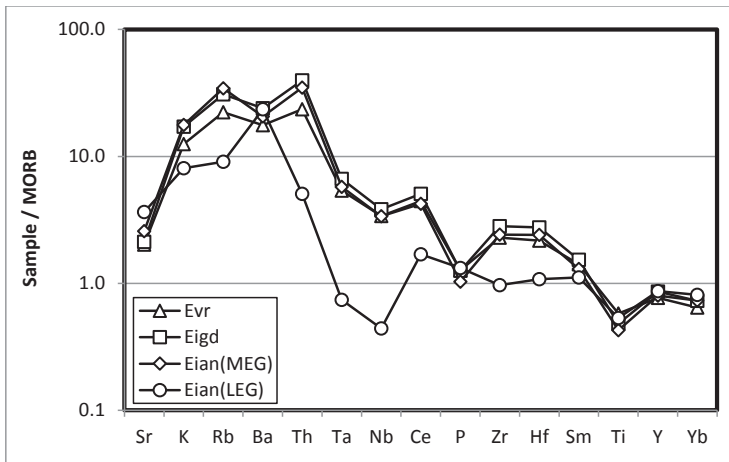


Figure 10E. MORB-normalized spider diagram showing K-Rb-Ba-Th enrichments and Ta-Nb depletions characteristic of subduction-related magmas. Plotted values are averages for each unit (Appendix D and *Data Supplement*). Note the close similarity of patterns for Eigd, Evr, and Eian (MEG), suggestive of a common origin. Available information suggests a syn-tectonic ~44 Ma igneous complex with several intrusive and extrusive lithologic types.

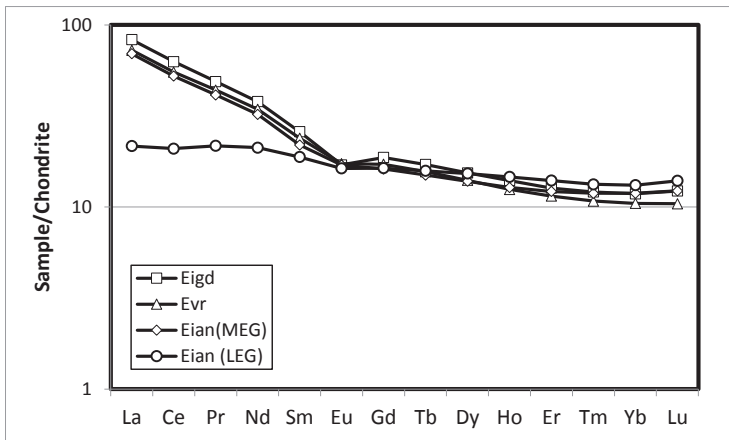


Figure 10F. Average REE contents of Eocene igneous units normalized to chondrite values of Boynton (1984).

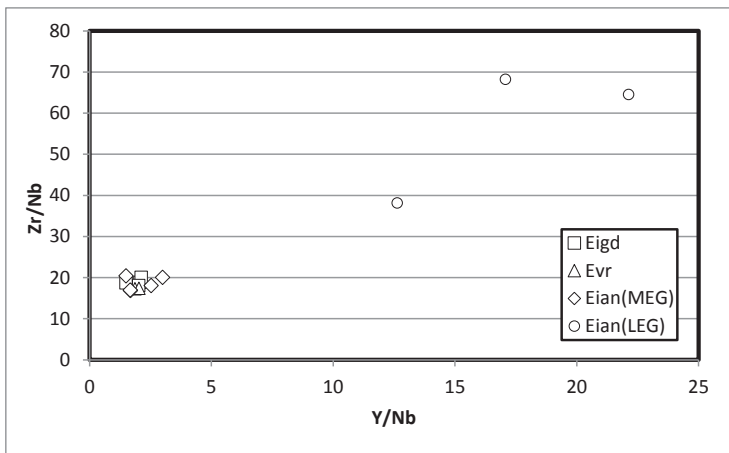


Figure 10G. Comparison of high field strength element ratios among Eocene igneous samples. The tight clustering of Eigd, Evr, and Eian (MEG) samples suggests a common origin for these units that is distinct from that of the Eian (LEG) samples.

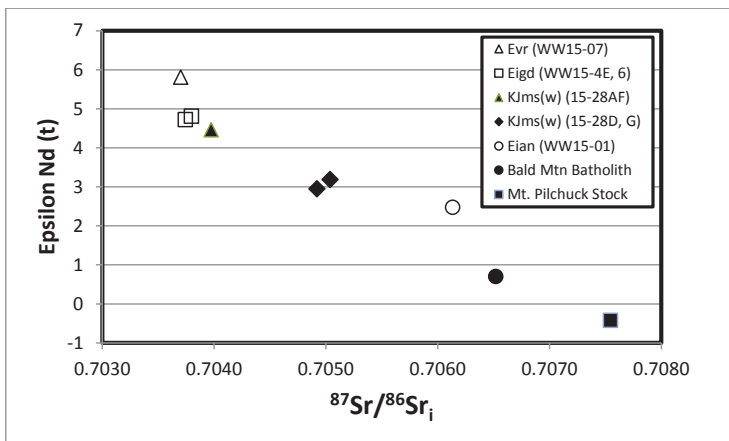


Figure 10H. Sr-Nd isotopic compositions. Note the similarity of Eigd and Evr samples. Their high ϵ_{Nd} and low $^{87}Sr/^{86}Sr$ values argue against derivation from KJms_w argillite or from the source of the Pilchuck and Bald Mountain plutons. WMB volcanic lithic metasandstone (15-28AF) could be representative of the Eigd/Evr source, although we suspect that the structurally low (aluminous) meta-arkosic sedimentary petrofacies is a good candidate for the “S-type” Bald Mountain and Mount Pilchuck plutons. See Appendix E.

serpentinite has Al/Si (5.36), Mg/Si (0.89), V/Mg (69.09), and Y/Mg (1.41) ratios similar to those of modern abyssal peridotites (Niu, 2004; Deschamps and others, 2013). However, it is not clear if this serpentinite belongs to the WMB or is a structurally-emplaced fragment of Eastern mélangé belt.

ISOSTATIC GRAVITY AND AEROMAGNETIC ANALYSES

High-quality aeromagnetic data define the geomagnetic anomalies in the quadrangle (Fig. 11; Blakely and others, 1999). Very few gravity data existed in the quadrangle prior to our work (Finn, 1991), therefore we collected ~140 new gravity stations to define isostatic gravity anomalies. We use both of these data sets to constrain our structural interpretations. Extensive sampling and measurement of density and magnetic susceptibility for units in this and six neighboring quadrangles (Dragovich and others, 2010a,b, 2011a,b, 2012, 2013, 2014a, 2015) provide strong support for predicting geophysical anomalies in terms of subsurface geologic units (Fig. 12), as well as a means for interpreting map-view anomalies in terms of subsurface geologic units and faults. Densities and magnetic susceptibilities used for modeling do not deviate from measured values except for metagabbro (unit KJigb_w), which did not crop out on the quadrangle, and Eocene rhyolite (unit Evr), for which we only had two samples (model value is 2,500 kg/m³ whereas measured values average 2,550). The KJigb_w density and susceptibility used for modeling is quite similar to that measured and used for modeling in previous quadrangles, particularly Lake Roesiger (Dragovich and others, 2015).

An aeromagnetic high in the middle of the quadrangle dominates the geophysical anomalies (SP1 and SP2 on Fig. 11). It has a broader wavelength signal (8 km) than those observed over metagabbro bodies to the south (especially in the Lake Roesiger quadrangle—3.5 km; Dragovich and others, 2015) and the gradient on the edges of the anomaly is less steep (58 nT/km on average vs. 95 nT/km in Lake Roesiger). These observations indicate that the source is likely a more deep-seated structure. The gravitational anomaly trend is similar to other areas along the eastern edge of the Everett and Seattle basins, with a high to the east (WM in Fig. 11) where the western mélangé belt is exposed at the surface or sits just under a thin veneer of Quaternary sediments. From that point, the gradient trends west, creating the lowest values along the western edge and in the southwestern corner of the quadrangle.

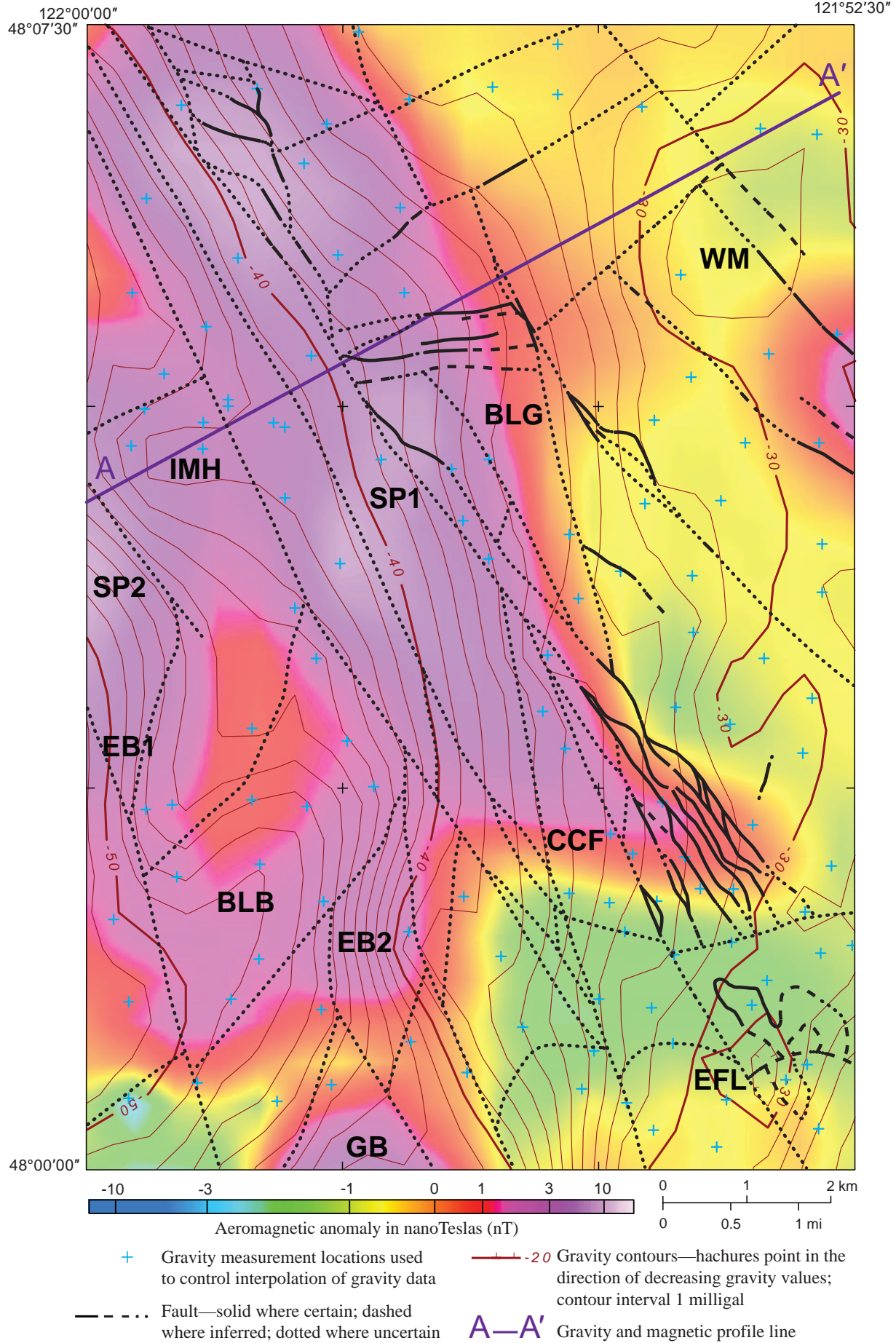
The large, northwest-trending aeromagnetic anomaly at SP1 is collocated with outcrops of ultramafic rocks, particularly serpentinite (unit KJu_w). This area also coincides with the start of the westward-trending gravity gradient, indicating lower density rocks under the area. Given the surface exposures of KJu_w, we must explain the gravity gradient by other means than simply the existence of sediment infill along the edge of the Everett basin, and the low density of our samples give us the key. Our measurements of KJu_w samples indicate a very high magnetic susceptibility (averaging 42 × 10⁻³ SI), at the high end of published ranges (Telford, 1990), and very low density (2,570 kg/m³) compared to the bulk of the Western mélangé belt making up the crust in this region (which average 2,720 kg/m³). These properties can account for the pairing of

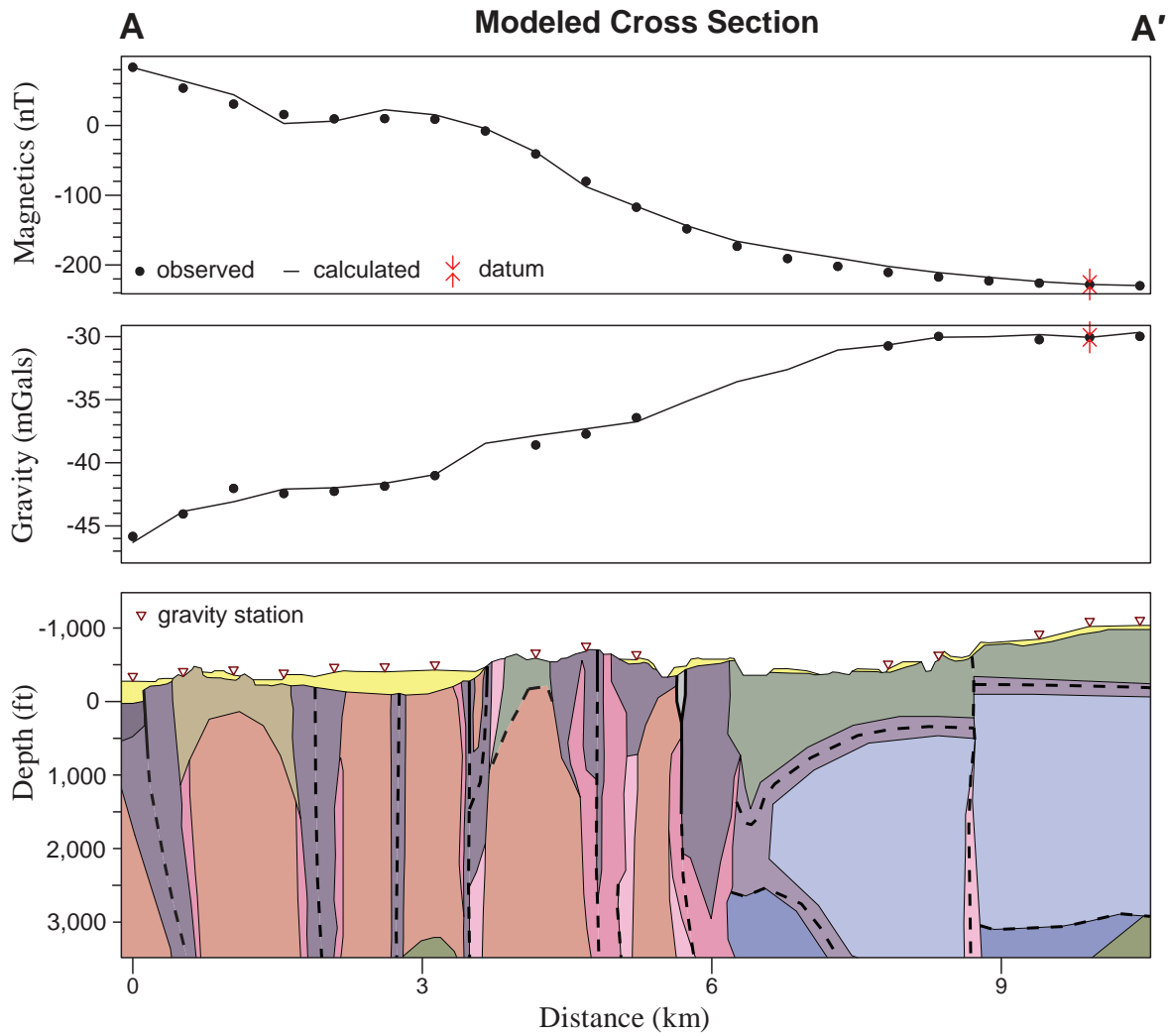
high magnetic and lower gravity anomalies in the center of the quadrangle.

In addition to the ultramafic rocks, we interpret KJigb_w at depth underneath much of the aeromagnetic anomaly at SP1, but this is solely based on modeling the gravity and magnetic anomaly data (Fig. 12). There is a clear tradeoff in magnetism between units KJu_w and KJigb_w, each having a similarly high magnetic susceptibility. Gabbroic phases of unit Eian could also trade off with these other units, but it is of such small volume that we cannot distinguish it from the metagabbro of the western mélangé belt. It is clear that there is a massive amount of magnetic rock below the surface to account for the strength of the aeromagnetic anomaly SP1. However, in the modeling process, using only KJu_w results in a gravitational anomaly that is too low to match the data. Because it has a high density, placing some KJigb_w at depth underneath the ultramafic rocks helps increase the modeled magnetic anomaly to fit the data and simultaneously keeps the modeled gravity anomaly at a more reasonable (higher) value and closely match the gravity data. The modeled thickness of the metagabbro is a tenuous hypothesis, but we are encouraged that what fits our data here is consistent with other models in the region, especially in the Lake Roesiger quadrangle, where exposure of metagabbro and lack of overlying magnetic lithology helps constrain thickness with greater confidence. The final modeled thickness (existing largely below the cross-section limits in Fig. 12) is 1,470 m at its thickest, largely within fault zones (consistent with 1,000 m in Lake Roesiger or 1,563 m in the Lake Chaplin quadrangles) and closer to ~560 m elsewhere (consistent with ~470 m in Lake Roesiger and ~370 m in Lake Chaplin). Units KJu_w and KJigb_w both clearly extend east of the Granite Falls fault zone, based on our modeling. Similar to Lake Roesiger, the metagabbro body appears to taper into a wedge shape to the east in order to fit the gentler gradient in the aeromagnetic anomaly heading eastward. There is one spot where we interpret gabbro close to the surface along the southern border of the quadrangle (GB in Fig. 12). This anomaly is continuous with an aeromagnetic high clearly associated with a northwest-trending metagabbro body mapped on the Lake Roesiger quadrangle.

Another important tradeoff to note is between three volumetrically significant low density units: Eocene intrusive rocks (especially Eigd), metasedimentary rocks of the Western mélangé belt (unit KJms_w) and KJu_w. As noted above, when used for modeling, KJu_w changes the predicted magnetic anomaly significantly, so there are limits to its use in map interpretation and modeling. To help make predicted gravity lower in our model, we included a fair amount of Eigd under

Figure 11 (facing page). Aeromagnetic anomaly and isostatic gravity map of the Granite Falls quadrangle. Base map is reduced-to-pole aeromagnetic anomaly, filtered (upward continued and differenced with original grid) to bring out magnetic anomalies originating from near-surface sources. Gravity is contoured in red and blue crosses mark gravity measurement locations. BLG, aeromagnetic gradient associated with the Boyd Lake fault; CCF, aeromagnetic gradient associated with the Carpenter Creek fault; EB1 and EB2, gravity gradients associated with the edge of the Everett basin; EFL, Explorer Falls gravity low; GB, meta gabbro unit KJigb_w near the surface; IMH, Iron Mountain fault zone-associated gravity high; BLB, Bosworth Lake basin gravity low; SP1 and SP2, northwest trending aeromagnetic highs associated with serpentinite at depth; WM, western mélangé belt gravity high.





Density contrast (kg/m ³)	Susceptibility	Geologic units
Quaternary deposits		
$\Delta\rho = -660$	$\chi = 2.5$	undifferentiated Quaternary deposits
Eocene Intrusives and Volcanics		
$\Delta\rho = -170$	$\chi = 4.0$	Evr
$\Delta\rho = -20$	$\chi = 0.3$	Eigd
$\Delta\rho = -40$	$\chi = 3.4$	Eian
Western mélangé belt		
$\Delta\rho = -30$	$\chi = 0.2$	metasedimentary, unit KJms _W
$\Delta\rho = 50$	$\chi = 0.3$	phyllite, unit KJph _W
$\Delta\rho = 170$	$\chi = 55$	metagabbro, unit KJimgb _W
$\Delta\rho = 50$	$\chi = 0.3$	undivided unit KJm _W , excluding metagabbro
$\Delta\rho = -100$	$\chi = 42$	ultramafic, unit KJu _W
$\Delta\rho = 80$	$\chi = 0.4$	listvenite, unit KJu _{Wl}
Tectonic zones		
$\Delta\rho = -140$	$\chi = 1.2$	cataclasite of unit Φ EC and KJu _W
$\Delta\rho = -10$	$\chi = 1.2$	cataclasite of unit KJph _W
$\Delta\rho = -100$ to -60	$\chi = 1.2$	cataclasite of unit KJu _W and Eian

Figure 12. Geophysical model A coincides with lithologic Cross Section A–A’ (at 2.5x vertical exaggeration) and show the match of modeled density and magnetic susceptibility of rock packages from the cross section to the observed gravity and aeromagnetic values. Here we use the total field magnetic anomaly to interpret both the shallow and deep-seated structures that contribute to the magnetic anomalies of the region, unlike in Figure 11, which focuses on near-surface structures. Aeromagnetic data sampling distance along A–A’ is approximately twice the flightline spacing. Gravity data points are shown where good data control exists within 1.5 km of the line. The models extend to infinity in both directions perpendicular to the profiles. $\Delta\rho$ is the density contrast relative to normal crust (2,670 in kg/m³) used for the model; χ is magnetic susceptibility (used in the model) in SI units x 1,000. Bold, solid lines show fault locations that are well constrained by the geophysical data and geologic mapping; dashed lines are less certain at depth.

the KJigbw at depth (below the section shown in Fig. 12). While interpreting a source body for the dikes observed across the quadrangle is reasonable, we could have alternatively interpreted a much smaller volume source, and included more KJmsw at depth below the quadrangle. The dikes themselves (both Eigd and Eian) are completely unresolvable by our modeling because of the density tradeoff with KJuW, therefore they are included in our model to be consistent with the structural interpretation. We would also like to note that the depth of the KJph/ KJmsw boundary at the eastern edge of the geophysical model (Fig. 12) is highly dependent on the broader gradient set up by the Everett basin depth/sediment density to the west of the quadrangle, therefore this depth should be considered with caution. While we can make a reasonable estimate of Everett basin structure, changes to that interpretation could affect the steepness of the broad east-west gravity gradient predicted across our model line.

Eocene and younger tectonism imprints the geophysics in a couple of areas on the map. In contrast to nearby quadrangles, Quaternary sediment here is rather thin and well data give us high quality stratigraphic constraints. Therefore, we do not use changes in Quaternary sediment thickness to help fit the gravity data during our modeling process. The southwest corner of the quadrangle is clearly within the Everett basin. Modeling of Cross Section A (Fig. 12) indicates the start of the Everett basin just west of the quadrangle boundary, coinciding approximately with gradient EB1 (Fig. 11). Gradient EB2 also most likely bounds the Everett basin, due to similarity in gradient steepness (both are much stronger gradients than at SP1). Therefore, we interpret Bosworth Lake basin, a gravity low (BLB on Fig. 11), as an arm of the Everett basin. It is likely that a significant portion of its origin is due to Eocene age extension, consistent with other interpretations in this report (See *Regional and Local Eocene Tectonics and Magmatism*). However, if the gradients at EB1 and EB2 are currently collocated with and at least partially due to the most active strands within the WCFZ (indicated by the strength of the gradients), the zone containing the Bosworth Lake basin would be a transpressional step within the right lateral Woods Creek fault zone, at odds with evidence for pre-Hamm subsidence (see *Structurally Controlled Basins and Valleys*). This story would be consistent with our hypothesis of a switch of tectonic strain in the Pleistocene (see *Northeast-Trending Pleistocene Transtensional Basins*). It is important to emphasize, however, that if the gradients at EB1 and EB2 originate largely from Eocene-age structures, their existence may be inconsequential for the more recent tectonic story of the Woods Creek and other fault zones.

Other east-northeast striking features are worth noting in the geophysical data. There is a separate and distinctive gravity anomaly high north of the Bosworth Lake Basin (IMH on Fig. 11). Because its strike is parallel to the Iron Mountain fault zone, we hypothesize a genetic relationship. In this case, the gradient bounding the northern edge of the high would be interpreted to indicate a down-to-the north structural interpretation along the unnamed fault collinear with the Iron Mountain fault zone. The Carpenter Creek fault zone is notable for its lack of evidence in the gravity data, indicating

that it bounds rocks of similar densities; therefore, any recent activity has failed to preserve sediments thick enough to affect the gravity. However, it shows a strong east-trending gradient in the aeromagnetic data (CCF in Fig. 11). This indicates it bounds the southern extension of strongly magnetic unit KJuW in this location. Because the strongest part of the gradient is north of the mapped surface trace, the fault could dip to the north, but other observations (structural, associated microseismicity and distribution of surface sedimentation) all indicate a dip to the south. Therefore, we prefer the interpretation that the maximum gradient is north of the fault due to non-magnetic unit tz bordering the fault. The preservation of the structurally higher magnetic unit KJuW north of the fault indicates an overall relative downward displacement of the northern fault block over time.

A small gravity low exists at EFL (Fig. 11) and is slightly enigmatic in origin. Though an inspection of the gravity stations constraining this low indicates no problems with the data, we have very few data to detail a feature of this size. Well data in this area indicate the existence of a greater thickness of sediment in this area, thus supporting its existence. We suspect it has origins related to the Explorer Falls basin, but we leave further interpretation for future study.

With the exception of fault-related features detailed above, we note that unlike many other quadrangles mapped to the south of Granite Falls, fault locations here are not well-delineated by the geophysical data, especially the strands within the Granite Falls fault zone. The primary units responsible for the aeromagnetic and gravity gradients (particularly at SP1 and SP2) seem to cross the northwest trending faults with little consequence to their thickness across many of the faults. In addition, there is some flexibility in where we make thickness changes of units KJigbw and KJuW to help fit the aeromagnetic data, and they may or may not be exactly coincident with mapped faults. Because of the tradeoffs denoted above, tectonized units are also not well-delineated by the geophysics. We do use tz units in our modeling (generally 20 kg/m³ less dense than the host rock) to be consistent with mapping and structural interpretations, but their size and geometry is not well-constrained by the geophysical data. Because tz zones have been measured to be consistently non-magnetic in this and other quadrangles in the region, they cannot be too wide at depth, because highly magnetic rocks are needed in the near subsurface in our model (Fig. 12) to fit the aeromagnetic anomalies across the profile, but that is the only support we can give for their existence and size at depth.

DISCUSSION

Mesozoic to Tertiary Tectonics of the Western Mélange Belt

EASTERN AND WESTERN MÉLANGE BELTS—CORRELATION OF ULTRAMAFIC ROCKS IN THE MAP AREA

Tabor (1994) suggested that the Eastern and Western mélange belts were thrust over the Northwest Cascades System—a set of nappe-bounding thrusts and associated structures containing Mesozoic and older rocks, likened to a regional mélange

by Brown (2012). Tabor and others (2002, p. 25) indicated that the Eastern mélangé belt is thrust over the Western mélangé belt (WMB) and state that “The eastern mélangé belt and a probable correlative mélangé, the highly mixed Trafton terrane of Whetten and others (1988), appear to be structurally high”. Tabor and Booth (1985) and Tabor and others (2002) show these regional thrusts to be folded. These relations indicate that both regionally and locally or intraformationally thrusting appears to be the primary mechanism for obduction of these accretionary rocks.

Ultramafic rocks occur widely in the Granite Falls fault zone (GFFZ), as a gently tilted body in the subsurface along the easternmost part of the Everett basin (Cross Section A). We follow Tabor and others (2002) and correlate ultramafic rocks and the metasomatized equivalent listwänite bodies (units KJu_w and KJu_{wl}) with the Western mélangé belt. However, ultramafic bodies are rare in the Western mélangé belt outside of the Granite Falls quadrangle; there is one small mass of serpentinite in the Rattlesnake Mountain fault zone near North Bend (Dragovich and others, 2009c) and some small bodies along the fault bordering the northeastern part of the Bald Mountain pluton east of the map area (Dungan, 1974; Tabor and others, 2002). Conversely, ultramafic rocks are common in the Eastern mélangé belt (EMB) east and northeast of the map area (Tabor and others, 2002). They indicate (p. 26): “The eastern mélangé belt displays many of the same lithologies and the same degree of disruption as the western mélangé belt, but it is predominantly greenstone and chert and contains numerous pods of ultramafic rocks and gabbro.” Thus, ultramafic rocks in the Granite Falls quadrangle may correlate with those in the EMB. Tabor and others (2002, p. 26) state:

“Ultramafic rocks, including serpentinite, metaperidotite, and metaclinopyroxenite, are characteristically scattered throughout the eastern mélangé belt. Dungan (1974, p. 48–53, 94) describes some ultramafic blocks with primary cumulus textures and others as harzburgite and dunite tectonite. Metamorphic minerals, mostly confined to rocks north of the South Fork of the Stillaguamish River, are tremolite, talc, and olivine. Dungan (1974) and Vance and Dungan (1977) give mineral analyses and parageneses. Vance and others (1980, p. 362–367) describe these rocks and, based on regional considerations, suggest that they are Jurassic in age. They consider the ultramafic rocks and associated gabbro (TKeg) to be part of a metamorphosed and dismembered ophiolite complex imbricated in the oceanic and volcanic rocks of the eastern mélangé belt along Tertiary high-angle faults. We consider this imbrication within the mélangé to be mostly due to mélangé mixing, probably a combination of olistostromal and tectonic processes, but additional displacement by high-angle faulting is also likely.”

We conjecture (Fig. 8) that ultramafic bodies in the map area are the basal portion of the Eastern mélangé belt and

demarcate the deformed thrust or tectonic contact between the two mélangé belts. From mapping and geophysical analyses of the map area, we postulate that this Cretaceous thrust contact is displaced by later Tertiary and younger high-angle faulting along the edge of the Everett basin (Cross Sections A and B, see *Everett Basin and Vertical Tectonics along the Granite Falls Fault Zone*). Currently, we suspect only the ultramafite has potential to be correlative with the EMB, but we urge future workers to consider other protoliths within this strongly tectonized zone, including the metachert, greenstone and metagabbro mapped in the eastern part of the GFFZ.

METAMORPHIC GRADE, STRATIGRAPHY, AND STRUCTURAL STACKING OF THE WMB

The WMB contains outcrop- to mountain-sized phacoids of metagabbro, metadiabase, amphibolite, and metatonalite that are metamorphosed to greenschist or amphibolite facies. In the study area, metasedimentary and metavolcanic rocks are predominantly in the prehnite-pumpellyite facies, whereas greenschist to amphibolite facies metasedimentary and metavolcanic rocks found in the highest grade of the WMB occur in uplifted blocks. This is a regional grade change whereby, “the eastern part of the Western [mélangé] belt is more thoroughly metamorphosed than the rest of the belt; in the general area of the lower Sultan Basin the disrupted rocks grade to slate, phyllite, and semischist and contain minor greenschist and chert” (Tabor and others, 1993, p. 12). Dragovich and others (2014a, 2015) suggest that some or all of the meta-intrusive rocks lie within the Lake Chaplain nappe, a structural unit bound by the Sultan River and Lake Chaplain thrusts and composed mostly of Jurassic (150–170 Ma) metagabbro and metatonalite (Fig. 8). The intensity of deformation in the mélangé is greatest in the Lake Chaplain nappe where the meta-intrusive rocks appear to be deformed at most scales. These higher grade meta-igneous rocks are structurally confined to the Lake Chaplain nappe, locally resulting in ‘jumps’ in metamorphic grade. This observation is further borne out in the Granite Falls quadrangle where high-grade metamorphic rocks of the Lake Chaplain nappe are mapped in uplifted areas.

The juxtaposition of low-grade rocks above and below higher grade rocks most likely is a result of late- to post-metamorphism thrust stacking and Tertiary high-angle faulting. This is seen in the southeastern corner of the map area around significant site 38L, where metagabbro is thrust over metasedimentary rocks along a thick zone of sheared metagabbro and metasedimentary rocks (unit tz), forming a klippe of the Lake Chaplain nappe (Fig. 8). Tectonic fabrics in unit tz above and below the thrust are similar to thrust fabrics mapped in quadrangles to the south; an S-C mylonite in this tectonic zone near the Sultan River thrust indicates a north-northwest thrust direction for this klippe (Fig. 3). The model of Dragovich and others (2014a, 2015) in which older Jurassic–Cretaceous arc components were thrust over younger metasedimentary rocks that have a granitic source, is further substantiated in this quadrangle by the sole occurrence of arkosic petrofacies metasedimentary rocks at significant site 36N along the southern boundary of the map area. The Lake Chaplain nappe is exposed in this area and is thought to represent the structurally

lowest position in the Granite Falls quadrangle south of the Carpenter Creek fault (Fig. 8). Exposure of this structural level south of the Carpenter Creek fault is consistent with mapping to the south of the Granite Falls quadrangle where the arkosic petrofacies is observed to be structurally below the Lake Chaplain nappe metagabbro klippen. The lack of exposed meta-arkose and rarity of metagabbro in the WMB north of the Carpenter Creek fault locally and regionally may indicate that this structure predates the Eocene and perhaps demarks a fundamental Mesozoic tectonic boundary, such as a major obduction surface that has a distinct history of rejuvenation. Although this structural geometry is speculative, it is clear that this fault zone is the locus of a major change in structural level exposed north and south of this fault zone.

The Western Mélange Belt Structural/Stratigraphic End-members—Regular Volcanic Arc Stratigraphy and Local Structural Dismemberment in Thrust Dislocation Zones

Our mapping from the North Bend quadrangle northward to the Granite Falls quadrangle indicates the WMB contains abundant near-arc volcanoclastic sediments that were deposited in an accretionary prism. In some areas these strata include regularly folded stratigraphic successions with generally homoclinal fold limbs. This “regular stratigraphy” typically displays little or no obvious mélange-like structure. However, a few key areas in nappes record moderate to extreme disruption with a marked increase in metamorphic grade. These include the Lake Chaplain nappe described above as well as an inferred folded thrust zone containing exotic tectonic fragments in the northeastern part of the map area.

In the Granite Falls quadrangle, the inferred depositional environment for the WMB is marine, near-arc sedimentary basins, perhaps a forearc, dominated by volcanic lithic metasedimentary rocks. East of the GFFZ and north of the Carpenter Creek fault, regularly stratified metasedimentary rocks folded around the Chitwood Lake and Worthy Creek synclines display minimal mélange disruption and contain unit KJmsw volcanoclastic rocks and metatuffaceous sandstones as well as andesitic metatuff beds. Our new detrital zircon ages for volcanoclastic metasandstone (sample 15–28AF) suggests a ~166 Ma Jurassic volcanic arc proximal to the accretionary complex dominated by volcanoclastic metasedimentary rocks and metatuff. Combined with mapping, the new age information, petrography, and geochemistry suggest an accretionary complex adjacent to an island arc volcanic chain that is distant or shielded from the craton. This Jurassic volcanoclastic and near arc sequence is structurally high and overlies the Cretaceous arkosic petrofacies. The arkosic petrofacies is a late Cretaceous sequence for which petrography, geochemistry, and detrital U-Pb ages suggest a craton granitic provenance (Dragovich and others, 2014a, 2015; Sauer and others, 2014; Brown, 2012)(Fig. C3; Table C1). Brown (2012, pp. 805–806) describes detrital zircon peaks in the arkosic petrofacies as follows:

“The dominant populations are in the range of 87–93 Ma, with groupings at 87, 91, and 93 Ma. The mean age of the youngest population of 11

zircons is 87.3 ± 1 Ma, which establishes a maximum depositional age.”

The current information of Dragovich and others (2014a, 2015, this study) and Sauer and others (2014) indicate that: (1) the arkosic petrofacies is locally as young as 74 Ma, and (2) the arkosic petrofacies is everywhere structurally low in the WMB and below the Lake Chaplain thrust (Fig. 8). Dumitru and others (2016) note a pattern of detrital ages across the Cordillera:

“Upper Cretaceous sandstones from 17 localities from California to southeastern Alaska (United States) contain unexpectedly large populations of detrital zircons with Proterozoic U-Pb ages, with age peaks at 1800–1650 and 1380 Ma. These peaks are indicative of a sediment source region in the southern part of the Proterozoic Belt Supergroup basin in central Idaho, which hosts 1800–1650 Ma detrital zircons and which was intruded by rift-related 1380 Ma bimodal plutons and sills.”

Regional depositional ages for WMB arkosic samples (Table C1) support the contention of Dragovich and others (2014a), Sauer and others (2014) and Brown (2012) that the arkosic petrofacies contains detritus from the Idaho Batholith source area. The petrography, geochemistry, and detrital U-Pb ages for the WMB indicates an accretionary complex along a Jurassic island arc that in the later Cretaceous became sourced by craton detritus, including detritus from the Idaho Batholith area.

We suspect that the distribution of marble and quartz muscovite schist bodies demarcates a folded major accretionary surface or surfaces, such as a major thrust plane. (Also see unit KJmsw.) Both marble and quartz muscovite schist bodies: (1) have an exotic nature relative to nearby rock types; and (2) occur in apparent linear belts near mapped faults. Tabor (2002, p. 4) stated that, “in the [WMB], fossil ages are Late Jurassic and Early Cretaceous except for marble which is Permian and may be olistostromal” and also noted, (p.25) “the linearity of limestone outcrops east of Granite Falls” parallel to the regional structural grain. Marble bodies in the quadrangle are located at significant sites 15L, 17V, and 7F that broadly align with two other bodies northwest and southeast of these sites outside the quadrangle (Danner, 1966). This northwest-trending belt is coincident with the exotic schist bodies and broadly aligns with the Pilchuck fault zone (Pilchuck River faults nos. 1 and 2) in the Granite Falls quadrangle as shown on Figure 1. Quartz muscovite schist outcrops are found at significant sites 35K and 203Z along the Worthy Creek fault and Pilchuck River fault no. 2 and are interpreted as in-sheared tectonic bodies. These amphibolite-facies metachert bodies are completely recrystallized and contain a D2 crenulation that contrasts with the surrounding lower grade WMB metasedimentary rocks. Wiebe (1963, p.7) described a body of quartz mica phyllite along our informally named Pilchuck River fault no. 2 east of the map area and concludes that this is due to tectonic emplacement because of the “contrast in structure and

in metamorphic grade” relative to the nearby metasedimentary rocks. Most of these tectonic bodies occur adjacent to larger bodies of moderate-grade phyllite of the WMB, suggesting a genetic tie between the emplacement history of these bodies and the moderate- to high-grade rocks in the accretionary complex. This is illustrated on the cross sections where: (1) folded thrusts are inferred to separate moderate-grade phyllite from metasedimentary rocks at depth (both sections), and (2) quartz mica schist is inferred to be folded around the Chitwood Lake syncline and tectonically emplaced along the high-angle Worthy Creek fault. Although the contact with surrounding lower-grade metasedimentary rocks is poorly exposed, we conjecture that the marble and schist bodies are in-sheared along accretion surface(s), hinting at folded thrust structures.

Although much work remains, we suspect that an olistostromal origin of the marble—landsliding from an older carbonate-rich terrane into the lower accretionary prism—is unlikely given the current known age and structure of the WMB. Further work may show that (1) these marbles are tectonic bodies dispersed along an accretionary surface or surfaces such as a thrust or a similar type of obduction surface; and (2) thrusting are responsible for the tectonic emplacement of these Paleozoic marble and quartz mica schist bodies and other exotic fragments. We describe the WMB east of the GFFZ as a fairly thin mélangé or thrust zones between broadly folded, stratigraphically coherent WMB strata. Similar structural and compositional relations whereby “disrupted strata (broken formation) in which we can still see stratigraphically coherent, different units as well as well-developed block-in-matrix features making a transition to zones of slightly boudinaged beds” have been described in the Appennines and Appalachians, as well as in the Franciscan Complex of California and on Antarctica by Festa and others (2010, p. 1086 and references therein). They also document that:

“...true mélangé zones are restricted to (1) thin, elongated and coalescent fault zones, (2) large-scale thrust fault zones associated with fault thickening processes, and (3) plate boundaries with thick (~1,000–2,000 m) mélangé zones.”

Regional and Local Eocene Tectonics and Magmatism

TRANSTENSIONAL STRUCTURES—A HISTORY OF REGIONAL TRANSTENSION AND BASIN INVERSION

Early to middle Eocene regional transtension is well documented in western Washington by many studies including Heller and others (1987). They posit:

“non-marine basins that formed during this phase were caused by extension possibly associated with transcurrent faulting. Rapid sedimentation in both marine and nonmarine basins during this time consisted dominantly of sandstone derived from Cretaceous plutonic sources far to the east.”

These basins were commonly bounded by extensional or oblique slip faults. Haugerud and others (1994, p.18) indicate that:

“Mackin and Cary (1965) envisioned Basin and Range-like topography for the Cascade Range at this time. Uplift was possibly driven by transtensional forces of the Challis event. In the Oligocene much of the relief may have been eroded away, for sediments of the quartz-rich Wenatchee Formation suggest tectonic quiescence.”

Eocene extensional structures are also evident in the Granite Falls quadrangle. These include the Pilchuck River, Granite Falls, Carpenter Creek, and Iron Mountain fault zones. We also suspect the Bosworth Lake basin and, particularly, the Explorer Falls basin (EFB) developed as a result of this regional stress regime. Eocene magmatism (~43–50 Ma) in the Pilchuck River valley has resulted in widespread intrusion and localized extrusion across that area. This activity is also broadly synchronous with magmatism associated with the volcanic rocks of Mount Persis (Dragovich and others, 2013).

Regional and Proximal Examples of Extensional Eocene Faults Bounding Fluvial Basins

Structural and stratigraphic data, facies trends, and provenance relations indicate that several east-trending fluvial basins within western Washington were probably bounded by normal or oblique-normal faults during the Eocene. Regionally, syn-tectonic basin deposition is well established for the Chuckanut basin in Whatcom County, where the basin-bounding Boulder Creek fault was an active normal fault during deposition of the early Eocene Bellingham Bay Member (Johnson, 1982). Fluvial arkose of this member contains exotic detritus from the Omineca Belt of north-central Washington and little locally derived sediment. Later Eocene units had a more locally derived lithic-dominated provenance as a result of basin instability (Johnson, 1982; Evans and Ristow, 1994). The Boulder Creek fault east of Bellingham is now an active reverse fault in response to north–south compression (Kelsey and others, 2012; Siedlecki, 2008, Barnett and others, 2006). The Monroe fault to the south of the map area was also a basin-bounding normal fault during deposition of the Eocene volcanic rocks of Mount Persis (Fig. 1). The lower Skykomish River valley parallels this major reverse fault, which juxtaposes Eocene volcanic rocks against Jurassic–Cretaceous rocks of the WMB. As with the Boulder Creek fault, the Monroe fault was later rejuvenated by regional north-south compression as a reverse structure, and is still potentially active (Dragovich and others, 2011a,b, 2013, 2014b). Similarly, Johnson and others (1994) indicate that the Seattle fault switched from an extensional to compressional reverse fault in the late Eocene after the regional transtension episode documented by Heller and others (1987).

Local Examples of Nonmarine Basins in the Pilchuck River Valley

Early Eocene feldspathic fluvial sandstone deposits in the adjacent Lake Chaplain quadrangle contain only minor detritus from the WMB and have exotic plutonic provenance. These

sandstones contain monocrystalline quartz, K-spar, plagioclase, and some polycrystalline quartz, muscovite, and biotite; they were exposed as a result of westward tilting and erosion of the easternmost part of the EFB in the Lake Chaplain quadrangle. The sandstone deposits are compositionally mature and similar to the unnamed feldspathic sandstone of the Pilchuck River valley mapped directly east of the Granite Falls quadrangle by Tabor and others (2002)(Fig. 1) who describe (p. 28):

“...well-indurated fluviatile feldspathic sandstone and conglomerate with shaley beds and locally with leaf fossils are preserved in a down-faulted block along the south side of the Pilchuck River fault. We assume the sandstone and conglomerate are at least slightly older than the early middle Eocene rhyolite of Hanson Lake and probably were deposited at a much higher structural level than the Mount Pilchuck stock of the same age and the questionably older Bald Mountain pluton. Neither the sandstone and conglomerate nor the underlying mélangé south of the Pilchuck River Fault show thermal metamorphism common in rocks surrounding the Mount Pilchuck stock and Bald Mountain pluton northeast of the fault (Wiebe, 1963, p. 41). They may correlate with the oldest part of the early and middle Eocene Swauk Formation (about 50 Ma), exposed about 55 km to the southeast, or with the lowest part of the Chuckanut Formation exposed about 45 km to the northwest.”

We suggest these early Eocene sedimentary rocks represent the oldest part of a wide transtensional basin that existed between the Pilchuck River fault of Tabor and others (2002) and the Three Lakes Hill fault of Dragovich and others (2014a, 2015)(Fig. 1). The provenance for the Chuckanut and Swauk Formations is the distant Omenica structural complex of northeastern Washington (Johnson, 1982), indicating deposition before major local basin instability. The compositional maturity and lack of significant amounts of locally derived detritus in these early Eocene deposits suggest that local uplift and basin instability did not occur until the later Eocene or during deposition of unit Φ_{E_C} . The sandstone provenance of the younger unit Φ_{E_C} deposits, as documented by Dragovich and others (2015), suggests major basin instability across the EFB in the mid- to-late Eocene and probably reflects Eocene transtensional basin development documented regionally. Unit Φ_{E_C} lithic sandstones adjacent to the Three Lake fault near Lake Roesiger have a strong local WMB provenance probably as a result of extension across this fault. These relations are best explained by overall normal faulting and uplift along the EFB basin margin resulting in the shedding of abundant WMB detritus into the EFB. Provenance information generally advises that basin instability increased in the later part of the Eocene and early Oligocene as transtensional local block uplift.

The amount of WMB-derived metasedimentary rock fragments (60–80%) in the lithic sandstones is similar to the amount in lithic sands of unit Q_{Cphl} (70–95%), and this

population of grains is conspicuously absent from the Eocene feldspathic sandstone deposits along the axis of the EFB. This supports our hypothesis that extension and basin inversion is a reoccurring structural theme in the Tertiary and Quaternary for the Pilchuck River valley with renewed basin down-warping in the early- to mid-Pleistocene. We suspect that this cycle of basin development / inversion has been a persistent theme in western Washington.

Magmatism and Extensional Structures in the Pilchuck River Valley East of the Granite Falls Quadrangle

East of the map area, the Mount Pilchuck and Bald Mountain intrusions are S-type granitoids whose chemical and mineralogical similarities to one another have been previously recognized (Dungan, 1974, p. 31–34; Campbell, 1991, p. 59–66; Tabor and others, 2002). A new preliminary U-Pb single zircon age of 49.667 ± 0.068 Ma for the Mount Pilchuck stock (Michael Eddy, MIT, written commun., 2016) is similar to the 49 Ma K-Ar ages reported by Yeats and Engels (1971) and Tabor and others (2002). The Hansen Lake rhyolite, an S-type extrusive body containing garnet and cordierite, has been interpreted as an extrusive equivalent of these intrusive bodies by Tabor and others (2002) and Wiebe (1963, p. 20). Our new whole-rock analyses (Data Supplement) and Sr-Nd isotope data (Table E1) from Mount Pilchuck and Bald Mountain support the conjecture of Tabor and others (2002) that these plutonic bodies were derived from the same ‘old continental basement’ source. The elevated initial $^{87}\text{Sr}/^{86}\text{Sr}$ ratios (0.7065–0.7075) and peraluminous chemistry of these plutons are indicative of a metasedimentary source; the low ϵNd values (+0.70 to -0.42) yield late Proterozoic depleted mantle model ages (675–535 Ma). Model ages represent estimates of how long the elements in these rocks have been in the crust, not direct measurements of the age of the inferred metasedimentary source rocks, but it is noteworthy that these model ages are significantly older than those obtained for other units in the map area (90 – 430 Ma; Table E2).

Eocene intrusions in the Pilchuck River valley, including the Bald Mountain and Mount Pilchuck stocks, are epizonal to mesozonal plutons whose emplacement was largely to completely structurally controlled by bounding faults. Although mapping by Tabor and others (2002) suggests the Mount Pilchuck stock is not completely bounded by faults, Wiebe (1963, p.36) indicates that “it is probable that both phases [were] controlled by [the Pilchuck River] fault zone.” Tabor and others (2002, p.27) noted that:

“The Bald Mountain pluton is clearly truncated by the northwest-trending Pilchuck River fault. We think that the Mount Pilchuck stock cuts at least one strand of this fault, although Wiebe (1963, plate 1) shows the fault cutting the stock.”

Subsequent southwest-side-down normal and (or) oblique strike-slip movement along the Pilchuck River fault zone has exhumed these intrusions, juxtaposing them with their Hansen Lake extrusive equivalents, as well as with the extensional fluvial basin. Uplift of the WMB phyllite in the structural

block between Pilchuck River faults no. 1 and 2 in the quadrangle suggests that a cross-fault exists between these major faults east of the area and could explain the disparate uplift history between the Mount Pilchuck area and the Granite Falls quadrangle.

In conclusion, the Hansen Lake rhyolite and “S-type intrusives” east of the map area constitute a probable ~49 Ma comagmatic package that is slightly older than the ~44 Ma metaluminous Granite Falls stock (unit E_{igd}) and associated volcanic rocks that are discussed below. We view the latter, including exposures of the Hansen Lake rhyolite (unit E_{vr}) in the Granite Falls quadrangle, as a separate and slightly younger magmatic center within the broader Eocene (43–50 Ma) igneous complex preserved in the Pilchuck River valley.

Magmatism and Extensional Structures in the Granite Falls Quadrangle

Our new mapping, age information, and geochemistry suggest a co-magmatic history for the Granite Falls stock (unit E_{igd}) and associated MEG dikes (unit E_{ian}). Structural control of magma emplacement is evident around the Granite Falls stock in the northern part of the Granite Falls quadrangle, where a contact complex bordering the main granodiorite phase is dominated by dikes that intrude faults. This contact complex consists of intermediate to felsic aphanitic to porphyritic bodies and mafic to intermediate, medium-grained intrusive bodies that were largely syn-tectonically intruded along the structural contact with the WMB country rock. Published dates of ~44–45 Ma on the Granite Falls Stock (Yeats and Engels, 1971) are similar to our new ~43 Ma age for unit E_{vr} rhyolite and our ~44 Ma date on a unit E_{ian} dike (samples 15–26H and 15–40W#1 respectively, Appendix C) in the Iron Mountain fault zone. Cross cutting fault, dike, and pluton relations in and near the contact complex preserve a history of intrusion into transtensional dilation zone similar to a “pull-apart” common to strike-slip fault zones. Together with the observed field relations, these ages indicate syn-tectonic intrusion into a shallow crustal dilatational zone—a process we term the “pull-apart basin” intrusive model (Fig. 7). This model explains several observations including: (1) dikes that intrude along faults and are cut again by later faults; (2) contact complexes and dikes with conjugate ENE and NNW trends; (3) intrusion of granodiorite into the dike complex but also dikes cutting the main phase granodiorite body; and (4) whole-rock, geochemical, and isotopic information that indicates that the dikes, specifically those of the more enriched group (MEG) are comagmatic with the stock (See *Geochemistry* for further observations.)

Contact metamorphism (biotite zone) of some E_{ian} dikes surrounding the main stock suggests that the oldest dikes injected into early extensional structures were reheated by later dike and stock magmas. In our model, intrusive space was created either by dilation of individual faults or by a complex of faults that produced a rectangular dilation space for larger intrusive bodies (Fig. 7). Within the overall transtensional stress regime we envision normal strike slip faulting on the northwest trending faults and (oblique) normal faulting on the conjugate northeast trending faults. These pull-apart structures were conjugate to the Granite Falls fault zone whereby

the northeast-trending faults accommodate magma intrusion. This “pull-apart” basin model for intrusion is consistent with Eocene structural information documented locally and regionally for small to large fluvial basins, as well as some of the thick volcanic Eocene successions preserved in extensional regimes, such as the volcanic rocks of Mount Persis south of the Monroe fault (Fig. 1)(Dragovich and others, 2014b).

Our mapping, combined with new elemental and isotope data and U-Pb dates, shows that the Hansen Lake rhyolite (unit E_{vr}) exposed directly southwest of the stock—the Pilchuck Bend Formation of Danner (1957)—is comagmatic with the Granite Falls stock. This is illustrated in Cross Section A where unit E_{igd} bodies and unit E_{ian} dikes underlie and are the source for the extrusive rocks of the complex. Following Tabor and others (2002) we suspect that granodiorite masses intruded to the near surface and underlie much of the northern part of the map area. It also seems likely that unit E_{ian} dikes were feeders not only for the granodiorite but also for the surficial unit E_{vr}. The fact that the dike and stock intrusive bodies are syn-tectonic and fault bounded suggests that the intrusive plumbing system for unit E_{vr} is also structurally controlled by extensional structures below unit E_{vr}. This finding is consistent with a component of vertical offset along the Granite Falls fault zone and overall down-dropping of crustal blocks across this fault zone towards the Everett basin. (See *Everett Basin and Vertical Tectonics along the Granite Falls Fault Zone.*)

REGIONAL PLATE TECTONICS AND MAGMATISM

In the Granite Falls quadrangle, as throughout much of the Pacific Northwest, the early to middle Eocene was a time of compositionally diverse magmatism, extension, and crustal uplift. It is likely that the large-scale tectonic processes responsible for this activity on a regional scale were also responsible for much of the Eocene activity within the map area. The magmatism, extension, and basin formation that occurred from the Yukon to Montana between ~52 – 44 Ma is commonly referred to as the Challis Event. Several authors have attributed this activity to subduction of a spreading ridge, and the resulting formation of one or more slab windows beneath the Pacific Northwest (e.g., Haeussler and others, 2003; Madsen and others, 2006; McCrory and Wilson, 2013; Wells and others, 2014). This hypothesis is consistent with reconstructions of Eocene plate geometry that show one or more spreading ridges intersecting the Cascadia margin, and it explains several features of the Granite Falls and adjoining quadrangles, including: (1) compositionally diverse forearc magmatism that includes peraluminous rocks potentially derived from melting of accreted metasedimentary material, and (2) uplift in response to subduction of buoyant young oceanic lithosphere. Eddy and others (2015) indicate that, “Early Eocene near-trench magmatism on southern Vancouver Island and in western Washington includes peraluminous granites that represent melts derived from forearc metasedimentary rocks and dacitic rocks with adakitic geochemistry that may represent melts derived from subducted basalt or underplated mafic crust.”

Alternatively, the Challis Event has been attributed to rollback and breakoff of the Farallon slab in response to

the ~50 Ma accretion of the Siletzia Terrane (Tepper, 2016). Geologic phenomena associated with slab breakoff (or detachment) include: (1) a short-lived episode of magmatism occurring within a linear belt above the zone of rupture, and (2) crustal uplift in response to upwelling of hot asthenospheric mantle and (or) rebound after detachment of the deeper portion of the slab. Because these phenomena are very similar to those resulting from ridge subduction, it is difficult to unequivocally distinguish between the two tectonic models on the basis of geologic features within the map area. However, seismic imaging that reveals upper mantle features beneath the Pacific Northwest that are interpreted as detached fragments of the Farallon slab (Schmandt and Humphreys, 2011), and a magmatic age progression in eastern Washington that is consistent with slab rollback (Tepper, 2016) thus providing independent support for the slab breakoff model. Early Eocene igneous units in the Granite Falls quadrangle appear to be part of a 49- to 44-Ma magmatic belt that roughly parallels the eastern edge of the Siletzia terrane inferred in the subsurface (Trehu and others, 1994). The Granite Falls stock and related rocks including rhyolite extrusions are in the right location and of the appropriate age to be manifestations of Farallon slab breakoff similar to findings of MacDonald and others (2013) for the rocks of Mount Persis.

Fault Zones in the Study Area

REGIONAL FAULTS

Geologic mapping of the Granite Falls quadrangle continues our efforts to better understand fault zones locally and regionally, including the southern Whidbey Island (SWIF), Cherry Creek (CCFZ), Woods Creek (WCFZ), and Monroe fault zones and the Everett and Explorer Falls basins (EFB)(Fig. 1). Sherrod and others (2008) mapped the SWIF from Whidbey Island to the Maltby quadrangle west of the Lake Roesiger area. In a series of six geologic maps, Dragovich and others (2007, 2009a,c, 2010b, 2011a, 2012) traced the Rattlesnake Mountain fault zone and correlated it with the SWIF. All of these studies indicate that the SWIF is a strike-slip fault zone with several active or potentially active segments. Southeast of the present map area, the CCFZ is a locally active left-lateral, northeast-striking strike-slip fault zone (Fig. 1) that is likely a conjugate of the SWIF (Dragovich and others, 2011, 2012, 2013, 2014a). The northwest-striking, right-lateral WCFZ may be linked to the CCFZ southeast of the study area (Dragovich and others, 2015). Strands of the WCFZ and the Woods Lake fault merge with the Granite Falls fault zone, as discussed below.

Woods Creek Fault Zone

The Woods Creek fault zone (WCFZ) is a four-mile-wide series of northwest-striking sub-parallel strike-slip and oblique-slip faults in the Lake Roesiger quadrangle directly south of the map area. The Woods Lake fault is a strand of this fault zone that was originally mapped in the adjacent Lake Chaplain quadrangle on the basis of geomorphic lineaments, geophysical anomalies, and shallow seismicity; and was spatially correlated with a north–northwest-trending tectonic zone

(unit tz) observed at the surface and modeled in the subsurface (Dragovich and others, 2014a). Surface mapping and subsurface data, show that many strands of the WCFZ have an overall right-lateral-oblique sense of slip and that the fault zone as a whole accommodates west-side-down movement. Additional constraints from surface mapping, geophysics and subsurface data show a significant increase in the thickness of sedimentary rocks (unit OE_c) in the Everett basin directly west of the WCFZ. A component of vertical motion along the WCFZ fault strands is best exemplified by the dramatic increase in Tertiary sedimentary rocks directly west of the fault zone as evidenced by the abundant subsurface data in the westernmost part as well as directly west of the map area. This finding is supported by the geophysical information with the overall oblique sense of motion derived from other considerations including the kinematics of the fault strands observed in the field.

Granite Falls Fault Zone

We informally name the Granite Falls fault zone (GFFZ) for the strike-slip to oblique-slip fault zone mapped northwest of the Carpenter Creek fault and trending to the northwest corner of the map area. We separate this from the Woods Creek fault zone south of the Carpenter Creek fault but do connect some fault strands from the south into the GFFZ on the basis of field mapping and geophysical analyses. Overall, both zones can be considered part of a regional system that bounds the eastern part of the Everett basin. We speculate above that the GFFZ dissects a broad body of serpentinitized ultramafic rocks that may demark the lowermost portion of the Eastern mélangé belt (Cross Section A and B). Part of our rationale for informally naming the GFFZ as a separate entity from the WCFZ is our suspicion that some of the fault strands bounding the alpine ultramafic bodies in the GFFZ originated during Cretaceous accretion or that similar type structures north of the Carpenter Creek originated in the Eocene and continue to the present. Alpine ultramafic bodies are by definition exotic, fault bounded tectonic fragments of the mantle that nearly everywhere have a complex structure. In this instance the tectonic fragments were likely emplaced during Cretaceous thrusting of the exotic alpine ultramafic bodies over the supracrustal WMB metasedimentary and metavolcanic rocks and were later cut by the GFFZ.

Like the Woods Creek fault zone to the south, most kinematic indicators on fault strands of the GFFZ—such as en echelon veins, shallowly raking slickenlines on steep fractures and fault planes, and rare S-C mylonites in serpentinite—suggest right-lateral or dextral-oblique offset. Unlike the Woods Creek fault zone, the GFFZ contains widespread bodies of ultramafite. Adjacent to fault strands, bedding of the WMB has been locally transposed sub-parallel to the GFFZ fault strands (map sheet). We agree with Danner (1957, p.368), who indicated “Great slickensided surfaces are parallel to the [north-northwest] strike of the ridge and mostly horizontal indicating a predominant strike slip movement. The writer believes this may be a great altered fault zone.” We are similarly impressed by the amount of brittle strain observed in the GFFZ as indicated by the density and wide distribution of thick tectonic zones along northwest-trending and steep

fault strands. We semi-quantitatively estimate that the GFFZ contains ~35–60 percent modestly to strongly tectonized rock, including moderately fractured rock types to areas of intense cataclasis.

The formation of listwänite bodies (unit KJU_W) within the GFFZ may be largely the result of metasomatism of the ultramafic bodies by magmatic and (or) hydrothermal fluids related to Eocene intrusions along the GFFZ fault strands (Cross Sections A and B). Utilizing supporting geophysical anomalies associated with serpentinites [MA1] and structural evidence, we commonly map GFFZ fault strands near listwänite bodies because the metasomatic replacement process is strongly aided by circulation of fluids along structural discontinuities like faults. This is supported both by (1) the spatial association of listwänite bodies with serpentinite, and (2) the geometry of secondary faults and fractures within the tectonized listwänite bodies consistent with nearby mapped fault discontinuities. Hansen and others (2005, p. 228) wrote that:

“Our field mapping [in British Columbia] confirms the structural control of listwänite development along the basal décollement and along a transecting network of sets of steeply dipping joints and fractures. Although the joint and fracture systems served as the primary conduit for infiltration of CO₂-bearing fluid, pervasive carbonate alteration extends from a few centimeters to many tens of meters outward from the primary structural controls into intact bedrock.”

The GFFZ is thought to continue to the north-northwest where it may correlate with other right-lateral faults, such as the Mount Washington and McMurray fault zones in the McMurray quadrangle 20 miles northwest of Granite Falls, forming the eastern structural boundary of the Everett basin. The McMurray fault zone of Dragovich and DeOme (2006) follows the valley southeast of Lake McMurray and merges with the Darrington-Devils Mountain fault zone. (See *Everett Basin and Vertical Tectonics Along the Granite Falls Fault Zone* for further information.) Dragovich and DeOme (2006) further conjectured that the northwest-trending Lake McMurray fault is a major Cascade Mountains bounding fault that may extend considerably south of the Lake McMurray area, perhaps even as far as the Skykomish River where the structure may correlate with the (regionally defined) Lake Chaplain fault of Cheney (1987). The Lake Chaplain fault broadly aligns with the Woods Lake fault of Dragovich and others (2014a) and this study, but is oblique to other structures that we map and thus we have abandoned that fault name. However, even though we do not follow the “Lake Chaplain fault” terminology, we do concur with Cheney (1987) that an important regional fault or faults follow the structural boundary between the Everett basin and the Cascades as defined in this document and Dragovich and DeOme (2006).

We informally name the Boyd Lake fault for the easternmost fault strand in the GFFZ. This fault demarks the easternmost oblique-slip movement of the GFFZ, is truncated by the Carpenter Creek fault on the south, and continues north past the Wayside mine, where it is covered by Quaternary deposits.

This north-trending sub-vertical fault is coincident with several structural and stratigraphic changes in the WMB including: (1) the easternmost exposure of ultramafic rocks and listwänites (see the high BLG aeromagnetic gradient coincident with this fault zone on Figure 11); and (2) the change from strongly tectonized ultramafic, metavolcanic, and metasedimentary rocks in the GFFZ to largely stratigraphically coherent distal turbidites of the WMB. These turbidites are systematically folded by the Chitwood Lake and Worthy Creek synclines and the Worthy Creek anticline east of the Boyd Lake fault. These folded WMB metasedimentary rocks strike west-northwest to northwest in a slight angular discordance to the north-northwest-striking, steep Boyd Lake fault. This discordance is probably a result of fault drag of these folded structures by the overall dextral strike-slip GFFZ. As discussed with *Isostatic Gravity and Aeromagnetic Analyses*, the spatial correlation of the magnetic highs with the ultramafic rocks within the GFFZ and on the edge of the Everett basin is strong and distinct. (Also see *Everett Basin and Vertical Tectonics Along the Granite Falls Fault Zone*.) The termination of this aeromagnetic high and the easternmost occurrences of the causative ultramafic bodies by the Boyd Lake fault may be indicative of substantial vertical offset along this fault and the down-dropping of the thrust contact between the eastern and western mélange belts west of the fault. This model is stipulated upon the conjecture that the ultramafic bodies generally define the thrust between the mélange belts as illustrated in Figure 8.

Iron Mountain Fault Zone

We informally name the sub-vertical west-trending zone of widespread cataclastic shear mapped across most of Iron Mountain as the Iron Mountain fault zone. It is defined by a wide zone of mildly to strongly tectonized WMB metasedimentary strata with subvertical to steeply northerly dipping bedded surfaces that are transposed sub-parallel to the steeply dipping faults. The fault zone is exceptionally well-exposed in the large Iron Mountain quarry. The fault zone is >650 m thick and exposes sections containing numerous sub-vertical meter- to several meter-thick cataclastic zones that are locally more than 100 m thick. The broad fault zone is intruded by several Eocene dikes and displays sub-vertical zones of mild to intense hydrothermal alteration that is genetically related to the igneous intrusions. Sub-vertical alteration zones 20 m thick pervade the quarry and in some parts constitute 20 percent of the exposed rock mass. We interpret the pervasive Iron Mountain alteration as generally Eocene in age and related to the intermediate to felsic intrusions driving hydrothermal cells in the fault zone. Records from two historical mine operations near the town of Granite Falls give insights to subsurface geology of the Iron Mountain fault zone consistent with structural observations. In a 1928 report on the Wayside mine (significant site WM), Hancock interpreted ore formation as granodiorite-intruded metasedimentary country rock and indicated that pyrite, chalcopyrite, and bornite secondary mineralization formed “along sheared zones which traverse the granodiorite rocks, the strike of these rocks being northeast and southwest with a nearly vertical dip.” Sauers (1974) indicated two populations of ore-bearing veins, one that strikes

northeast-southwest and another striking east–west. Sauers (1967) mapped a NNW-trending ‘silica-carbonate dike’ cross cutting the NE-SW structural fabric near the Wayside mine. This study interprets that finding as a fault-bounded body of unit KJ_{UW1}. Kaiser (1934) also described an E–W striking shear zone in the Yankee Boy mine (significant site YBM) and indicated a steep dip to the north. Both mines are now abandoned and inaccessible, but good exposure of the Iron Mountain fault zone and related alteration zones are found in the active and expansive Iron Mountain Quarry.

The Iron Mountain fault zone is interpreted to be an Eocene oblique-slip normal fault zone bounding a complex of extensional structures along the easternmost part of the GFFZ. This “pull-apart basin” model of formation is supported by the extensive diking and related alteration zones that pervade this steep, east-west trending fault zone. Steep faults and cataclastic zones are intruded by several sub-vertical rhyolites to dacite porphyritic dikes that are typically 2 to 4 meters thick (Fig. 6). We obtained a single zircon age of ~44 Ma from the plagioclase porphyry dacite/rhyolite at age site 15–40W#1. This dike is an offshoot of the Granite Falls stock intrusive complex and likely dates Eocene transtension across this northeast-trending fault zone. The width and intensity of fault deformation in this fault zone indicate that this is a major fault, probably of significant lateral extent. We suspect that this fault zone is part of a family of poorly exposed extensional faults that generally follow the northeasterly Canyon Creek and North Fork Stillaguamish ‘structural trend’ in the northeastern part of the map area. (See *Isostatic Gravity and Aeromagnetic Analyses*).

Worthy Creek Fault

The Worthy Creek fault is a major northwest-trending oblique-slip fault. This discrete fault zone follows thin to wide tectonic zones (unit tz) and merges to the west with the Boyd Lake fault, the easternmost part of the broad GFFZ. The fault follows Worthy Creek and appears to continue to the east of the map area along a strong lineament and overall parallels the Pilchuck River faults, as well as the Chitwood Lake and Worthy Creek synclines. These major structures fold well-stratified metasedimentary and metavolcanic rocks of the WMB in panels adjacent to the fault. A sub-vertical fault is indicated by the general straight fault trace and kinematics of the unit tz exposures around the fault. As shown on Cross Section B, an exotic tectonic body of quartz mica schist exposed along the Worthy Creek fault (significant site 35K) may reside on a folded thrust that is transposed into the steep Worthy Creek fault. Although a conjecture, we suspect this tectonic body is an emergent fault sliver formed by folding of a buried thrust. (See *Thrusting, High-Grade Metamorphic Rocks and Tectonic Bodies*.)

Eocene to Plio-Pleistocene Tectonics

STRUCTURALLY CONTROLLED BASINS AND VALLEYS—EOCENE STRUCTURAL CONTROL OF NEOTECTONIC STRUCTURES

The strong structural control on Pleistocene nonglacial depocenters documented here adds to a growing list of structurally controlled river valleys and other basins in the area, including

those of the Snoqualmie River (SWIF and Rattlesnake Mountain fault zone) and Skykomish River (Monroe fault and folds). We speculate that the bounding faults of the EFB may be part of an intersecting set of Tertiary normal faults (along with the Carpenter Creek fault), but further study is warranted (Fig. 1). We suggest that the Bosworth Lake basin is a structurally controlled depocenter that merges to the west with the much larger Everett basin (Fig. 1). Above we presented our “pull-apart” basin model for emplacement of Eocene intrusive rocks within the GFFZ—this northeast-trending basin formation was established in the Eocene and appears to be a precursor to Pleistocene basin formation. A recurring mapping theme for the Snoqualmie-Skykomish and Pilchuck River areas is that transtensional development of fault zones and basins in the early to middle Eocene produced the basic structural architecture for many of the potentially active to active structures mapped in the area. The general lack of Oligocene to Pliocene igneous or sedimentary rocks or deposits in the region mostly precludes investigations into the prospect of structural activity during that timeframe. Our mapping may indicate that these northeast-trending Tertiary basins are locally rejuvenated in the Pleistocene depocenters that preserve locally thick fluvial sediment sequences.

Explorer Falls Basin

The Explorer Falls basin (EFB) is a fault-bound graben that preserves Tertiary sedimentary rocks (unit Φ_{Ec}) and a thick succession of Pleistocene nonglacial strata (Dragovich and others, 2014a, 2015). The EFB was initially mapped in the northwestern part of the Lake Chaplain quadrangle and then westward into the Lake Roesiger quadrangle, where it merges stratigraphically with the Everett basin (Fig. 1). As discussed further below, the EFB likely originated as an Eocene (~45–50 Ma) extensional structure; later north-south compression resulted in inversion of Tertiary to Pleistocene basin fill consistent with the complex basin-margin fault kinematics we have described, and the general lack of imprint on the gravity data in the region. The EFB is at least 8 km wide and 16 km long and is bound by the Carpenter Creek fault on the north and the Three Lakes Hill fault on the south. This study confirms the tentative results of Dragovich and others (2014a, 2015) and finds that: (1) deposits with a Cascade Range provenance (unit Q_{Cph}) are confined to the basin axis and form a thick sequence of Pleistocene alluvium, (2) alluvial deposits with a local provenance (unit Q_{Cphl}) are found in a mappable band along the east-northeast-striking basin-bounding faults, (3) basin deposits are tilted or folded—and locally uplifted—to form an inverted basin, and (4) Tertiary strata of unit Φ_{Ec} are preserved in the EFB and locally form the basement for Pleistocene deposits. As shown in Figure 4, we envision a precursor to the Pilchuck River flowing westward from the Cascade Range during the Pleistocene. Deposits of this river system interfingered with alluvial fans shed across active basin margin faults. Deformation of the basin after deposition of the Pleistocene basin fill locally tilted, uplifted, and warped these deposits.

Unconsolidated deposits in the EFB were previously correlated by Dragovich and others (2014a, 2015) with a

pre-Hamm Creek interglacial interval due to the weathering characteristics and several IRSL ages that indicated an early to middle Pleistocene age (>370–540 ka; Dragovich and others, 2015). We use composition, sedimentology, geochemistry, stratigraphic architecture, age, and detrital zircon ages to show that the nonglacial alluvium preserved in the EFB is a Pleistocene deposit of the ancient Pilchuck River. We use the term Pilchuck River provenance (PP; Table 1) to refer to sediment derived from the Cascade Range that are broadly similar to sediment of the modern and ancient Skykomish River (Table 1). See Dragovich and others (2015) for a comparison of PP with Skykomish River provenance (SP), as well as for information about thickness and detrital ages for EFB Pleistocene sediments. We use the term local provenance (LP; Table 1) to refer to locally derived Pleistocene alluvium (unit QC_{ph}). As compared to its distribution in the Lake Chaplain and Lake Roesiger quadrangles, unit QC_{ph} is exposed as a discontinuous band directly south of the Carpenter Creek fault. We ascribed spotty outcropping of these Pleistocene alluvial fan deposits to (1) burial by younger glacial deposits, and (2) erosion due to uplift along the Pilchuck River anticline growth fold as schematically illustrated on Figure 3. The geographic distribution of the basin-margin alluvial fan deposits (unit QC_{ph}) provides compelling evidence for the extent of this Pleistocene basin (Fig. 4). LP sediments—with ~50–90 percent WMB metasedimentary clasts—are mapped as broad bands along the Carpenter Creek fault on the north in the Granite Falls quadrangle and the Three Lakes Hill fault on the south in the Lake Roesiger and Lake Chaplain quadrangles. These sediments interfinger basinward with unit QC_{ph} in several places (this study; Dragovich and others, 2014a, 2015). Although the active basin-bounding faults were likely transtensional in the early to mid-Pleistocene, we now suspect that many segments of the Carpenter Creek fault have been rejuvenated as reverse faults due to active north-south contraction as indicated by (1) folded Pleistocene sediments across the Pilchuck River anticline, and (2) some earthquake hypocenters and focal mechanisms. (See *Carpenter Creek Fault Zone* below.)

Carpenter Creek Fault Zone

The Carpenter Creek fault (CCF) of Dragovich and others (2015) parallels an east-northeast-trending geomorphic lineament along the Pilchuck River and Carpenter Creek within the Granite Falls and Verlot quadrangles and probably intersects the extension of the Worthy Creek fault east of the map area. The CCF also aligns with prominent tectonic zones (unit tz) and a distinct magnetic gradient (CCF in Fig. 11), which help suggest a major fault. These west-trending anomalies and lineaments are coincident with a striking change in structural level for the WMB basement across this fault. A potentially active to active fault zone is supported by: (1) the Pilchuck River anticline, a tentatively proposed growth fold structure that parallels the CCF, and (2) the Carpenter Creek earthquake cluster, respectively.

Several compositional, stratigraphic, geophysical and structural changes across the CCF lineament support our mapping of a major fault. South of the CCF, PP sediments of the Hamm Creek and pre-Hamm Creek nonglacial units define the



Figure 13. Slickenlines on a steeply-dipping fault exposed in the rock quarry directly north of the Carpenter Creek fault (CCF) at significant site 9M where cataclastically deformed Western mélange belt greenstone (unit tz) is exceptionally well exposed. The east-northeast strike of the fault and steep plunge of the slickenlines illustrated here are generally consistent with the CCF as a high-angle, oblique-slip fault zone with both reverse and normal movement. This brittle deformation has tectonically intercalated metavolcanic and metasedimentary rocks within the WMB. In the northern part of this large quarry, unit tz grades into less disrupted WMB away from the CCF.

northernmost part of the EFB fill (Fig. 3). Significantly, unit QC_{ph} contains minor but conspicuous serpentinite grains (to ~10%); this is relevant because it more strongly ties the source of this locally derived sediment to unit KJU_w that is only exposed north of the CCF. Substantial vertical motion of the CCF is consistent with the juxtaposition of different structural levels for the WMB across the CCF, including the exposure of the Lake Chaplain nappe in the southeastern corner of the map area only south of the fault. “Tectonite” is also observed locally along the fault. A rock quarry at significant site 9M reveals extensively tectonized WMB greenstone directly north of the Pilchuck River. This greenstone has steeply plunging slickenlines on steeply dipping west- to west-southwest-striking faults and fractures correlated with the CCF in this quarry (Fig. 13). This deformation is generally sub-parallel to the east-west orientation of the strong, linear aeromagnetic gradient that aligns with the CCF subsidiary tectonic zone exposures found in this large quarry. (See *Isostatic Gravity and Aeromagnetic Analyses* for further information.) Also, several east-northeast-trending andesite dikes (unit E_{ian}) along the Pilchuck River (Figs. 5 and 6) likely reflect Eocene extension during the initiation of the EFB. These hypocrySTALLINE dikes are 0.5–2 m thick and dip steeply and cross cut the cleavage in WMB metasedimentary country rock. Pilchuck River dikes are post-metamorphic and probably originated from the same ~44 Ma magmatism as dikes farther north in the quadrangle (see Age Site 15–40W#1, Appendix C). Further work on these dikes may help document Eocene extension across this basin-bounding fault.

The Carpenter Creek earthquake cluster forms a band of seismicity south of the CCF in the southernmost part of the Granite Falls quadrangle and the northernmost part of the Lake Roesiger quadrangles, as well as in the Verlot quadrangle (this study, Dragovich and others, 2015). This cluster of hypocenters

includes a significant number of reverse focal mechanisms, consistent with a currently active reverse fault (Appendix B and Fig. B1). Of the 35 earthquakes that have focal mechanisms in the cluster, 15 earthquakes give general reverse mechanisms and five quakes give left-lateral strike-slip mechanisms if a west-striking preferred fault plane is chosen (Fig. B1). The dominance of reverse or “thrust” focal mechanisms relative to normal and strike-slip fault types in the Carpenter Creek earthquake cluster is clearly illustrated on the focal mechanism ternary diagram (Fig. B2) provided in Appendix B. We include the July 1, 2016 moderate earthquake ($M=3.4$) and temporally related aftershocks in the Carpenter Creek earthquake cluster because all instrumental historical data show the CCF area has a cluster of earthquakes forming a “swarm”. However, the 35 recent earthquakes generally northeast of Lake Roesiger are likely a main-shock and aftershock sequence in a portion of the cluster. We suspect that (1) the variation in the earthquake types (for example, the normal fault focal mechanisms) within the CCF zone is due to seismogenic fault locking along some fault strands within the larger fault zone; and (2) the microseismicity is the result of smaller strains associated with parts of the stress field not relieved by the larger events. In this model past offset along portions of the CCF main strand has seismically loaded other structures that are kinematically tied to the fault zone such as antithetic faults and folds leading to variable offset mechanisms.

We map the CCF as an oblique-slip reverse fault with a component of left-lateral strike separation on the basis of map information and focal mechanisms, combined with some of the fault, fracture, and slickenline data (Fig. 13). Additionally, as noted by Dragovich and others (2015), the location of the earthquake cluster south of the mapped fault is consistent with a southerly dip for the CCF (Fig. 3). As inferred by Dragovich and others (2015) in the Lake Roesiger area, some of the low-level seismic activity we associate with the CCF could be related to antithetic motion on the northwest-trending structures. In a few places, some of the left-lateral, west-trending preferred solutions could be right-lateral north-south fault motions on the cross-cutting faults; and therefore correlation of earthquakes near the intersection of these intersecting structures with individual fault strands requires further information (see *Woods Creek Fault Zone* below).

Except in the Bosworth Lake basin, ancient PP alluvium occurs only south of the CCF consistent with the model of a Pleistocene fluvial basin, in the southeastern part of the map area. Our new mapping and geochronology in this area, however, reveals a possible growth fold that we informally name the Pilchuck River anticline along the northernmost part of the EFB. Mapping and IRSL ages suggest that the northernmost portion of the EFB contains PP sediments of the Whidbey Formation and Hamm Creek nonglacial unit (as well as LP of the Hamm Creek unit) that are preserved along the northern limb of the Pilchuck River anticline. As schematically represented in Figure 3, growth folding is tentatively indicated by the stratigraphic younging of this PP alluvium (Table 1) representing three nonglacial or interglacial intervals (during pre-Hamm Creek, Hamm Creek, and the Whidbey Formation) toward the CCF. This younging occurs as northerly tilted

Pleistocene nonglacial alluvium descends in elevation to the Pilchuck River suggesting systematic tilting of ancient Pilchuck alluvium as the anticline compressed above the active CCF.

We interpret the structural and stratigraphic relations to indicate an anticline in which Whidbey, Hamm Creek, and pre-Hamm Creek fluvial sediments inset against each other along its northern limb. Our tentative growth fold model is inferred from three major lines of evidence: (1) the IRSL ages across the fold, (2) elevation of the formations across the anticline, and (3) overall folded geometry of the PP sediments across the anticline. IRSL ages include: (1) elevated Q_{Cph} dated at >370 ka directly south of the anticline axis in the southernmost part of the quadrangle; (2) younger inset Q_{Ch} at 490 to 616 feet elevation along the northern limb of the anticline and dated as 237 and 263 ka; and (3) younger Q_{Cw} Whidbey Formation sediments dated at 117 ka near the Pilchuck River at about 520 ft elevation. Important in this interpretation is the overall decrease in nonglacial strata IRSL ages with elevation towards the modern Pilchuck River. We interpret the available information to indicate that the Pilchuck River was pinned along the northernmost part of the EFB between the compressional CCF and the growing Pilchuck anticline during the late Pleistocene (after ~ 190 – 300 ka). This folding suggests the CCF has been a compressional reverse or reverse oblique slip structure since deposition of Hamm Creek unit PP alluvium in the Late Pleistocene (~ 190 – 300 ka; Appendix A).

The general orientation of the cleavage and bedding planes in the WMB basement and overlying PP nonglacial deposits generally fit the anticlinal axis. Bedding orientations in the Explorer Falls basin Quaternary sedimentary fill (units Q_{Cph} , Q_{Cphl} , Q_{Ch} , and Q_{Chl}) also generally fit the fold geometry, but some anomalies were also observed. This is likely partially due to weathering, which results in creeping or general mass-wasting of these ancient overbank fluvial sediments on moderately steep to steep slopes. Although the growth fold model explains the current geochronologic and structural information, further work is needed to test the Pilchuck Valley anticline growth fold hypothesis. Some of the additional information needed includes (1) more geochronologic constraints across the anticline including testing the proposed “younging” direction across the northern limb of the fold, and (2) more structural data is needed to fully test our growth fold hypothesis. Also, further work is needed to elucidate the relationship between the Woods Creek fault zone and the CCF. Geophysical data combined with map relations suggest that some strands of the Woods Creek fault zone offset the CCF producing fault-bounded crustal blocks across a dissected basin, particularly in the southwestern part of the map area.

Bosworth Lake Basin

The informally named Bosworth Lake basin (BLB) is a deep, northeast-trending Pleistocene basin west of the Granite Falls fault zone east and west of Bosworth Lake. The BLB was discovered using a combination of surface and subsurface mapping supported by geophysical analyses and numerous water well logs across the basin. Subsurface records indicate the basin contains a very thick sequence of nonglacial alluvium (units Q_{Cph} and Q_{Ch}) deposited during the Hamm Creek

and pre-Hamm Creek interglacial intervals. The weathered fluvial PP sand and silt is very similar to sediments in the Explorer Falls basin (EFB) in that there is a distinct mélange belt and granitic Cascade provenance (Table 1); it has abundant monocrystalline quartz, plagioclase, and mica with lesser mélange belt-derived metasedimentary and granitic clasts and hornblende. Detrital mica (to 30%) is likely derived from foliate mélange belt metasedimentary rocks and higher grade phyllite as well as from Tertiary granitic rocks. Several sand petrography samples contain a trace of tourmaline we suspect is derived from Pleistocene erosion of the Eocene contact complex rocks intruding the Granite Falls fault zone east or northeast of the basin. Multiple moderately deep to deep wells (>400 ft) penetrate the BLB. From ~230 wells in the basin area, we selected 32 wells that are both accurately located and whose logs contain detailed stratigraphic information. These wells consistently record thick sediment dominated by well-stratified, medium-bedded to laminated sand, silt, and clay with rare gravel interbeds interpreted primarily as overbank fluvial deposits. Most well records (and observed outcrops) report peat, logs, sticks, fossil plants or other organic material at multiple stratigraphic levels, confirming their nonglacial origin. Many of these wells are represented on Cross Section B, which follows the BLB axis.

Our geochronology (Appendix A) indicates that the exposed strata in the BLB are correlative with the Hamm Creek interglacial deposits (~170–218 ka). Water-well lithologic logs (for example: W777, W203, and W197) and available depth to rock information suggest ~210 ft of Quaternary basin fill sediment near Bosworth Lake that deepens to at least ~400–500 ft elsewhere in the basin (map sheet). A strong, low gravity anomaly (BLB in Fig. 11) clearly indicates the presence of the thickest sediment within the quadrangle and therefore we posit that there may be still older nonglacial deposits lower in the basin; thus we infer Q_{Cph} below Hamm Creek nonglacial deposits (unit Q_{Ch}) mapped at the surface. Although we suspect that the BLB is a composite basin containing both Hamm Creek and pre-Hamm Creek nonglacial deposits (Cross Section B), the basin could be simply the result of Hamm Creek deposition in a subsiding late Pleistocene basin. The basin boundaries mapped as queried extensional faults were identified on the basis of the gravity and well/geotechnical boring information that suggest shallower bedrock directly north and south of the BLB. We speculate here that the Eocene Hansen Lake rhyolite (unit E_{vr}) exposed north of the BLB may suggest uplift of this bedrock block directly west of the GFFZ and north of the BLB where the younger fluvial and marine Tertiary rocks (units O_{Ec} and O_{En}) have been eroded possibly as a result of episodic emergence of this block. Alternatively, unit E_{vr} formed a persistent paleotopographic high that remained emergent over time, causing later Tertiary and Quaternary deposition to wrap around this volcanic highland.

The relation between the EFB and the BLB is poorly understood. The EFB is likely a rejuvenated Eocene fluvial basin; further study may indicate the BLB is also. The distribution of units Q_{Cph} and Q_{Cphl} indicate that these two basins may merge west of Woods Creek fault no. 3 in the southwestern corner of the Granite Falls quadrangle or along

the easternmost part of the Everett basin as discussed below. Finally, more work is needed to determine the temporal and spatial relationship between deposition of unit Q_{Ch} PP sediments in both the Bosworth Lake and Explorer Falls basins during the Late Pleistocene and if the alluviation switched due to local basin inversion, folding or other forces that generally pushed the ancient and modern Pilchuck River in a northwesterly direction during the Quaternary.

NORTHEAST-TRENDING PLEISTOCENE TRANSTENSIONAL BASINS—POSSIBLE REGIONAL TECTONIC IMPLICATIONS

Structural and stratigraphic relationships across the EFB, as well as the general nature of the seismicity on the Carpenter Creek fault, may indicate a switch from transtension to transpression after deposition of the Hamm Creek nonglacial interval. In summary, there was a ‘tectonic switch’ from transtension to transpression across the EFB in the late Pleistocene at ~190–300 ka. This tectonic control poses an enigma: northeast-trending Pleistocene extensional basins across the map area are inconsistent with the current north-south compression documented for example, by Wells and others (1998); they are more consistent with northeast-directed maximum compressional strain and (or) oblique subduction of the Juan De Fuca plate. In other words, the EFB implies a period of generally NNW–SSE directed extension across the basin whereas the current seismicity, structure and regional tectonics suggest generally north-south directed compression across the EFB generally and the bounding CCF in particular.

As a possible solution to the ‘tectonic enigma’, we speculate that changing stress fields rejuvenated ENE- or NE-striking basin-bounding faults as extensional structures to contractional structures to account for inversion of the EFB and the nature of the current seismicity which implies the CCF bounding the northern part of the basin is an overall reverse fault. This inferred ‘tectonic switch’ between subduction-parallel and north-south-dominant compressional vectors may be controlled by unrecognized, long-term tectonic switches that control the degree of compression delivered to the forearc as a result of oblique subduction. Miller and others (2001, p.172) indicated that:

“Both impingement of the Sierra Nevada block and oblique subduction have been invoked as processes that drive Oregon forearc migration [Wang 1996; Wells and others, 1998]. The kinematics, taken with the geometry of the subduction zone, invite speculation. Vancouver Island, which is part of Wrangellia, arguably forms a more rigid backstop against which the inland penetration of a Pacific transform component terminates. In this view, the Oregon and Washington forearc migrates in front of the impinging Sierra Nevada block. The northern margin of the migrating forearc also coincides with the limit of oblique subduction, however, implying a different origin. The bight in the continent margin results in nearly orthogonal convergence along Vancouver

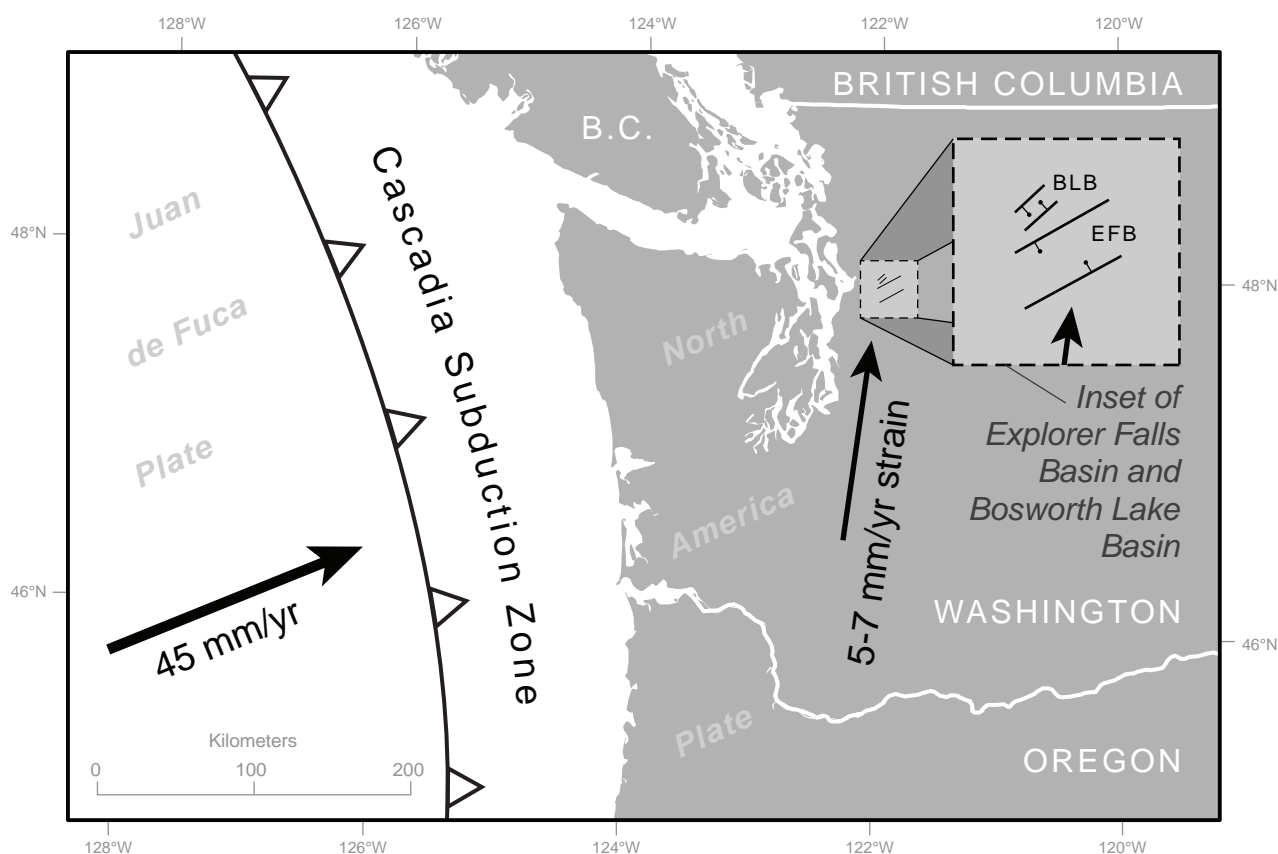


Figure 14. Regional neotectonic context of the Granite Falls Quadrangle. Bounding faults of the Explorer Falls Basin (EFB) and the Bosworth Lake Basin (BLB) are shown. North-south strain vectors are adapted from Magee and Zoback (1992) and Werner and others (1991). Tectonic vector for subduction of the Juan De Fuca plate is taken from Wang (2000). We conjecture that the extensional development of the EFB in the Early to Middle Pleistocene may be due to compression related to subduction of the Juan De Fuca plate due to “tectonic switching” from north-south compression. As the figure illustrates, the east-northeast extensional faults for the basin are not generally consistent with a north-south maximum compression vector thus raising the question, “can northeast directed strain related to the Juan De Fuca plate periodically cycle with north-south compression as the primary strain direction in the Cascadia forearc?”

Island, where forearc migration is absent, and moderately oblique convergence farther south, where forearc migration is relatively rapid. This implies that oblique subduction [of the Juan De Fuca plate] drives forearc migration.”

In the oblique subduction model, the northwest-trending transpressional deformational response to oblique subduction is accompanied by northeast-trending extensional structures similar to the tectonic regime of the Eocene. Overall, north-northeast-directed extension indicates a switch from N–S compression to perhaps more NE–SW compression, consistent with the basin orientations—and more consistent with compression generally related to subduction as shown in Figure 14. In summary, the NE-trending basin-bounding faults are most consistent with the Juan de Fuca plate subduction vector in the early Pleistocene or during deposition of the Explorer Falls basin fill. A later transition to N–S “margin parallel” compression resulted in rejuvenation of the bounding faults as reverse structures; this compression also results in growth folding and the inversion of basin fill.

Lewis (2003, p.185) wrote:

“Although we find seismogenic evidence for active north-directed shortening across much

of the Washington Cascadia margin, it is noteworthy that a variety of geologic data have been interpreted to reflect Cenozoic northeast directed shortening in the Olympic Range. In particular, analyses of rock fabrics and fission tracks suggest that the exhumation history of the Olympic Range is best explained by northeast directed underthrusting along the Cascadia subduction zone (Brandon and others, 1998, and references therein). The fact that many geologic observations from the Olympic Peninsula have not been explained by north-south shortening highlights both the complexity of the region and the importance of exploring the relation between the rock record and ongoing deformation.”

We speculate that ‘tectonic switching’ might be a factor in some structural domains of the Washington forearc. However, a few (of many) questions raised by our “tectonic switching hypothesis” include:

- Does the weakness of the subduction zone thrust fault (Wang, 2000) preclude inland shallow crustal deformation solely due to plate subduction?

- Could this weakness actually tectonically cycle as a result of a change in stress/strain relations related to subduction zone seismic cycles?
- Could stress-strain relations in the subducting Juan de Fuca slab and adjacent forearc cycle lead to increased subduction-related strain in the forearc region over the longer time frames (~0.2–1.0+ m.y.)?
- Could the hypothesized switch in compression directions have occurred at other times besides Eocene regional transtension (related to slab breakoff) and Pleistocene extension (possibly related to subduction as the primary compression vector)?
- Could the hypothesized switch in compression be related to smaller stress domains related to tectonic block rotations in the forearc, or is it generally related to transpression/transension northeast of the southern Whidbey Island fault zone?
- We tentatively relate the observed rejuvenated structures to regional tectonics but acknowledge that further work is necessary to determine the ultimate causes of the multi-faceted slip history on faults in the Granite Falls region. Whether ‘tectonic switching’ or continual reorganization of smaller stress domains in the forearc as deformation progresses are responsible for the complex fault history we observe requires further information including careful study of the uplift and subsidence history of the area. This information can be used to test models and investigate the questions we forwarded above.

EVERETT BASIN AND VERTICAL TECTONICS ALONG THE GRANITE FALLS FAULT ZONE

The Everett basin is a regional geophysical and stratigraphic feature composed of a thick sequence of Tertiary to Quaternary rocks and sediments that lie north of the Southern Whidbey Island fault zone (Fig. 1) and south of the Darrington-Devils Mountain fault zone (DDMFZ; Johnson and others, 1996). Structural control of the basin by the Woods Creek fault zone directly to the south in the Lake Roesiger quadrangle was documented by Dragovich and others (2015). In that area, substantial vertical offset (>600 m) is documented across some northwest-trending fault strands using surface mapping, geophysics and subsurface data including oil and gas wells logs. This study further documents that the easternmost part of the Everett basin is structurally controlled by oblique- to strike-slip fault zones, including the Granite Falls fault zone (GFFZ) along its easternmost boundary. We correlate the GFFZ with the Lake McMurray fault of Dragovich and DeOme (2006) on-strike with the GFFZ northwest of the map area (Fig. 1). The Lake McMurray fault merges with the DDMFZ, and together these faults bound the eastern and northern parts of the Everett basin. The southern part of that basin is structurally controlled by the southern Whidbey Island fault zone (SWIF; Sherrod and others, 2008). The GFFZ and other high-angle fault zones (for example, the Cherry Creek fault zone) appear to have aided exhumation of the Cascades; uplift of the Cascades across individual fault zone strands is documented

across steep northwest- to northeast-trending fault zones with an overall up-to-the-east sense of offset (Dragovich and others, 2013, 2014a, 2015).

Down-dropping of the ultramafic rocks along the easternmost part of the Everett basin (Cross Sections A and B) is consistent with other structural changes across the GFFZ, which include: (1) thickness and depositional facies trends for the rocks of Bulson Creek, (2) juxtaposition of different crustal levels of the Eocene intrusive and extrusive rocks, and (3) initiation of the Bosworth Lake basin along the easternmost edge of the Everett basin. Cross Section B best illustrates the vertical tectonics of the GFFZ, where the WMB basement is against thick Tertiary and Quaternary basin fill along the axis of the Bosworth Lake basin. This pattern is consistent with oblique-slip offset of the GFFZ and support the model that the easternmost part of the Everett basin is structurally controlled.

Tertiary Sedimentary and Igneous Rocks— Facies Changes and Vertical Tectonics

The thickness and depositional facies trends for the rocks of Bulson Creek change across the GFFZ to the west and into the Everett basin are related to vertical tectonics across the GFFZ. First, no rocks of Bulson Creek unconformably overlie the mélangé belt basement east of the GFFZ in the map area. Within the GFFZ the fluvial facies conglomerates and sandstones (unit Φ_{Ec}) vary from 1- to 2-m-thick deposits forming isolated erosional remnants in the eastern GFFZ to several-meter-thick bodies locally in the western part of the GFFZ. This thickness change probably reflects both uplift and erosion but perhaps also a Tertiary structural control to fluvial, deltaic and marine deposition. Directly east of the GFFZ and below the westernmost edge of the quadrangle, unit Φ_{En} significantly thickens and interfingers with the unit Φ_{En} marine facies. This thickness change is best illustrated on Cross Section B that shows how rocks of Bulson Creek change from isolated, meters-thick bodies in the GFFZ to very thick strata along the easternmost part of the Everett basin west of the GFFZ. This is best documented in the northwestern part of the map area where subsurface data documents siltstone and sandstone with interbedded coal and pumice under Quaternary sediments that are at least 45 m thick south of the South Fork Stillaguamish and perhaps more than ~100 m thick north of the river. The rocks of Bulson Creek thicken into the Everett basin and are likely faulted against the Western mélangé belt across western strands of the GFFZ. Danner (1957, p. 497) noted that:

“The outcrop of the Riverside formation appears to mark the eastern edge of a structural basin. All along the east side of the Stillaguamish River the dip steepens markedly as the 1,000-ft scarp of Mesozoic Sultan Unit [Western mélangé belt] rocks forming the western edge of the Jordan Uplands is approached. West of the river the dip is seldom more than 20°, dips as high as 75° were measured east of the river. A fault may be present but no definite evidence of it was found.”

Whetten and others (1988) followed this interpretation and mapped two NW-trending faults that project into the Granite Falls quadrangle.

As noted above the ~44 Ma Granite Falls stock and related intrusive bodies are the source for the nearby ~43 Ma rhyolitic to andesitic extrusive rocks exposed along the easternmost part of the Everett basin. (See units *Evr*, *Eian* and *Eigd* on Cross Section A.) Significant vertical or oblique-slip offset along strands of the GFFZ is indicated by these relations: supracrustal volcanic rocks are placed near intrusive bodies that are the general “plumbing” sources for the volcanic surficial deposits. Although the stock and related bodies are shallow-level intrusive masses, our model for Cross Section A (Fig. 12) suggests several hundreds of meters of overall uplift across the GFFZ whereby genetically related Eocene intrusive and extrusive rocks are juxtaposed across GFFZ fault strands. This uplift occurred after the igneous activity (~43 Ma) and may reflect continued tectonic activities associated with the GFFZ tectonic discontinuity. This vertical offset may generally reflect the on-going uplift of the Cascades directly east of the GFFZ and subsidence of the Everett basin which is well-documented directly west of the GFFZ (for example, Johnson and others, 1996, 2001).

Neotectonism in the Map Area

Here we report briefly on the neotectonic features noted in the Granite Falls quadrangle including noted instances of faulted and (or) liquefied Pleistocene sediment. Widespread and exceptionally well exposed liquefaction features including sand dikes and lateral spreading slump features are exposed in the large Menzel Lake gravel pit (significant site 10D)(Fig. 2). This pit is located within the GFFZ directly south-southeast of the City of Granite Falls. It exposes recessional Vashon glacial sand deposits that are loose deltaic or glacial lake sand facies within the Menzel Lake ice contact complex. We interpret the common small faults with normal displacement (Fig. 2) and thin sand dikes that intrude the faults as extensional liquefaction features. While we cannot discount the possibility that the liquefaction features are unrelated to local faults we have not observed intense liquefaction features such as these in other recessional sand deposits in the map area that might suggest locally severe shaking on regional structures. We also observed sheared Vashon till in a large outcrop exposed by scour from the Pilchuck River during very low flows during 2015 (significant site 201B)(observed on 7/28/2015). The feature might be a northwest-trending fault with steeply dipping spaced fractures along the discontinuity striking northwest sub-parallel to nearby strands of the Granite Falls fault zone. Although this might be a Quaternary fault, further study during low river flow is warranted around this site to discount the possibility that it is not a subglacial shear or a liquefaction feature. We observed tilted, sheared, or liquefied nonglacial sediments (unit *QCpf*) at significant site 43A in the southeastern corner of the map area where sand deposits also display chaotic deformational features such as small faults and (or) lateral spreading shear planes and perhaps liquefaction-induced slumping. Finally, we note that the “canyonization” of Canyon Creek, South Fork Stillaguamish River, and the Pilchuck River in the eastern

part of the map area might be related to neotectonism. This incision is particularly noteworthy within the eastern part of the map area or east of the GFFZ and is most prominent for the South Fork Stillaguamish River which is strongly incised from east of the City of Granite Falls to Verlot east of the map area where incision of the river is markedly reduced. Perhaps this area is undergoing net neotectonic uplift which would explain the general lack of thick Tertiary sedimentary or Pleistocene nonglacial deposits in this area. We note here that it seems that the inferred Quaternary course of the Pilchuck River has been diverted around this generally uplifted block and into the Explorer Falls, Bosworth Lake basins and the area represented by thick Tertiary sedimentary rocks below the northwestern part of the map area.

Vashon Recessional Lake and Delta Formation

Booth (1990) subdivided recessional outwash deposits into six stages of deglaciation and emphasized the importance of both ice-marginal and subglacial meltwater paths. For example, some of the southwest-trending valleys traversing the glacial uplands are the result of meltwater erosion and sedimentation in subglacial tunnels and open recessional valleys. Restricted fluvial and lake kame deposits (units *Qgjk* and *Qglr*) are either part of larger ice-contact complexes or are isolated accumulations that formed along the interface between the ice margin and deglaciated uplands. Our mapping confirms that ice-marginal meltwater followed several elevated pathways during glacial recession and deposited fluvial, deltaic, lacustrine, and ice-contact sediments.

The altitude of glacial lakes controlled the location of recessional outwash and smaller lakes in the region. Inset fluvial terraces and outwash channel landforms of unit *Qgof* are the result of fluvial incision or erosion in response to dropping glacial lake levels during deglaciation. These features are inset against slightly older ice-contact complexes in some parts of the map area. As observed in adjacent quadrangles, these terraces record Pleistocene south- and southwest-trending recessional meltwater pathways that descended to glacial Lake Skykomish or the later glacial Lake Snohomish elevations. Glacial runoff drained to the south and southeast to lower elevations across the Lake Roesiger and Lake Chaplain quadrangles. Drainage was first down the Lake Chaplain channel to the Sultan River delta into glacial Lake Skykomish. With additional recession the Woods Creek then Roesiger Creek, and Carpenter Creek channels opened draining to the Woods Creek delta at Monroe. The last glacial outwash drainage way to open was the lower Pilchuck channel draining to the glacial delta at Snohomish into glacial Lake Snohomish/Skykomish/Snoqualmie. At this stage the ice and upper Pilchuck delta at Granite Falls blocked the Pilchuck River from its original valley to the NW forcing it to flow to the SW at the present lower valley location forming a delta at the town of Snohomish.

Thorson (1989) indicated that “the lake sequence was complex because systematic northward retreat caused progressive uncovering of lower lake spillways, resulting in the coalescence of smaller lakes to form large ones at lower levels.” East of the quadrangle, Booth (1989) mapped thick ‘embankment’

deposits that marked significant glacial lake deposition centers during early stages of Vashon recession. Within the quadrangle, exposures of high-amplitude foreset beds record multiple stages of progressively lowering glacial lake levels (unit Qgod, significant sites 42X, 17F, 10D, 10P). The highest deltaic deposits are graded to ~915, ~790, ~600-, ~515-, and ~460-ft elevations. 'Glacial Lake Pilchuck' occupied much of the Pilchuck River valley during early Vashon Stade deglaciation. Nearby early glacial lakes of about the same time period would be glacial lake Skykomish of Dragovich and others (2013, 2014a, 2015) or glacial lake Stillaguamish of Newcomb (1952). These lakes occupied major valleys south and north of the map area. Although there were likely numerous lake levels during deglaciation, most recessional geomorphic features in the Granite Falls quadrangle can ultimately be tied to these water bodies; for example, Mountain Loop Highway ice contact complex features graded to glacial Lake Pilchuck.

The youngest large Vashon delta complex we mapped is the Granite Falls delta complex in the northwest corner of the quadrangle. This newly named deltaic and glacial lake feature is generally graded to a ~460-ft glacial lake elevation. For example, quarry excavation into one of these channels (significant site 10D) exposes high-amplitude (>10 m) foreset bed structures that indicate westward delta progradation. Lidar imagery shows several paleo-channels at the ~460-ft elevation that record possible drainage paths of the ancient South Fork Stillaguamish River and Canyon Creek. The Granite Falls and Canyon Creek delta complexes are graded to this elevation and could have been part of a large deltaic depocenter(s) that has since been incised by the modern South Fork Stillaguamish River. Multiple fluvial terrace levels record progressive down-cutting of the river to its present level.

ACKNOWLEDGMENTS

This geologic map was funded in part by the U.S. Geological Survey (USGS) National Cooperative Geologic Mapping Program under award no. G15AC00248. Special thanks to Kitty Reed for editorial assistance. We thank Mike Eddy for providing preliminary U-Pb ages and for general geologic discussions; Matt Holland (USGS) and John Bethel (King County) for field mapping assistance; Scott Kuehner and Bruce Nelson (both at U.W., Dept. of Earth and Space Sciences) for help with the isotopic analyses; Katherine Waters and Dylan Riger (students at Colorado College) for help with isostatic gravity surveys; Quinn Butler, Xianyu Meng, Todd Lau, and Eda Yagiz for assistance with portable seismometers; Glenn Thompson (Florida Gulf Coast Univ.) for microprobe data and interpretations; Scott Boroughs, Rick Conrey, and Charles Knaack (Washington State University) for geochemical analyses; Candace Passehl (USGS) for sampling and preparation of luminescence samples; Kirsten Sauer (University of Nevada, Reno) for geologic discussions and preparing a detrital zircon figure; and Eric Dingeldein and Tracy Trole (WSDOT), Jeff Jones (Snohomish County), and Sue Kahle and Theresa Olsen (USGS, Water Resources Division) for subsurface geologic information. Historical mine information was provided in part by Fred Cruger (Granite Falls Historical Society). Several landowners provided access to important outcrops; Jerry and Lanai

Hemstrom were particularly helpful. Kurt Siegfried (Cemex), Jim Burnett (Iron Mountain Quarry), and Rob Hild (Menzel Lake Gravel) provided access to excellent exposures in active quarries. We also thank our colleagues at the Washington Division of Geology and Earth Resources: Tim Walsh (for a review), Daniel Eungard (for well data), and Tara Salzer (for logistical support).

REFERENCES CITED

- Armstrong, J. E., 1981, Post-Vashon Wisconsin glaciation, Fraser Lowland, British Columbia: Geological Society of Canada Bulletin 322, 34 p.
- Associated Earth Sciences, Inc., 1994, Pilchuck West hydrogeology and pump tests results ground water application no. GI-26520, Snohomish County, Washington: Associated Earth Sciences, Inc., 1 v.
- Associated Earth Sciences, Inc., 2003, Proposed Snoqualmie Ridge II project—Environmental impact statement—Technical report on geology, soils, and groundwater: Associated Earth Sciences, Inc., [under contract to] Quadrant Corporation, 1 v.
- Barnett, E. A.; Kelsey, H. M.; Sherrod, B. L.; Blakely, R. J.; Hughes, J. F.; Schermer, E. R.; Haugerud, R. A.; Weaver, C. S.; Siedlecki, E., 2006, Active faulting at the northeast margin of the greater Puget Lowland—A paleoseismic and magnetic-anomaly study of the Kendall scarp, Whatcom County, northwest Washington [abstract]: Eos (American Geophysical Union Transactions), Abstract S31A-0183, v. 87, no. 52.
- Bhatia, M.R.; Crook, K.A., 1986, Trace element characteristics of graywackes and tectonic setting discrimination of sedimentary basins: Contributions to Mineralogy and Petrology, v. 92, no. 2, p.181-193.
- Blakely, R. J.; Wells, R. E.; Weaver, C. S., 1999, Puget Sound aeromagnetic maps and data: U.S. Geological Survey Open-File Report 99-0514. [<http://geopubs.wr.usgs.gov/open-file/of99-514/>]
- Booth, D. B., 1984, Glacier dynamics and the development of glacial landforms in the eastern Puget Lowland, Washington: University of Washington Doctor of Philosophy thesis, 217 p., 1 plate. [<http://hdl.handle.net/1773/6696>]
- Booth, D. B., 1986, The formation of ice-marginal embankments into ice-dammed lakes in the eastern Puget Lowland, Washington, U.S.A., during the late Pleistocene: Boreas, v. 15, no. 3, p. 247-263.
- Booth, D. B., 1990, Surficial geologic map of the Skykomish and Snoqualmie Rivers area, Snohomish and King Counties, Washington: U.S. Geological Survey Miscellaneous Investigations Series Map I-1745, 2 sheets, scale 1:50,000, with 22 p. text. [<http://pubs.er.usgs.gov/publication/i1745>]
- Boynton, W. V., 1984, Cosmochemistry of the rare earth elements—meteorite studies. In Henderson, R., editor, Rare Earth Element Geochemistry: Developments in Geochemistry 2, Elsevier, Ch. 3, p., 89-92.
- Brach-Papa, C.; Van Bocxstaele, M.; Ponzevera, E.; Quérel, C. R., 2009, Fit for purpose validated method for the determination of the strontium isotopic signature in mineral water samples by multi-collector inductively coupled plasma mass spectrometry—Spectrochimica Acta Part B: Atomic Spectroscopy, v. 64, no. 3, p. 229-234.
- Brandon, M. T.; Roden-Tice, M. K.; Garver, J. I., 1998, Late Cenozoic exhumation of the Cascadia accretionary wedge in the Olympic Mountains, northwest Washington State: Geological Society of America Bulletin, v. 110, no. 8, p. 985-1009, Data Repository item 9865.
- Broecker, W. S.; Kulp, J. L.; Tucek, C. S., 1956, Lamont natural radio-carbon measurements, III: Science, v. 124, no. 3213, p. 154-165.

- Brown, E. H., 2012, Obducted nappe sequence in the San Juan Islands—Northwest Cascades thrust system, Washington and British Columbia: *Canadian Journal of Earth Sciences* v. 49, no. 7, p. 796-817.
- Brown, N. D.; Forman, S. L., 2012, Evaluating a SAR TT-OSL protocol for dating fine-grained quartz within Late Pleistocene loess deposits in the Missouri and Mississippi river valleys, United States: *Quaternary Geochronology*, v. 12, p. 87-97.
- Campbell, A. R., 1991, Petrology and petrogenesis of the Lost Peak and Monument Peak stocks, Okanogan County, Washington: University of Washington Master of Science thesis, 136 p., 1 plate.
- Cann, J. R., 1970, Rb, Sr, Y, Zr, and Nb in some ocean floor basaltic rocks: *Earth and Planetary Science Letters*, v. 10, no. 1, p. 7-11.
- Capps, G.; Simmons, J. D.; Videgar, F. D., 1973, Geology of southern Snohomish County for land-use planning: Western Washington State College Department of Geology, 1 v.
- Cheney, E. S., 1987, Major Cenozoic faults in the northern Puget Lowland of Washington. In Schuster, J. E., editor, *Selected papers on the geology of Washington*: Washington Division of Geology and Earth Resources Bulletin 77, p. 149-168.
- Colman, S. M.; Pierce, K. L., 1981, Weathering rinds on andesitic and basaltic stones as a Quaternary age indicator, western United States: U.S. Geological Survey Professional Paper 1210, 56 p. [<http://pubs.er.usgs.gov/publication/pp1210>]
- Danner, W. R., 1957, A stratigraphic reconnaissance in the northwestern Cascade mountains and San Juan Islands of Washington State: University of Washington Doctor of Philosophy thesis, 3 v., 562 p., 7 plates.
- Danner, W. R., 1966, Limestone resources of western Washington; with a section on the Lime Mountain deposit, by G. W. Thorsen: Washington Division of Mines and Geology Bulletin 52, 474 p.
- Deschamps, F.; Godard, M.; Guillot, S.; Hattori, K., 2013, Geochemistry of subduction zone serpentinites—A review: *Lithos*, v. 178, p. 96-127.
- Dickinson, W. R., 1970, Interpreting detrital modes of graywacke and arkose: *Journal of Sedimentary Petrology*, v. 40, no. 2, p. 695-707.
- Dragovich, J. D., 2007, Sand point count and geochemical data in the Fall City and Carnation 7.5-minute quadrangles, King County, Washington: Washington Division of Geology and Earth Resources Open File Report 2007-3, 2 Microsoft Excel files and 6 p. text. [http://www.dnr.wa.gov/publications/ger_ofr2007-3_fall-city_supplement.zip]
- Dragovich, Joe D.; DeOme, Alex J., 2006, Geologic map of the McMurray 7.5-minute quadrangle, Skagit and Snohomish Counties, Washington, with a discussion of the evidence for Holocene activity on the Darrington-Devils Mountain fault zone: Washington Division of Geology and Earth Resources Geologic Map GM-61, 1 sheet, scale 1:24,000, with 18 p. text. [http://www.dnr.wa.gov/Publications/ger_gm61_geol_map_mcmurray_24k.zip]
- Dragovich, J. D.; Gilbertson, L. A.; Norman, D. K.; Anderson, G.; Petro, G. T., 2002a, Geologic map of the Utsalady and Conway 7.5-minute quadrangles, Skagit, Snohomish, and Island Counties, Washington: Washington Division of Geology and Earth Resources Open File Report 2002-5, 34 p., 2 plates, scale 1:24,000. [http://www.dnr.wa.gov/Publications/ger_ofr2002-5_geol_map_utsalady_conway_24k.zip]
- Dragovich, J. D.; Logan, R. L.; Schasse, H. W.; Walsh, T. J.; Lingley, W. S., Jr.; Norman, D. K.; Gerstel, W. J.; Lapen, T. J.; Schuster, J. E.; Meyers, K. D., 2002b, Geologic map of Washington—Northwest quadrant: Washington Division of Geology and Earth Resources Geologic Map GM-50, 3 sheets, scale 1:250,000, with 72 p. text. [http://www.dnr.wa.gov/publications/ger_gm50_geol_map_nw_wa_250k.pdf]
- Dragovich, J. D.; Anderson, M. L.; Walsh, T. J.; Johnson, B. L.; Adams, T. L., 2007, Geologic map of the Fall City 7.5-minute quadrangle, King County, Washington: Washington Division of Geology and Earth Resources Geologic Map GM-67, 1 sheet, scale 1:24,000. [http://www.dnr.wa.gov/publications/ger_gm67_geol_map_fallcity_24k.zip]
- Dragovich, J. D.; Littke, H. A.; Anderson, M. L.; Hartog, Renate; Wessel, G. R.; DuFrane, S. A.; Walsh, T. J.; MacDonald, J. H., Jr.; Mangano, J. F.; Cakir, Recep, 2009a, Geologic map of the Snoqualmie 7.5-minute quadrangle, King County, Washington: Washington Division of Geology and Earth Resources Geologic Map GM-75, 2 sheets, scale 1:24,000. [http://www.dnr.wa.gov/publications/ger_gm75_geol_map_snoqualmie_24k.zip]
- Dragovich, J. D.; Littke, H. A.; MacDonald, J. H., Jr.; DuFrane, S. A.; Anderson, M. L.; Wessel, G. R.; Hartog, Renate, 2009b, Geochemistry, geochronology, and sand point count data for the Snoqualmie 7.5-minute quadrangle, King County, Washington: Washington Division of Geology and Earth Resources Open File Report 2009-4, 35 p. text, with 3 Microsoft Excel files. [http://www.dnr.wa.gov/publications/ger_ofr2009-4_snoqualmie_suppl.zip]
- Dragovich, J. D.; Walsh, T. J.; Anderson, M. L.; Hartog, Renate; DuFrane, S. A.; Vervoot, Jeff; Williams, S. A.; Cakir, Recep; Stanton, K. D.; Wolff, F. E.; Norman, D. K.; Czajkowski, J. L., 2009c, Geologic map of the North Bend 7.5-minute quadrangle, King County, Washington, with a discussion of major faults, folds, and basins in the map area: Washington Division of Geology and Earth Resources Geologic Map GM-73, 1 sheet, scale 1:24,000. [http://www.dnr.wa.gov/publications/ger_gm73_geol_map_northbend_24k.zip]
- Dragovich, J. D.; Anderson, M. L.; MacDonald, J. H., Jr.; Mahan, S. A.; DuFrane, S. A.; Littke, H. A.; Wessel, G. R.; Saltonstall, J. H.; Koger, C. J.; Cakir, Recep, 2010a, Supplement to the geologic map of the Carnation 7.5-minute quadrangle, King County, Washington—Geochronologic, geochemical, point count, geophysical, earthquake, fault, and neotectonic data: Washington Division of Geology and Earth Resources Open File Report 2010-2, 42 p., 8 digital appendices. [http://www.dnr.wa.gov/publications/ger_ofr2010-2_carnation_supplement.zip]
- Dragovich, J. D.; Littke, H. A.; Anderson, M. L.; Wessel, G. R.; Koger, C. J.; Saltonstall, J. H.; MacDonald, J. H., Jr.; Mahan, S. A.; DuFrane, S. A., 2010b, Geologic map of the Carnation 7.5-minute quadrangle, King County, Washington: Washington Division of Geology and Earth Resources Open File Report 2010-1, 1 sheet, scale 1:24,000, with 21 p. text. [http://www.dnr.wa.gov/publications/ger_ofr2010-1_geol_map_carnation_24k.zip]
- Dragovich, J. D.; Anderson, M. L.; Mahan, S. A.; Koger, C. J.; Saltonstall, J. H.; MacDonald, J. H., Jr.; Wessel, G. R.; Stoker, B. A.; Bethel, J. P.; Labadie, J. E.; Cakir, Recep; Bowman, J. D.; DuFrane, S. A., 2011a, Geologic map of the Monroe 7.5-minute quadrangle, King and Snohomish Counties, Washington: Washington Division of Geology and Earth Resources Open File Report 2011-1, 1 sheet, scale 1:24,000, with 24 p. text. [http://www.dnr.wa.gov/publications/ger_ofr2011-1_geol_map_monroe_24k.zip]
- Dragovich, J. D.; Mahan, S. A.; Anderson, M. L.; MacDonald, J. H., Jr.; Wessel, G. R.; DuFrane, S. A.; Cakir, Recep; Bowman, J. D.; Littke, H. A., 2011b, Analytical data from the Monroe 7.5-minute quadrangle, King and Snohomish Counties, Washington—Supplement to Open File Report 2011-1: Washington Division of Geology and Earth Resources Open File Report 2011-2, 58 p., 2 plates, 2 Microsoft Excel files. [http://www.dnr.wa.gov/publications/ger_ofr2011-2_monroe_supplement.zip]

- Dragovich, J. D.; Anderson, M. L.; Mahan, S. A.; MacDonald, J. H., Jr.; McCabe, C. P.; Cakir, Recep; Stoker, B. A.; Villeneuve, N. M.; Smith, D. T.; Bethel, J. P., 2012, Geologic map of the Lake Joy 7.5-minute quadrangle, King County, Washington: Washington Division of Geology and Earth Resources Map Series 2012-01, 2 sheets, scale 1:24,000, with 79 p. text and 1 Excel file. [http://www.dnr.wa.gov/publications/ger_ms2012-01_geol_map_lake_joy_24k.zip]
- Dragovich, J. D.; Littke, H. A.; Mahan, S. A.; Anderson, M. L.; MacDonald, J. H., Jr.; Cakir, Recep; Stoker, B. A.; Koger, C. J.; Bethel, J. P.; DuFrane, S. A.; Smith, D. T.; Villeneuve, N. M., 2013, Geologic map of the Sultan 7.5-minute quadrangle, King and Snohomish Counties, Washington: Washington Division of Geology and Earth Resources Map Series 2013-01, 1 sheet, scale 1:24,000, with 52 p. text. [http://www.dnr.wa.gov/publications/ger_ms2013-01_geol_map_sultan_24k.zip]
- Dragovich, J. D.; Frattali, C. L.; H. A.; Anderson, M. L.; Mahan, S. A.; MacDonald, J. H., Jr.; Stoker, B. A.; Smith, D. T.; Koger, C. J.; Cakir, Recep; DuFrane, S. A.; Sauer, K. B., 2014a, Geologic map of the Lake Chaplain 7.5-minute quadrangle, Snohomish County, Washington: Washington Division of Geology and Earth Resources Map Series 2014-01, 1 sheet, scale 1:24,000, with 51 p. text. [http://www.dnr.wa.gov/publications/ger_ms2014-01_geol_map_lake_chaplain_24k.zip]
- Dragovich, J. D.; Mahan, S. A.; Anderson, M.; Macdonald, J. H., Jr.; Frattali, C.; Littke, H. A.; Stoker, B. A.; Koger, C. J.; Smith, D. T.; DuFrane, S. A., 2014b, The Monroe fault, anticline, and synclinal basin—A potentially active fault and fold system in the Skykomish River Valley, Snohomish County, Washington: Geological Society of America Abstracts with Programs, v. 46, no. 6, p. 779.
- Dragovich, J. D.; Mahan, S. A.; Anderson, M. L.; MacDonald, J. H., Jr.; Schilter, J. F.; Frattali, C. L.; Koger, C. J.; Smith, D. T.; Stoker, B. A.; DuFrane, Andrew; Eddy, M. P.; Cakir, Recep; Sauer, K. B., 2015, Geologic map of the Lake Roesiger 7.5-minute quadrangle, Snohomish County, Washington: Washington Division of Geology and Earth Resources Map Series 2015-01, 1 sheet, scale 1:24,000, 47 p. text. [http://www.dnr.wa.gov/publications/ger_ms2015-01_geol_map_lake_roesiger_24k.zip]
- Dumitru, T. A.; Elder, W. P.; Hourigan, J. K.; Chapman, A. D.; Graham, S. A.; Wakabayashi, John, 2016, Four cordilleran paleorivers that connected Sevier thrust zones in Idaho to depocenters in California, Washington, Wyoming, and, indirectly, Alaska: *Geology*, v. 44, no. 1, p. 75-78.
- Dungan, M. A., 1974, The origin, emplacement, and metamorphism of the Sultan mafic-ultramafic complex, North Cascades, Snohomish County, Washington: University of Washington Doctor of Philosophy thesis, 227 p., 3 plates.
- Eddy, M. P.; Bowring, S. A.; Umhoefer, P. J.; Miller, R. B.; McLean, N. M.; Donaghy, E. E., 2016, High-resolution temporal and stratigraphic record of Siletzia's accretion and triple junction migration from nonmarine sedimentary basins in central and western Washington: *Geological Society of America Bulletin*, v. 128, no. 3/4, p. 425-441.
- Evans, J. E.; Ristow, R. J., Jr., 1994, Depositional history of the southeastern outcrop belt of the Chuckanut Formation—Implications for the Darrington–Devil's Mountain and Straight Creek fault zones, Washington (U.S.A.): *Canadian Journal of Earth Sciences*, v. 31, no. 12, p. 1727-1743.
- Festa, A.; Pini, G. A.; Dilek, Y.; Codegone, G., 2010, Mélanges and mélange-forming processes—a historical overview and new concepts: *International Geology Review*, v. 52, no. 10-12, p. 1040-1105.
- Finn, C.; Phillips, W. M.; Williams, D. L., 1991, Gravity anomaly and terrain maps of Washington, scale 1:500,000 and 1:1,000,000, U.S. Geological Survey Geophysical Investigations Map GP-988.
- Frizzell, V. A., Jr.; Tabor, R. W.; Zartman, R. E.; Blome, C. D., 1987, Late Mesozoic or early Tertiary mélanges in the western Cascades of Washington. In Schuster, J. E., editor, Selected papers on the geology of Washington: Washington Division of Geology and Earth Resources Bulletin 77, p. 129-148. [http://www.dnr.wa.gov/publications/ger_b77_papers_on_wa_geology_pt2of3.pdf]
- Frost, B. R.; Barnes, C. G.; Collins, W. J.; Arculus, R. J.; Ellis, D. J.; Frost, C. D., 2001, A geochemical classification for granitic rocks: *Journal of Petrology*, v. 42, no. 11, p. 2033-2048.
- Fuller, R. E., 1925, The geology of the northeastern part of Cedar Lake quadrangle with special reference to the de-roofed Snoqualmie batholith: University of Washington Master of Science thesis, 96 p., 4 plates.
- Gaffney, A. M.; Blichert-Toft, J.; Nelson, B. K.; Bizzarro, M.; Rosing, M.; Albarede, F., 2007, Constraints on source-forming processes of West Greenland kimberlites inferred from Hf–Nd isotope systematics: *Geochimica et Cosmochimica Acta*, v. 71, no. 11, p. 2820-2836.
- Haeussler, P. J.; Bradley, D. C.; Wells, R. E.; Miller, M. L., 2003, Life and death of the Resurrection plate—Evidence for its existence and subduction in the northeastern Pacific in Paleocene–Eocene time: *Geological Society of America Bulletin*, v. 115, no. 7, p. 867-880.
- Harkins, S. A.; Appold, M. S.; Nelson, B. K.; Brewer, A. M.; Groves, I. M., 2008, Lead isotope constraints on the origin of nonsulfide zinc and sulfide zinc-lead deposits in the Flinders Ranges, South Australia: *Economic Geology*, v. 103, no. 2, p. 353-364.
- Harland, W. B.; Cox, A. V.; Llewellyn, P. G.; Pickton, C. A. G.; Smith, A. G.; Walters, R., 1982, A geologic time scale: Cambridge University Press, 131 p.
- Haugerud, R. A.; Brown, E. H.; Tabor, R. W.; Kriens, B. J.; McGroder, M. F., 1994, Late Cretaceous and early Tertiary orogeny in the North Cascades. In Swanson, D. A.; Haugerud, R. A., editors, *Geologic field trips in the Pacific Northwest*: University of Washington Department of Geological Sciences, v. 2, p. 2E 1-2E 53.
- Hancock, W. B., 1928, Mining Report of the Wayside Mine, Snohomish County, Washington: unpublished report dated May 21st, 1928 [Seattle, Wash.], 9 p. [Granite Falls Historical Museum].
- Hansen, H. P., 1947, Postglacial forest succession, climate and chronology in the Pacific Northwest: *American Philosophical Society Transactions*, new series, v. 37, part 1, p. 1-130.
- Hansen, L. D.; Dipple, G. M.; Gordon, T. M.; Kellett, D. A., 2005, Carbonated serpentinite (listwanite) at Atlin, British Columbia: A geological analogue to carbon dioxide sequestration: *The Canadian Mineralogist*, v. 43, no. 1, p. 225-239.
- Harland, W. B.; Cox, A. V.; Llewellyn, P. G.; Pickton, C. A. G.; Smith, A. G.; Walters, R., 1982, A geologic time scale: Cambridge University Press, 131 p.
- Heller, P. L.; Tabor, R. W.; Suczek, C. A., 1987, Paleogeographic evolution of the United States Pacific Northwest during Paleogene time: *Canadian Journal of Earth Sciences*, v. 24, no. 8, p. 1652-1667.
- Irvine, T. N.; Baragar, W. R. A., 1971, A guide to the chemical classification of the common volcanic rocks: *Canadian Journal of Earth Sciences*, v. 8, no. 5, p. 523-548.
- Irving, E.; Brandon, M. T., 1990, Paleomagnetism of the Flores volcanics, Vancouver Island, in place by Eocene time: *Canadian Journal of Earth Sciences*, v. 27, no. 6, p. 811-817.
- Jackson, S. E.; Pearson, N. J.; Griffin, W. L.; Belousova, E. A., 2004, The application of laser ablation-inductively coupled plasma-mass spectrometry to in-situ U-Pb zircon geochronology: *Chemical Geology*, v. 211, p. 47-69.

- Jett, G. A., 1986, Sedimentary petrology of the Western mélange belt, north Cascade Range, Washington: University of Wyoming Master of Science thesis, 85 p.
- Jett, G. A.; Heller, P. L., 1988, Tectonic significance of polymodal compositions in mélange sandstones, Western mélange belt, north Cascade Range, Washington: *Journal of Sedimentary Petrology*, v. 58, no. 1, p. 52-61.
- Johnson, D. M.; Hooper, P. R.; Conrey, R. M., 1999, XRF analysis of rocks and minerals for major and trace elements on a single low dilution Li-tetraborate fused bead: *Advances in X-ray Analysis*, v. 41, p. 843-867.
- Johnson, S. Y., 1982, Stratigraphy, sedimentology, and tectonic setting of the Eocene Chuckanut Formation, northwest Washington: University of Washington Doctor of Philosophy thesis, 221 p., 4 plates.
- Johnson, S. Y.; Potter, C. J.; Armentrout, J. M., 1994, Origin and evolution of the Seattle fault and Seattle basin, Washington: *Geology*, v. 22, no. 1, p. 71-74, 1 plate.
- Johnson, S. Y.; Potter, C. J.; Armentrout, J. M.; Miller, J. J.; Finn, C. A.; Weaver, C. S., 1996, The Southern Whidbey Island fault—An active structure in the Puget Lowland, Washington: *Geological Society of America Bulletin*, v. 108, no. 3, p. 334-354, 1 plate.
- Johnson, S. Y.; Dadisman, S. V.; Mosher, D. C.; Blakely, R. J.; Childs, J. R., 2001, Active tectonics of the Devils Mountain fault and related structures, northern Puget Lowland and eastern Strait of Juan de Fuca region, Pacific Northwest: U.S. Geological Survey Professional Paper 1643, 45 p., 2 plates. [<http://earthquake.usgs.gov/regional/pacnw/activefaults/dmf/>]
- Kaiser, A. E., 1934, The geology of the Yankee Boy mine, Snohomish County, Washington: University of Washington Bachelor of Science thesis, 20 p., 3 plates
- Kelsey, H. M.; Sherrod, B. L.; Blakely, R. J.; Haugerud, R. A., 2012, Holocene faulting in the Bellingham forearc basin—Upper-plate deformation at the northern end of the Cascadia subduction zone: *Journal of Geophysical Research*, v. 117, B03409, 26 p.
- Klepeis, K. A.; Crawford, M. L.; Gehrels, G., 1998, Structural history of the crustal-scale Coast shear zone north of Portland Canal, southeast Alaska and British Columbia: *Journal of Structural Geology*, v. 20, p. 883-904.
- Knaack, C.; Cornelius, S.; Hooper, P., 1994, Trace element analysis of rocks and minerals by ICP/MS: Department of Geology Washington State University Open-file Report, December 1994, 18 p.
- Knoll, K. M., 1967, Surficial geology of the Tolt River area, Washington: University of Washington Master of Science thesis, 91 p., 1 plate.
- Le Bas, M. J.; Le Maitre, R. W.; Streckeisen, A. L.; Zanettin, Bruno, 1986, A chemical classification of volcanic rocks based on the total alkali-silica diagram: *Journal of Petrology*, v. 27, part 3, p. 745-750.
- Le Maitre, R. W.; Streckeisen, A.; Zanettin, B.; Le Bas, M. J.; Bonin, B.; Bateman, P., editors, 2002, *Igneous rocks—A classification and glossary of terms*; 2nd ed.: Cambridge University Press, Cambridge, U.K., 256 p.
- Lees, J. M., 1999, Geotouch—Software for three and four-dimensional GIS in the earth sciences: *Computers & Geosciences*, v. 26, no. 7, p. 751-761.
- Lees, J. M., 2007, RFOC—Graphics for spherical distributions and earthquake focal mechanisms, graphics for statistics on a sphere, as applied to geological fault data, crystallography, earthquake focal mechanisms, radiation patterns, ternary plots and geographical/ geological maps: Comprehensive R Archive Network (CRAN). [accessed May 31, 2011, at <http://streaming.stat.iastate.edu/CRAN/web/packages/RFOC/index.html>].
- Lees, J. M., 2008, GEOMap—Topographic and geologic mapping: Comprehensive R Archive Network (CRAN) [accessed May 31, 2011, at <http://streaming.stat.iastate.edu/CRAN/web/packages/GEOMap/index.html>].
- Lewis, J. C.; Unruh, J. R.; Twiss, R. J., 2003, Seismogenic strain and motion of the Oregon coast block: *Geology*, v. 31, no. 2, p. 183-186.
- Lovseth, T. P., 1975, The Devils Mountain fault zone, northwestern Washington: University of Washington Master of Science thesis, 29 p.
- Ludwig, K. R., 2003, User's manual for Isoplot 3.00. A geochronological Toolkit for Microsoft Excel: Berkeley Geochronology Center, Special Publication No. 4a, 1 v.
- MacDonald, J. H., Jr.; Dragovich, J. D.; Littke, H. A.; Anderson, Megan; Dufrane, S. A., 2013, The volcanic rocks of Mount Persis: An Eocene continental arc that contains adakitic magmas [abstract]: *Geological Society of America Abstracts with Programs*, v. 45, no. 7, p. 392.
- MacDonald, J. H., Jr.; Dragovich, J. D.; Frattali, C. L.; Anderson, M. L.; Stoker, B. A.; Littke, H. A.; DuFrane, S. A.; Sauer, K.; Smith, D. T.; Koger, C. J., 2014, Geochemistry and metaigneous rocks from the Western mélange belt, Lake Chaplain, Snoqualmie, and Sultan 7.5-minute quadrangles, western Cascades, Washington—Evidence for a predominantly volcanic arc setting: *Geological Society of America, Abstracts with Programs*, v. 46, no. 6, p. 363.
- Mackin, J. H., 1941, Glacial geology of the Snoqualmie-Cedar area, Washington: *Journal of Geology*, v. 49, no. 5, p. 449-481.
- Mackin, J. H.; Cary, A. S., 1965, Origin of Cascade landscapes: Washington Division of Mines and Geology Information Circular 41, 35 p. [http://www.dnr.wa.gov/Publications/ger_ic41_origin_cascade_landscapes.pdf]
- Madsen, J. K.; Thorkelson, D. J.; Friedman, R. M.; Marshall, D. D., 2006, Cenozoic to Recent plate configurations in the Pacific Basin—Ridge subduction and slab window magmatism in western North America: *Geosphere*, v. 2, no. 1, p. 11-34.
- Magee, M. E.; Zoback, M. L., 1992, Wellbore breakout analysis for determining tectonic stress orientations in Washington State: U.S. Geological Survey Open-File Report 92-715, 56 p. [<http://pubs.er.usgs.gov/publication/ofr92715>]
- Marcus, K. L., 1991, The rocks of Bulson Creek—Eocene through Oligocene sedimentation and tectonics in the Lake McMurray area, Washington: *Washington Geology*, v. 19, no. 4, p. 14-15. [http://www.dnr.wa.gov/Publications/ger_washington_geology_1991_v19_no4.pdf]
- McCrory, P. A.; Wilson, D. S., 2013, A kinematic model for the formation of the Siletz-Crescent forearc terrane by capture of coherent fragments of the Farallon and Resurrection plates: *Tectonics*, 32, no. 3, p. 718-736, doi:10.1002/tect.20045.
- McDonough, W. F.; Sun, S. S., 1995, The composition of the Earth: *Chemical Geology*, v. 120, no. 3-4 p. 223-253.
- McFarland, C. R., 1981, Oil and gas exploration in Washington, 1900-1981: Washington Division of Geology and Earth Resources Information Circular 67R, 119 p. [http://www.dnr.wa.gov/publications/ger_ic67r_oil_gas_exploration_wa_1900-81.pdf]
- McLennan, S. M.; Taylor, S. R.; McCulloch M. T.; Maynard, J. B., 1990, Geochemical and Nd-Sr isotopic composition of deep-sea turbidites—Crustal evolution and plate tectonic associations: *Geochimica et Cosmochimica Acta*, v. 54, p. 2015-2050.
- Miller, M. M.; Johnson, D. J.; Rubin, C. M.; Dragert, H.; Wang, K.; Qamar, A. I.; Goldfinger, C., 2001, GPS-determination of along-strike variation in Cascadia margin kinematics—Implications for relative plate motion, subduction zone coupling, and permanent deformation: *Tectonics*, v. 20, no. 2, p. 161-176.

- Minard, J. P., 1981, Distribution and description of the geologic units in the Maltby quadrangle, Washington: U.S. Geological Survey Open- File Report 81-100, 4 p., 1 plate, scale 1:24,000. [http://ngmdb.usgs.gov/Prodesc/proddesc_11856.htm]
- Minard, J. P., 1985a, Geologic map of the Arlington East quadrangle, Snohomish County, Washington: U.S. Geological Survey Miscellaneous Field Studies Map MF-1739, 1 sheet, scale 1:24,000. [http://ngmdb.usgs.gov/Prodesc/proddesc_7431.htm]
- Minard, J. P., 1985b, Geologic map of the Lake Stevens quadrangle, Snohomish County, Washington: U.S. Geological Survey Miscellaneous Field Studies Map MF-1742, 1 sheet, scale 1:24,000. [http://ngmdb.usgs.gov/Prodesc/proddesc_7468.htm]
- Miyashiro, A., 1974, Volcanic rock series in island arcs and active continental margins: *American Journal of Science*, v. 274, no. 4, p. 321-355.
- Morrison, R. B., editor, 1991, Quaternary nonglacial geology—Conterminous U.S.: Geological Society of America DNAG Geology of North America, v. K-2, 672 p., 8 plates in accompanying case.
- Nelson, B. K., 1995, Fluid flow in subduction zones: Evidence from Nd- and Sr-isotope variations in metabasalts of the Franciscan Complex, California: *Contributions to Mineralogy and Petrology*, v. 119, p. 247-262.
- Newcomb, R. C., 1952, Ground-water resources of Snohomish County, Washington: U.S. Geological Survey Water-Supply Paper 1135, 133 p., 2 plates. [<http://pubs.er.usgs.gov/usgspubs/wsp/wspl1135>]
- Niu, Y., 2004, Bulk-rock major and trace element compositions of abyssal peridotites: Implications for mantle melting, melt extraction and post-melting processes beneath mid-ocean ridges: *Journal of Petrology*, v. 45, no. 12, p. 2423-2458.
- Ottmoller, L.; Voss, P.; Havskov, J.; 2016, SEISAN earthquake analysis software for Windows, Solaris, Linux, and MACOSX: National Geological Investigations of Denmark and Greenland (GEUS). [accessed at seis.gues.net]
- Pearce, J. A., 1996, A user's guide to basalt discrimination diagrams. In Wyman, D. A., editor, Trace element geochemistry of volcanic rocks—Applications for massive sulphide exploration: Geological Association of Canada Short Course Notes, v. 12, p. 79-113.
- Pearce, J. A., 2014, Immobile element fingerprinting of ophiolites: *Elements*, v. 10, no. 2, p. 101-108.
- Pessl, F., Jr.; Dethier, D. P.; Booth, D. B.; Minard, J. P., 1989, Surficial geologic map of the Port Townsend 30- by 60-minute quadrangle, Puget Sound region, Washington: U.S. Geological Survey Miscellaneous Investigations Series Map I-1198-F, 1 sheet, scale 1:100,000, 13 p. text.
- Pettijohn, F. J., 1957, *Sedimentary rocks*; 2nd ed.: Harper & Row, 718 p.
- Porter, S. C.; Swanson, T. W., 1998, Radiocarbon age constraints on rates of advance and retreat of the Puget lobe of the Cordilleran ice sheet during the last glaciation: *Quaternary Research*, v. 50, no. 3, p. 205-213.
- Prescott, J. R.; Hutton, J. T., 1994, Cosmic ray contributions to dose rates for luminescence and ESR dating—Large depths and long-term time variations: *Radiation Measurements*, v. 23, p. 497-500.
- Reasenber, P.; Oppenheimer D. H., 1985, FPFIT, FPLOT and FPPAGE; Fortran computer programs for calculating and displaying earthquake fault-plane solutions: U.S. Geological Survey Open-File Report 85-739, 109 p. [<https://pubs.er.usgs.gov/publication/ofr85739>]
- Ridolfi, F.; Renzulli, A. and Puerini, M., 2010, Stability and chemical equilibrium of amphibole in calc-alkaline magmas: an overview, new thermobarometric formulations and application to subduction-related volcanoes: *Contributions to Mineralogy and Petrology*, v. 160, no.1, pp.45-66.
- Rigg, G. B., 1958, Peat resources of Washington: Washington Division of Mines and Geology Bulletin 44, 272 p.
- Rigg, G. B.; Richardson, C. T., 1938, Profiles of some sphagnum bogs of the Pacific coast of North America: *Ecology*, v. 19, no. 3, p. 408-434.
- Robinson, L. F.; Henderson, G. M.; Slowey, N. C., 2002, U-Th dating of marine isotope stage 7 in Bahamas slope sediments: *Earth and Planetary Science Letters*, v. 196, no. 3, p. 175-187.
- Roser, B. P.; Korsch, R. J., 1988, Provenance signatures of sandstone- mudstone suites determined using discriminant function analysis of major-element data: *Chemical Geology*, v. 67, no. 1-2 p. 119-139.
- Roucoux, K. H.; Tzedakis, P. C.; Frogley, M. R.; Lawson, I. T.; Preece, R. C., 2008, Vegetation history of the marine isotope stage 7 interglacial complex at Ioannina, NW Greece: *Quaternary Science Reviews*, v. 27, no. 13, p. 1378-1395.
- Sauer, K.; Dragovich, J. D.; Macdonald, J. H., Jr.; Frattali, C.; Anderson, M.; DuFrane, S. A.; Gordon, S. M., 2014, Tectonic implications of detrital zircon geochronology and neodymium isotopes of the arkosic petrofacies of the Western mélange belt, Lake Chaplain quadrangle, western Cascades, Washington: *Geological Society of America Abstracts with Programs*, v. 46, no. 6, p. 363.
- Sauers, J. D., 1967, Ore zone, structural trend sketch map of Wayside Mine Area, Granite Falls, Wash: Unpublished map dated April 1967, [DGER mine files].
- Sauers, J., 1974, Update of Wayside Mine information: letter to Bill Reichert dated Jan. 30, 1974, 1 p. [DGER mine files].
- Schmandt, B.; Humphreys, E., 2011, Seismically imaged relict slab from the 55 Ma Siletzia accretion to the northwest United States: *Geology*, v. 39, no. 2, p. 175-178.
- Sherrod, B. L.; Blakely, R. J.; Weaver, C. S.; Kelsey, H. M.; Barnett, Elizabeth; Liberty, Lee; Meagher, K. L.; Pape, Kristin, 2008, Finding concealed active faults—Extending the southern Whidbey Island fault across the Puget Lowland, Washington: *Journal of Geophysical Research*, v. 113. [B05313, doi:10.1029/2007JB005060, 2008]
- Siedlecki, E. M., 2008, The geometry and earthquake history of the Boulder Creek fault—A paleoseismic, seismic refraction and ground penetrating radar study, Whatcom County, Washington: Western Washington University Master of Science thesis, 81 p., with CD containing appendices.
- Simonetti, A.; Heaman, L. M.; Hartlaub, R. P.; Creaser, R. A.; MacHattie, T. G.; Bohm, Christian, 2005, U-Pb zircon dating by laser ablation-MC-ICP-MS using a new multiple ion counting Faraday collector array: *Journal of Analytical Atomic Spectrometry*, v. 20, no. 8, p. 677-686.
- Sun, S.; McDonough, W. F., 1989, Chemical and isotopic systematic of oceanic basalts: Implications for mantle composition and processes. In Saunders, A. D.; Norry, M.J., editors, *Magmatism in the ocean basins*: Geological Society of London Special Publication 42, p. 313-345.
- Tabor, R. W., 1994, Late Mesozoic and possible early Tertiary accretion in western Washington State—The Helena-Haystack mélange and the Darrington-Devils Mountain fault zone: *Geological Society of America Bulletin*, v. 106, no. 2, p. 217-232.
- Tabor, R. W.; Booth, D. B., 1985, Folded thrust fault between major mélange units of the western North Cascades, Washington, and its relationship to the Shuksan thrust [abstract]: *Geological Society of America Abstracts with Programs*, v. 17, no. 6, p. 412.

- Tabor, R. W.; Frizzell, V. A., Jr.; Booth, D. B.; Waitt, R. B.; Whetten, J. T.; Zartman, R. E., 1993, Geologic map of the Skykomish River 30- by 60-minute quadrangle, Washington: U.S. Geological Survey Miscellaneous Investigations Series Map I-1963, 1 sheet, scale 1:100,000, 42 p. text. [<http://pubs.usgs.gov/imap/i1963/>]
- Tabor, R. W.; Frizzell, V. A., Jr.; Booth, D. B.; Waitt, R. B., 2000, Geologic map of the Snoqualmie Pass 30- by 60-minute quadrangle, Washington: U.S. Geological Survey Geologic Investigations Series Map I-2538, 1 sheet, scale 1:100,000, 57 p. text. [<http://pubs.usgs.gov/imap/i2538/>]
- Tabor, R. W.; Booth, D. B.; Vance, J. A.; Ford, A. B., 2002, Geologic map of the Sauk River 30- by 60-minute quadrangle, Washington: U.S. Geological Survey Geologic Investigations Series Map I-2592, 2 sheets, scale 1:100,000, with 67 p. text. [<http://pubs.er.usgs.gov/usgspubs/i/i2592>]
- Telford, W. M.; Geldart, L. P.; Sherrif, R. E., 1990, Applied Geophysics, 2nd edition, Cambridge University Press, Cambridge.
- Tepper, J. H., 2016, Eocene breakoff and rollback of the Farallon slab—An explanation for the Challis event?: Geological Society of America Abstracts with Programs, v. 48, no. 4, doi: 10.1130/abs/2016CD-274512.
- Tepper, J. H.; Clark, K.; Asmerom, Y.; McIntosh, W., 2004, Eocene adakites in the Cascadia forearc—Implications for the position of the Kula-Farallon ridge [abstract]: Geological Society of America Abstracts with Programs, v. 36, no. 6, p. 69.
- Thorson, R. M., 1989, Glacio-isostatic response of the Puget Sound area, Washington: Geological Society of America Bulletin, v. 101, no. 9, p. 1163-1174.
- Trehu, A. M.; Asudeh, Isa; Brocher, T. M.; Luetgert, J. H.; Mooney, W. D.; Nabelek, J. L.; Nakamura, Y., 1994, Crustal architecture of the Cascadia forearc: Science, v. 266, no. 5183, p. 237-243.
- Troost, K. G.; Booth, D. B.; Wisher, A. P.; Shimel, S. A., 2005, The geologic map of Seattle—A progress report: U.S. Geological Survey Open-File Report 2005-1252, version 1.0, 1 sheet, scale 1:24,000. [<http://pubs.usgs.gov/of/2005/1252/>]
- U.S. Geological Survey Geologic Names Committee, 2010, Divisions of geologic time—Major chronostratigraphic and geochronologic units: U.S. Geological Survey Fact Sheet 2010-3059, 2 p. [<http://pubs.usgs.gov/fs/2010/3059/>]
- Vance, J. A.; Dungan, M. A., 1977, Formation of peridotites by deserpentinization in the Darrington and Sultan areas, Cascade mountains, Washington: Geological Society of America Bulletin, v. 88, no. 10, p. 1497-1508.
- Vance, J. A.; Dungan, M. A.; Blanchard, D. P.; Rhodes, J. M., 1980, Tectonic setting and trace element geochemistry of Mesozoic ophiolitic rocks in western Washington: American Journal of Science, v. 280-A, p. 359-388.
- Varnes, D. J., 1978a, repr. 1995, Landslide classification system. In Dragovich, J. D.; Brunengo, M. J., Landslide map and inventory, Tilton River-Mineral Creek area, Lewis County, Washington: Washington Division of Geology and Earth Resources Open File Report 95-1, 165 p., Plate 3. [http://www.dnr.wa.gov/publications/ger_ofr95-1_lewis_co_landslides_plates.pdf]; http://www.dnr.wa.gov/publications/ger_ofr95-1_lewis_co_landslides_text.pdf]
- Varnes, D. J., 1978b, Slope movement types and processes. In Schuster, R. L.; Krizek, R. J., editors, Landslides—Analysis and control: National Academy of Sciences Transportation Research Board Special Report 176, p. 11-33, 1 plate.
- Wang, K., 1996, Simplified analysis of horizontal stresses in a buttressed forearc sliver at an oblique subduction zone: Geophysical Research Letters, v. 23, no. 16, p. 2021-2024.
- Wang, K., 2000, Stress-strain 'paradox,' plate coupling, and forearc seismicity at the Cascadia and Nankai subduction zones: Tectonophysics, v. 319, no. 4, p. 321-338.
- Weaver, C. E., 1912, A preliminary report on the Tertiary paleontology of western Washington: Washington Geological Survey Bulletin 15, 80 p.
- Weaver, C. E., 1937, Tertiary stratigraphy of western Washington and northwestern Oregon: University of Washington Publications in Geology, v. 4, 266 p.
- Weaver, C. E., 1942, Paleontology of the marine Tertiary formations of Oregon and Washington—Part I, Coelenterata, Vermes, Echinodermata, Molluscoidea, Pelecypoda, Scaphopoda: University of Washington Publications in Geology, v. 5, pt. 1, 268 p.
- Wells, R. E.; Blakely, R. J.; Weaver, C. S., 1998, Tectonics and earthquake potential of Cascadia—Effects of rotation and northward transport of forearc crustal blocks in Oregon and Washington [abstract]: Eos (American Geophysical Union Transactions), v. 79, no. 24, Supplement, p. W115.
- Wells, R. E.; Weaver, C. S.; Blakely, R. J., 1998, Fore-arc migration in Cascadia and its neotectonic significance: Geology, v. 26, no. 8, p. 759-762.
- Wells, Ray; Burkry, David; Friedman, Richard; Pyle, Doug; Duncan, Robert; Haessler, Peter; Wooden, Joe, 2014, Geologic history of Siletzia, a large igneous province in the Oregon and Washington Coast Range—Correlation to the geomagnetic polarity timescale and implications for a long-lived Yellowstone hotspot: Geosphere, July 14th, 2014, 28 p. doi:10.1130/GES01018.1.
- Werner, K. S.; Graven, E. P.; Berkman, T. A.; Parker, M. J., 1991, Direction of maximum horizontal compression in western Oregon determined by borehole breakouts: Tectonics, v. 10, no. 5, p. 948-958.
- Whetten, J. T.; Carroll, P. R.; Gower, H. D.; Brown, E. H.; Pessl, Fred, Jr., 1988, Bedrock geologic map of the Port Townsend quadrangle, Washington: U.S. Geological Survey Miscellaneous Investigations Series Map I-1988-G, scale 1:100,000. [http://ngmdb.usgs.gov/prodesc/proddesc_9030.htm]
- Wiebe, R. A., 1963, The geology of Mount Pilchuck: University of Washington Master of Science thesis, 53 p.
- Wiebe, R. A., 1968, Plagioclase stratigraphy—A record of magmatic conditions and events in a granite stock: American Journal of Science, v. 266, no. 8, p. 690-703.
- Williams, I. A., 1998, U-Th-Pb Geochronology by ion microprobe. In McKibben, M.; Shanks, W.; Ridley, W., editors, Applications of Microanalytical Techniques to Understanding Mineralization Process: Reviews in Economic Geology, v.7, p. 1-48.
- Williams, I. S.; Compston, W.; Black, L. P.; Ireland, T. R.; Foster, J. J., 1984, Unsupported radiogenic Pb in zircon—a cause of anomalously high Pb-Pb, U-Pb and Th-Pb ages: Contributions to Mineralogy and Petrology, v. 88, no.4, p.322-327.
- Wolfe, J. A.; Forest, C. E.; Molnar, P., 1998, Paleobotanical evidence of Eocene and Oligocene paleoaltitudes in midlatitude western North America: Geological Society of America Bulletin, v. 110, no. 5, p. 664-678.
- Yeats, R. S.; Engels, J. C., 1971, Potassium-argon ages of plutons in the Skykomish-Stillaguamish areas, North Cascades, Washington: U.S. Geological Survey Professional Paper 750-D, p. D34-D38. [<http://pubs.er.usgs.gov/publication/pp750D>]
- Zoback, M. L., 1992, Constraints on intraplate deformation. In Jacobson, M. L., compiler, National Earthquake Hazards Reduction Program, summaries of technical reports Volume XXXIII: U.S. Geological Survey Open-File Report 92-258, p. 749-754.

Appendix A. Infrared Stimulated Luminescence Age Data

Infrared Stimulated Luminescence ages for sediment samples are presented in Table A1. See Dragovich and others (2011b) for a discussion of the infrared stimulated luminescence methodology. Petrographic and geochemical examination of sand from the age sites, combined with deposit stratigraphy, indicate Cascade Range (ancient Pilchuck River) provenance (PP; Table 1) is indicated for these deposits mapped in the Pleistocene Explorer Falls and Bosworth Lake basins. PP deposits include sediments of the Whidbey Formation, Hamm Creek formation and pre-Hamm Creek formation interglacial interval (units Qcwpv, Qch, and Qcph). The sample inventory in the Data Supplement spreadsheet provides the list of the various geochronology and geochemistry samples analyzed during our study including samples with multiple analyses.

Table A1. Infrared stimulated luminescence ages (IRSL) from the Granite Falls 7.5-minute quadrangle, including elemental concentrations, total dose rates, equivalent doses, and ages from fine-grained feldspar using post infrared IRSL. Sample numbers are bold. See map sheet for sample locations. Gy, Gray (unit of absorbed radiation creating luminescence); WMB, Western mélange belt; PP, Pilchuck River provenance (Table 1). See Description of Map Units for further information and Appendix D for sand geochemistry of the indicated age sites. Analyses performed by Shannon Mahan, USGS.

IRSL Sample ID (geologic unit)		Water content (%) ^a	K (%) ^b	U (ppm) ^b	Th (ppm) ^b	Equivalent dose (Gy)	Total dose rate (Gy/ka)	Age ^d
33A (Qch)		11 (42)	1.04 ±0.04	1.10 ±0.15	2.92 ±0.34	436 ±55.8	1.84 ±0.11	237 ±33.6
TRS	sec. 8, T27N R7E	Dense, thinly bedded medium and fine sand with silt. Mica rich (~20%) with significant subangular to angular monocrystalline quartz (~20%). Has some polycrystalline quartz (~10%), plagioclase (~10%), metasedimentary lithic grains (~10%), substantial hornblende (~10%) and noteworthy potassium feldspar (4%). Other lithic grains include sedimentary, granitic, and volcanic lithic grains (~10%) as well as greenstone (2%). Other noted grains are epidote, pyroxene, and opaque minerals (~4-5%). Likely PP provenance with monocrystalline quartz, hornblende, white mica, and biotite. The occurrence of charcoal fragments in the sand is also suggestive of a nonglacial deposit. Relatively strong granitic provenance may indicate tapping of the broader Pilchuck River basin (Dragovich and others, 2015) and erosion of the extensive Index batholith and thus overcoming the low drainage divide with Spada Lake of the Sultan River basin in the Late Pleistocene (MIS 7). See Appendix C for sand geochemistry of sample 33A.						
Lat/long. (degrees)	47.960233 -121.968986							
Elev. (ft)	~535							
Material	sand to silt							
Provenance	PP							
33B (Qch)		11 (36)	1.76 ±0.05	1.18 ±0.23	5.38 ±0.55	786 ±114	2.99 ±0.18	263 ±40.6
TRS	sec. 8, T29N R7E	Dense, massive weathered silt, sand and pebbly sand. Petrographically, sand contains monocrystalline quartz (~25%), polycrystalline quartz (~15%), metasedimentary clasts (~20%), plagioclase (~15%) and mica (~10%). Also contains potassium feldspar (~5%), granitic lithic grains (~5%), volcanic lithic/greenstone grains (~3%) and hornblende grains (~2%). May contain some sedimentary clasts. Relatively high metasedimentary grain content and overall polymitic composition consistent with proximity of this deposit with interbedded, locally-derived Qcph. The relatively high mica, monocrystalline quartz, granitic lithic content and hornblende content overall is consistent with PP basin provenance. Sediment does not contain brown oxide or other weathering products that are relatively abundant in the older part of the Early to Middle Pleistocene part of the Explorer Falls basin. For example, compare to unit Qcph of Dragovich and others (2015). See Appendix C for sand geochemistry of sample 33B. This IRSL age on feldspars is heavily weighted toward the younger grain population (9 of 20 aliquots; 790 Gy or 263 ka). The other population of equivalent doses (natural luminescence) returns an age of 322 ka (OIS9). The range of ages for the feldspar post IR-IRSL is 222-304 ka and we suspect the sample is closer to 300 ka due to the weathering of the grains and the substantially dominant older IRSL population subset although it is impossible to rule out that the older IRSL ages could be a result of partial bleaching during transport.						
Lat/long. (degrees)	48.013114 -121.926058							
Elev. (ft)	~615							
Material	coarse sand							
Provenance	PP							
33D (Qcwpv)		18 (40)	1.14 ±0.04	1.27 ±0.24	3.27 ±0.29	336 ±28.5	2.87 ±0.16	117 ±12
TRS	sec. 2, T28N R7E	Dense medium to coarse sand and pebbly coarse sand with lenticular interbeds of silt in a large outcrop above the Pilchuck River. These nonglacial beds are overlain by gravelly silt of unit Qglv. Sand contains metasedimentary clasts (~22%), monocrystalline quartz (~20%), polycrystalline quartz (~15%), and plagioclase (~10%) with some potassium feldspar (~8%) and hornblende (~5%). Variable lithic grains including volcanic lithic grains/greenstone (~5%) and granitic lithic grains (~5%). Contains minor metamorphic and sedimentary lithic grains (~5%) and a few pyroxene, serpentine, epidote and chlorite grains (~5%). Overall looks like PP provenance with a distinct mélange and granitic source. The relatively high percentage of metasedimentary and polycrystalline quartz grains with minor serpentine clasts suggests a partial local contribution from the nearby highlands. See Appendix C for sand geochemistry of sample 33D. OSL on quartz was also performed using thermal transfer-OSL and the age was 117 ±19 ka, confirming the feldspar age.						
Lat/long. (degrees)	48.026236 -121.882289							
Elev. (ft)	~570							
Material	silt and sand							
Provenance	PP							

IRSL Sample ID (geologic unit)		Water content (%) ^a	K (%) ^b	U (ppm) ^b	Th (ppm) ^b	Equivalent dose (Gy)	Total dose rate (Gy/ka)	Age ^d
33E (Qc _H)		19 (35)	1.05 ±0.04	1.34 ±0.20	4.32 ±0.30	273 ±20.5 ^e	1.61 ±0.08 ^e	170 ±15 ^e
TRS	sec. 36, T30N R6E	Dense massive to subtly laminated silty sand, sandy silt and silt with rare very thin lenticular pebble beds containing some vein quartz. A thin-section of a silty fine sand bed reveals abundant angular monocrystalline quartz (~25%) and white mica and biotite (~30%), with lesser plagioclase (~10%) and some polycrystalline quartz (~5%) in a silty fine matrix (~20%) with brown cryptocrystalline weathering masses (~10%). Also contains a trace of tourmaline, epidote and chlorite. Other sand petrography samples from unit Qc _H in the Bosworth Lake area also suggest PP provenance with much mica, monocrystalline quartz, plagioclase and some polycrystalline quartz, potassium feldspar and a trace of tourmaline (up to 4%). Some of the mica from this sample could be eroded from phyllite in the eastern or western mélange belts to the east. The range of ages for the quartz TT-OSL is 155-185 ka and we suspect the sample is closer to 185 ka due to the weathering of the grains and the substantially dominant older OSL population subset although it is impossible to rule out that the older OSL ages could be a result of partial bleaching during transport						
Lat/long. (degrees)	48.032455 -121.988719							
Elev. (ft)	~581							
Material	Silty sand and silt							
Provenance	PP							
34B (Qc _H)		24 (56)	1.11 ±0.05	1.38 ±0.26	4.20 ±0.40	335 ±36.9 ^e	1.53 ±0.09 ^e	218 ±29.5 ^e
TRS	sec. 1, T29N R6E	Dense, stratified sand, silt, and organic silt. Strata are mostly thinly bedded, tilted to the west, and contain flattened sedge fossils along bedding planes. Sands are composed of monocrystalline quartz (~20%), mica (~20%), plagioclase (~20%), polycrystalline quartz (~7-8%) and hornblende (~5%) with some potassium feldspar (~3%). Contains variable lithic grains (~15%) including some volcanic lithic grains/greenstone as well as scattered brown, cryptocrystalline weathering products between the sand grains (~10%). We also noted a few pyroxene and high grade metamorphic clasts. This sand has a dominant granitic Cascade source similar to other PP deposits. Volcanic lithic grains were likely partially derived from Eocene volcanic sources to the east or northeast. The proportion of metasedimentary lithic grains is low relative to average PP provenance sands but some mica found in this sample is likely from phyllite or other metasedimentary mélange sources as noted for other Qc _H and Qc _{PH} sands in the map area. See Appendix C for sand geochemistry of sample 34B.						
Lat/long. (degrees)	48.039116 -121.972343							
Elev. (ft)	~642							
Material	medium sand to silt							
Provenance	PP							
34D (Qc _{WPV})		16 (32)	1.11 ±0.04	1.25 ±0.22	3.75 ±0.29	179 ±13.4	2.13 ±0.11	83.9 ±5.15
TRS	sec. 3, T30N R7E	Dense, laminated to thickly bedded, medium and fine sand, with silt exposed in a large river bank exposure adjacent to Canyon Creek in the northeast part of the map area. Sand samples are composed of monocrystalline quartz (20%), plagioclase (15%), polycrystalline quartz (~15-25%), with some potassium feldspar (5%) and hornblende (~2-3%). Lithic grain types include volcanic lithic grains/greenstone (~10%), sedimentary/metasedimentary lithic grains (~13%) and granitic/metamorphic lithic grains (~5%). Contains minor epidote, opaque mineral grains and pyroxene (~5%) and rare tourmaline. Sands differ substantially from the composition of modern Canyon Creek alluvium (unit Qa) next to the Qc _{WPV} deposit. Unit Qa is rich in mélange belt lithic detritus. Unit Qc _{WPV} sands here have a general PP composition but with a diverse lithic clast composition more consistent with the expansive Pilchuck Valley mélange belt and granitic sources.						
Lat/long. (degrees)	48.123227 -121.891541							
Elev. (ft)	~580							
Material	sand to silt							
Provenance	PP							

^a Field moisture, with figures in parentheses indicating the complete sample saturation %. Ages calculated using approximately 50% of saturation values.

^b Analyses obtained using high-resolution gamma spectrometry (HPGe detector).

^c Cosmic doses and attenuation with depth were calculated using the methods of Prescott and Hutton (1994). See text for details. Cosmic doses varied from 0.19 to 0.05 Gy/ka.

^d Dose rate and age for fine-grained 250–180 microns K-feldspar, post IR2³⁰C; fade of 3.4%/decade. Exponential + linear fit used on equivalent dose; age was generated from the weighted mean, errors to one sigma; ages and errors rounded.

^e Dose rate and age for fine-grained 250–180 micron sized quartz. Exponential + linear fit used on single aliquot regeneration equivalent doses; age was generated from the weighted mean, errors to one sigma; ages and errors rounded. The quartz was run as thermal transfer-OSL using protocols from Brown (2013).

Appendix B. Seismicity in and near the Granite Falls 7.5-minute Quadrangle

We present earthquake epicenters and focal mechanisms reported by the Pacific Northwest Seismic Network (PNSN) around the Granite Falls quadrangle to provide a sense of fault movement at depth. See Data Supplement for the earthquake data. This broader area (Fig. B1) contains 507 epicenters and 55 focal mechanisms, including 33 previously unpublished focal mechanisms. Hypocenter depths less than 40 km are interpreted as crustal events. The focal mechanisms, along with ternary plots of the Carpenter Creek fault zone events are depicted in Figures B1 and B2 using the RFOC software package of Lees (1999, 2007, and 2008) in which the 20 new focal mechanisms were calculated in SEISAN Earthquake Analysis package (Ottomoller and others, 2016)[<http://seisan.info>]. The 20 additional focal mechanisms were determined using the FPFIT method (Reasenber and Oppenheimer, 1985) by picking first-motion P-wave polarities on the vertical component of seismograms gathered from the Incorporated Research Institutions for Seismology (IRIS)[<http://www.iris.edu>]. A constant seismic-velocity model of the Puget Sound was assumed during all analyses, as well as consideration for possible reversed polarity seismic stations during each event. In addition, we deployed two portable seismographs near the southeastern corner of the quadrangle in an effort to provide additional constraints to seismogenic events recorded at stations S1 and S2 shown in Fig. M3. Three crustal events were recorded near the map area during the span of this project (since July 2015), but were not significant enough to provide any further sense of fault movement in the mapping area.

Earthquake hypocenters in the area are concentrated in the southern portion of the Granite Falls Quadrangle, and in the Lake Roesiger, Lake Chaplain, and Verlot, quadrangles to the south, southeast and east, respectively. Earthquake activity in the northern portion of the Granite Falls Quadrangle is relatively limited, and generally restricted to very shallow (possibly quarry blast) events.

In the southern portion of the Granite Falls Quadrangle, there is a NE–SW trending cluster of hypocenters at depths typically between 12 and 20 km. This east-northeast concentrated band of seismicity was informally named the Carpenter Creek earthquake cluster by Dragovich and others (2015) and was attributed to displacement along the Carpenter Creek fault bounding the northern extent of the Explorer Falls basin (EFB) (see Carpenter Creek Fault). In the EFB, both the Three Lakes Hill fault and the Carpenter Creek fault are spatially associated with relatively shallow earthquakes (Dragovich and others, 2015). We tentatively project the Carpenter Creek fault into the adjoining Verlot quadrangle along a lineament observed in lidar (Fig. 1), and follow the suggestion of Dragovich and others (2015) that this fault is associated with the Carpenter Creek earthquake cluster located just south of the lineament (Fig. B1). Although further work is required, the correlation of this cluster with the Carpenter Creek fault is generally strengthened by: (1) the number of reverse-offset focal mechanisms in the cluster (Fig. B2), (2) our new mapping of the Pilchuck River

growth fold directly south of the Carpenter Creek fault, and (3) geologic evidence that suggests the basin-bounding fault for the EFB strikes northeast and dips steeply south in this area. (See *Explorer Falls Basin and Carpenter Creek Fault* for further information). Our local seismic array detected the July 1st, 2016 moderate earthquake (M3.4) generally northeast of Lake Roesiger. This earthquake as well as the temporally related smaller earthquakes are included in the Carpenter Creek earthquake cluster because overall all instrumental historical data show the CCF area has a cluster of earthquakes that we generally relate to the Carpenter Creek fault at depth. However, the 35 recent earthquakes generally northeast of Lake Roesiger are likely a main-shock and aftershock sequence.

The Pilchuck River fault (PRF) follows a NW-SE trend along the southern flank of Mount Pilchuck to the east of the Granite Falls Quadrangle. As mapped by Tabor and others (2002), the PRF is shown to be cut by the Eocene Mount Pilchuck stock and thus inactive. However, Weibe (1963) mapped the fault as cutting the Mount Pilchuck stock, suggesting deformation that was synchronous with or post-dated Eocene intrusion. Strong topographic lineaments along portions of the PRF, visible on lidar, might be fault scarps, and may indicate young Quaternary displacement along the fault (Ralph Haugerud, USGS, written commun., 2016). Earthquake hypocenters along the trace of the PRF are sparse and of generally very small magnitude (≤ 1.0) and thus we interpret this seismicity dataset as lacking conclusive evidence for modern activity along the PRF.

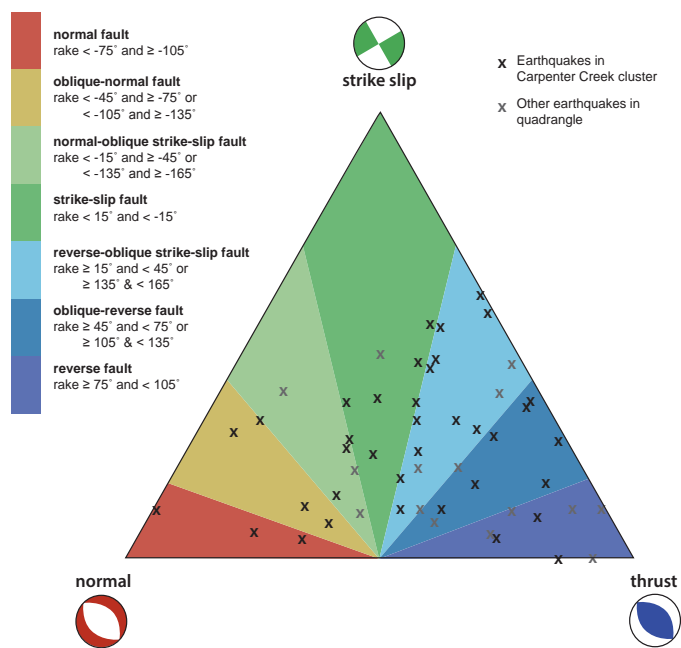


Figure B2. Earthquake focal mechanism ternary diagram.

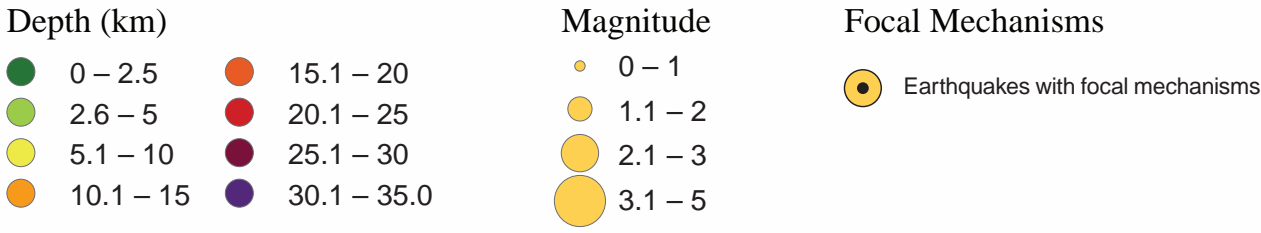
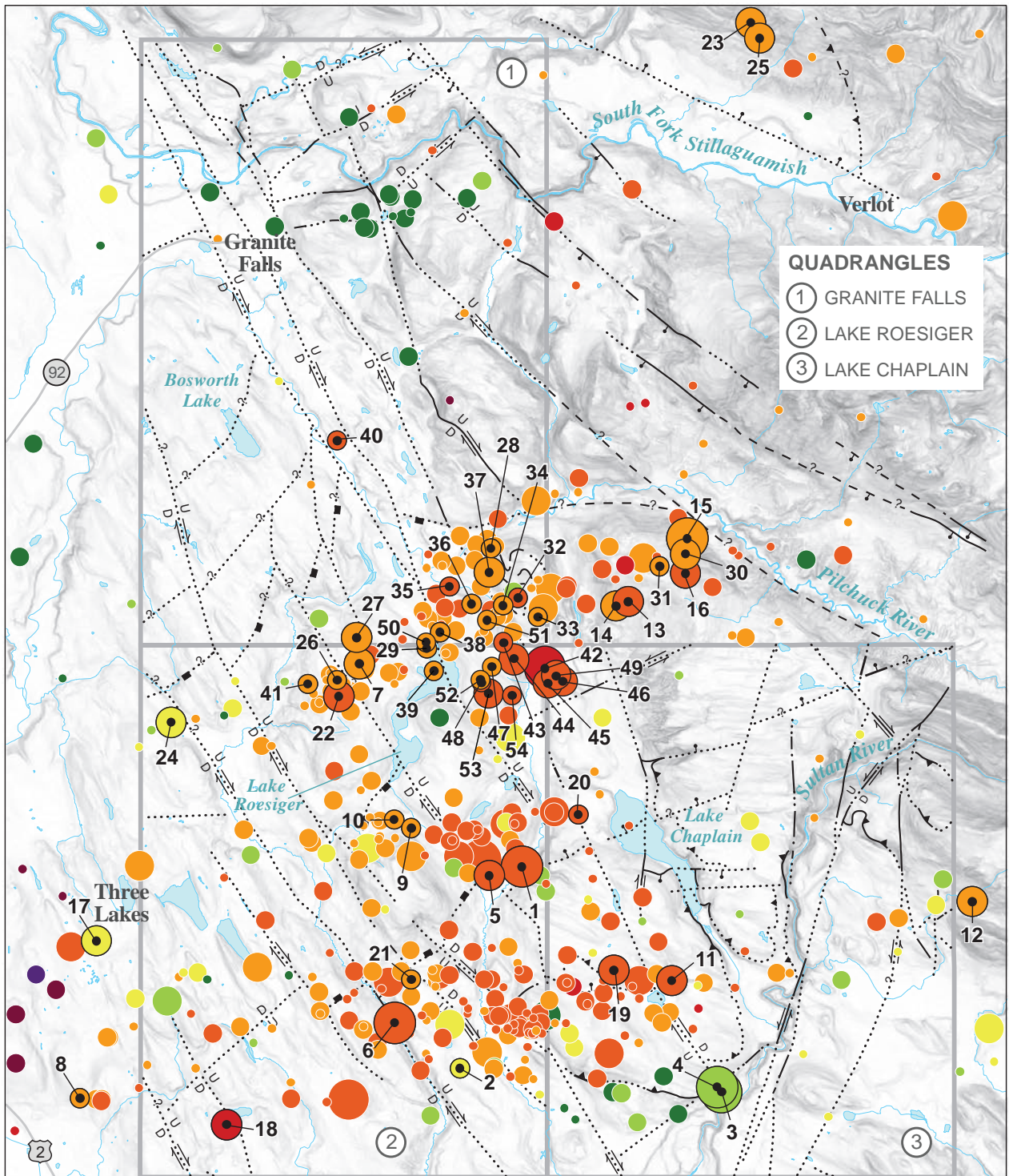


Figure B1. Earthquake epicenters in and around the Granite Falls, Lake Roesiger, and Lake Chaplain 7.5-minute quadrangles (gray boxes) with focal mechanisms for selected seismic events. Faults are simplified from our current mapping (see Map Sheet for explanation of fault symbology), Whetten and others (1988), Tabor and others (2002), and Dragovich and others (2014a, 2015).

Appendix C. U-Pb Zircon Geochronology

Methods

See Data Supplement for the single zircon U-Pb data. The sample inventory in the Data Supplement spreadsheet provides the list of the various geochronology and geochemistry samples analyzed during our study including samples with multiple analyses.

We separated zircons using standard crushing, gravimetric, and magnetic techniques. Zircon grains were randomly selected for analysis and annealed at 1,000° C for 48 hours. After cooling we mounted the grains in a standard 1-in. epoxy grain mount which was polished to expose the grain centers. Cathodo-luminescence images were taken to aid in identifying suitable areas for analysis, avoiding areas such as cracks, inherited cores, inclusions, and metamorphic zones.

Analyses were conducted at the Canadian Centre for Isotopic Microanalysis (CCIM) plasma mass spectrometry lab using procedures modified from Simonetti and others (2005). The analytical setup consists of a New Wave UP-213 laser ablation system and DSN-100 desolvating nebulizer “Y connected” to a Nu I plasma multi-collector inductively coupled plasma mass spectrometer (MC-ICPMS). We operated the laser at 40 µm beam diameter, 4 Hz repetition rate at a fluence of ~3 J/cm². Data were collected statically in 30 one second integrations. Prior to and during each analytical session we analyzed zircon reference materials GJ1 (Jackson and others, 2004) and 94-35 (Klepeis and others, 1998) repeatedly to correct for U-Pb fractionation and instrument bias/drift, and to assess data quality. During all analyses a 0.5 ppb Tl solution was aspirated using the DSN-100. The simultaneous measurement of Tl allows estimation of Pb isotope mass bias (β) by applying an exponential mass fractionation law, assuming $\beta_{Tl} \approx \beta_{Pb}$, and a natural ²⁰⁵Tl/²⁰³Tl of 2.3871. For further details, see Simonetti and others (2005).

All data were reduced offline using an Excel-based program. The uncertainties we report here are a quadratic combination of the standard error of a single measurement and the standard deviation of the zircon reference means. Overall standard reproducibility is approximately 3% (2 σ) for ²⁰⁶Pb/²³⁸U and ~1% for ²⁰⁷Pb/²⁰⁶Pb. For young zircons only ²⁰⁶Pb/²³⁸U ages are reported due to the low abundance of ²⁰⁷Pb. We corrected for common Pb using the “²⁰⁷Pb” method (Williams, 1998) which assumes grains are concordant, but does not require accurate measurement of ²⁰⁴Pb, which is difficult due to ²⁰⁴Hg present in the argon gas of the ICP. For all but a few analyses, the resulting ²⁰⁶Pb/²³⁸U ages are well within analytical uncertainties of the apparent ages. We calculated intercept ages and plotted concordia diagrams using the software of Ludwig (2003).

Sample 15-26H—Rhyolite of Hansen Lake (Unit Evr)

We obtained a sample along the bank of the Pilchuck River southwest of the town of Granite Falls (site 26H on map

sheet). The results are shown in Figure C1 and Supplementary Table C. These “rhyolites” are very well exposed along the Pilchuck River southwest of the City of Granite Falls where they form 2–10-meter-high outcroppings that follow the river for at least 100 m. The flows are mostly massive and homogeneous, but sometimes exhibit columnar jointing or locally brecciated flow tops and are geochemically classified as trachyandesites to dacites (Appendix D). Individual flows are many meters thick. The rubby flow tops and columns both indicate that the flows dip 60–70° to the north. See the ‘Pilchuck Bend Formation’ described by Danner (1957) for further field observations. Petrographically these flows display radiating plagioclase (35%) forming both microphenocrysts as well as few larger euhedral phenocrysts that are up to 3–4 mm long. These phenocrysts strongly replaced by calcite locally. Quartz (30%) occurs as individual microphenocrysts as well as a disseminated interstitial and fine-grained matrix with some disseminated, fine-grained potassium feldspar (22%). A few small grains of subhedral potassium feldspar also noted. Interstitial glass is replaced by fine clear green chlorite (10%). Also contains accessory sphene and opaque minerals (3%). Completely chloritized grains might be relict mafic microphenocrysts. The age and composition of these flows and the nearby Granite Falls Stock suggest they are broadly genetically related 43–44 Ma igneous bodies that intruded into or near the Granite Falls fault zone. See Appendices D and E for whole rock and isotope geochemistry for this andesite sample and Regional and Local Eocene Tectonics and Magmatism for a discussion of contemporaneous magmatic units.

Sample 15-40W#1—Dike of unit Eian

A family of east-northeast trending Eocene dikes intrude the steep structural grain of the Iron Mountain fault zone. Dikes are widespread and exceptionally well-exposed in the expansive Iron Mountain quarry where rhyolitic to dacitic porphyry dikes and medium-grained granodiorite dikes form igneous injection features that are typically ~2–10 meters wide. These dikes intrude sub-vertical, ENE-trending cataclastic fault and fracture zones that are extensively exposed on the mountain. Hydrothermal alteration zones are also east-northeast trending and are common on the property. (See Iron Mountain Fault Zone for further information.) The dacite/rhyolite (Appendix D) porphyry dike at site 15-40W#1 is shown in Figure 5.

The sampled porphyry contains blocky, subhedral to euhedral plagioclase (up to 4 mm, 37%) sitting in chloritized glass (50%) containing substantial microphyritic plagioclase, a few small anhedral quartz grains (8%) and opaque minerals (5%). A trace of disseminated potassium feldspar occurs in the glass and minor calcite and epidote occur as replacement minerals. This rock is hydrothermally altered with strong chloritization and some sericite. Other porphyry dike samples examined from the Iron Mountain quarry are of similar composition.

Sample 15-28AF—Volcaniclastic Metasandstone in the Western Mélange Belt

We sampled a massive, coarse grained, volcaniclastic metasandstone (unit KJms_w) from the central part of the map area directly east of the Boyd Lake fault. Samples were obtained from a 2–8 meter high road cut outcropping. These sandstones contain subangular to angular plagioclase (25–35%), monocrystalline quartz (25%) and volcanic lithic grains (25–45%) with scattered augite grains (3–8%). Contains some metamorphic chlorite and pumpellyite (3–7%). Many of the detrital grains are locally embayed volcanic quartz. A volcanic provenance for these sandstone beds is suggested by the mineral and lithic composition (intermediate to felsic volcanic lithic grains, augite and embayed quartz). A simple volcanic provenance for these metasandstone as indicated by the individual zircon age peak, volcaniclastic nature and lack of exotic detrital minerals in the petrographically examined metasandstones at or near the sample site. See Appendices D and E for whole rock and isotope geochemistry for this metasandstone sample. We are unsure if the one Precambrian zircon is the result of contamination or reveals a limited cratonal detrital source near the arc.

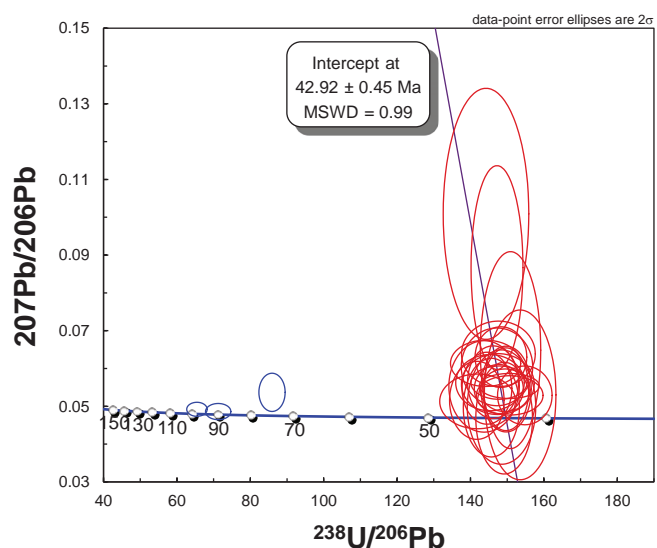


Figure C1. Concordia diagram for sample 15-26H (unit Evr), collected in the Pilchuck river southwest of the town of Granite Falls. Blue ellipses are thought to represent xenocrystic zircon grains of an unknown origin, perhaps inherited into ascending magma from country rock. Data point error ellipses are 2σ

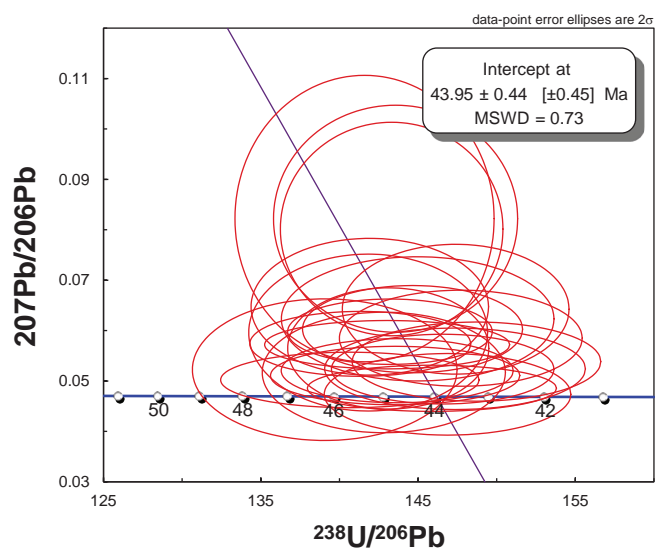


Figure C2. Concordia diagram for sample 15-40W#1 (unit Eian), a porphyritic dike sampled in the Iron Mountain Quarry east of the town of Granite Falls. Data point error ellipses are 2σ

Table C1. Regional detrital zircon age information for the five dated Western mélange belt (WMB) samples. See Figure C3 for compiled zircon age histograms. See Jett and Heller (1988) for description of arkosic and lithic metasandstone petrofacies; their lithic petrofacies is similar to the volcanic (arc) provenance of Dragovich and others (2014a, 2015). The three youngest (late Cretaceous) arkosic facies samples are below the Lake Chaplain nappe. Because of the mid-Cretaceous volcanic lithic meta-argillite is near the Lake Chaplain nappe (but is complicated by Eocene strike-slip fault deformation); the oldest Jurassic volcanic lithic sandstone is above the nappe.

Sample (depositional petrofacies)	Maximum depositional age	Major detrital minerals	Precambrian (cratonic) provenance	Reference and notes
13-35J (Arkosic)	74 Ma	Monocrystalline quartz (~40%), plagioclase (~40%), and potassium-feldspar (~20%) rich with lesser but significant biotite and mica (~15%) with a trace of granitic lithic grains.	Precambrian peaks at ~1375 and ~1680 Ma	Dragovich and others (2014a) who suggest that the two-mica granitic source for this petrofacies might be the Idaho Batholith. Similarly, Dumitru and others (2016) demonstrate that “Oage peaks at 1800–1650 and ~1380 Ma [the ‘Lemhi doublet’ of their Type E zircon age distribution] Oare indicative of a sediment source region in the southern part of the Proterozoic Belt Supergroup basin in central Idaho, which hosts 1800–1650 Ma detrital zircons and which was intruded by rift-related 1380 Ma bimodal plutons and sills.”
WMB-1 (Arkosic)	87 Ma	Quartz (~35%), potassium feldspar and plagioclase (~60%), siltstone–shale lithic grains (~5%), and volcanic lithic grains (trace).	Precambrian zircon grains dated at 1128, 1360, 1843, 1849, and 2306 Ma	Brown (2012) notes that “Jett and Heller’s (1988) point count analysis of 34 samples of arkosic rocks from this area indicates (percentages with standard deviation) the following: monocrystalline quartz, 32 ±6; plagioclase, 47 ±5; K-feldspar, 5 ±5, lithic fragments, 16 ±7.”
08-45J (Arkosic)	87 Ma	Monocrystalline quartz, potassium feldspar, plagioclase, chert scattered muscovite and some chlorite in minor matrix; scattered microlitic volcanic lithic clasts and few sedimentary lithic clasts; rare green or brown detrital hornblende	Devoid of Precambrian detrital zircons	Dragovich and others (2009b). Sample located east of Tokul Creek in the northeastern part of the Snoqualmie quadrangle. Well bedded grey-green lithic wacke metasandstone with distinct turbidite planar bedding and distinct thin to thick beds of black meta-argillite with little or no fracturing or faulting. Strong stratification and stratification combined with the low amount of strain indicates large block of undisturbed metasediments within mélange. No mélange matrix observed in the immediate area. Mature composition and angularity of grains suggests 1 cycle sediments for most grains.
14-39S (Lithic volcanic arc)	110 Ma	Monocrystalline quartz (~30%), plagioclase (~25%), polycrystalline quartz (~15%), lithic fragments dominated by felsic to intermediate microlitic volcanic grains (~20%), and some detrital mica. Metamorphic minerals include epidote, chlorite, and pumpellyite	Eleven Precambrian zircon grains dated between 1032 and 2121 Ma.	Dragovich and others (2015). Sample is from a 1–3 m-high outcrop; whole-rock geochemistry and has a mafic volcanic arc affinity. This sample occurs within the Woods Creek fault zone and is locally strongly fractured. The outcrop exposes meta-argillite, locally with thin sub-vertical beds of fine-grained lithofeldspathic metasandstone that strike northwest and parallel the Woods Creek fault zone. A moderately strong cleavage is sub-parallel to the discontinuous bedding. Metagabbro is faulted against these metasedimentary rocks on the west side of the property.
15-28AF (Lithic volcanic arc)	166 Ma	Plagioclase (25-35%), monocrystalline quartz (25%) and volcanic lithic grains (25-45%) with scattered augite grains (3-8%); some metamorphic chlorite and pumpellyite (3-7%). Many of the quartz grains are embayed volcanic quartz.	The one Precambrian zircon might be the result of contamination.	This study. An Island arc depositional environment distal to the craton is suggested by the detrital zircon age information in combination with field mapping and metasandstone geochemistry. Depositional age is similar to the 150-170 Ma age for the WMB intrusive (arc) rocks of the complex.

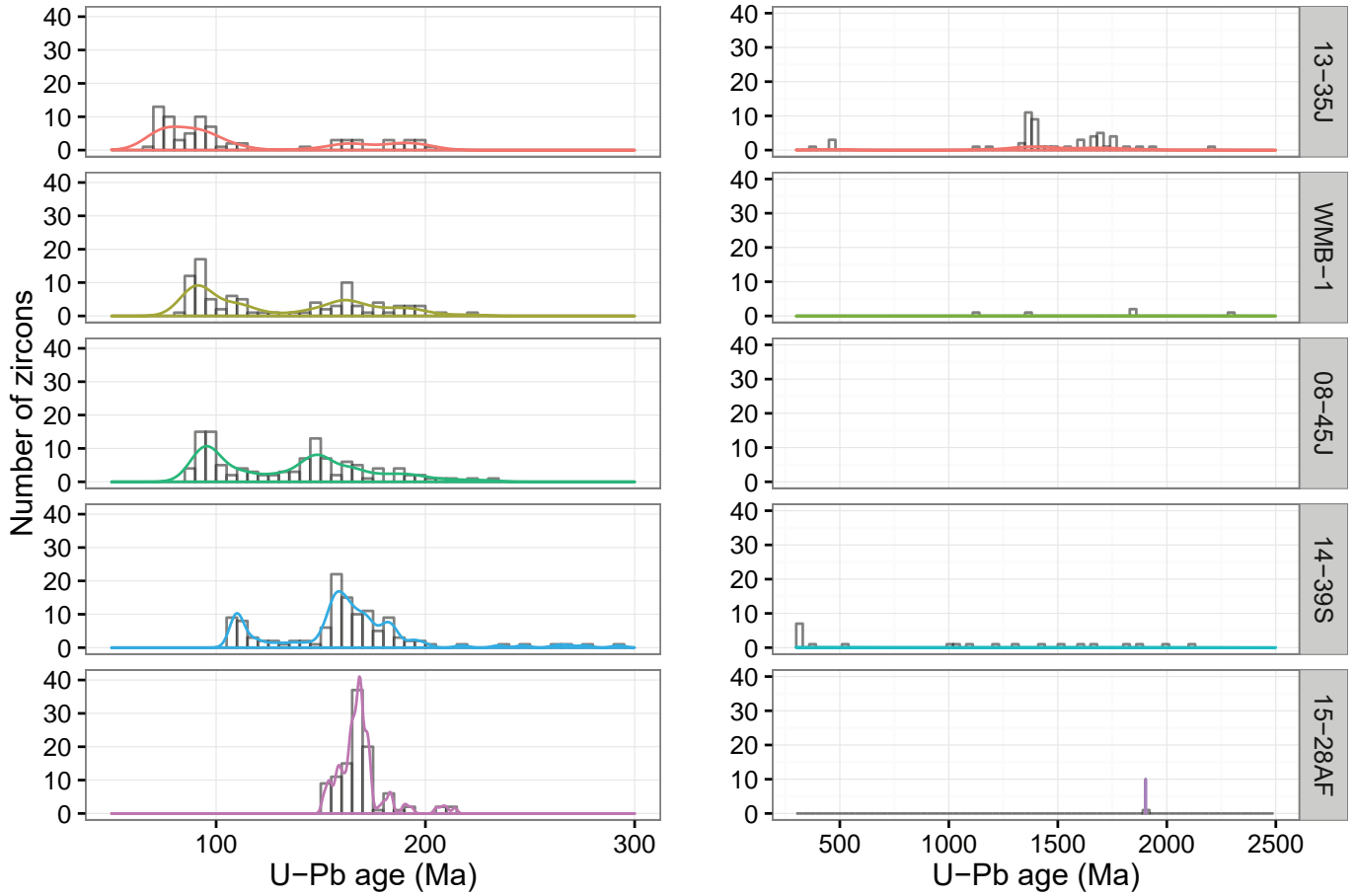
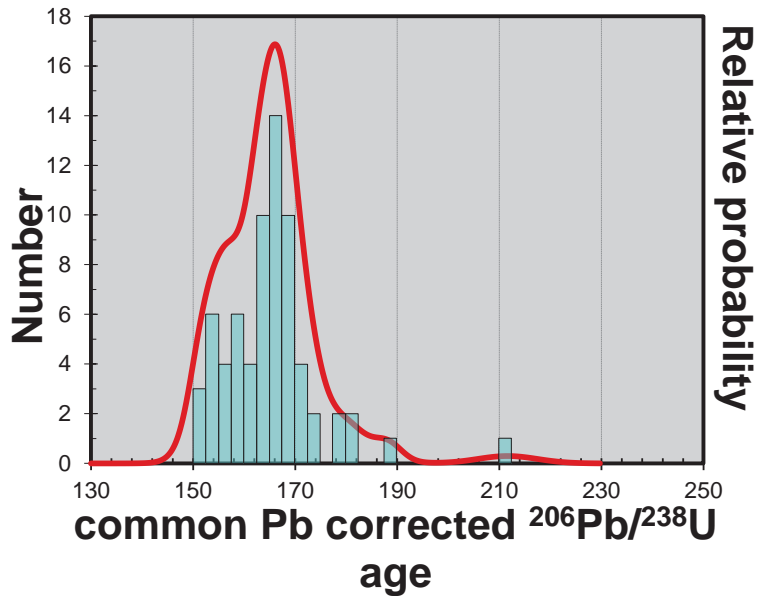


Figure C3. Probability density plot with histogram for all WMB metasandstone samples. See Table C1 for individual sample information and interpretation. Age is generally inversely correlated with structural level within the WMB consistent accretionary tectonics and thrusting.

Figure C4. Probability density plot for sample 15-28AF, a volcanoclastic metasandstone of the Western mélangé belt. The significant age population is noted at 165.6 ± 1.4 Ma. See Figure C3 and the *Data Supplement* for the one Precambrian zircon age obtained from this sample.



Appendix D. Geochemical Data

The data is presented in the Data Supplement. The sample inventory in the Data Supplement spreadsheet provides the list of the various geochronology and geochemistry samples analyzed during our study including samples with multiple analyses.

Whole-rock major- and trace-element analyses were performed on nonglacial sand and rock using x-ray fluorescence (XRF) and inductively coupled plasma source mass spectrometry (ICP-MS) at the GeoAnalytical Laboratory of Washington State University (WSU). Grinding of samples was completed at WSU using a tungsten carbide mill for XRF analyses and iron equipment for ICP-MS analyses. Estimates of accuracy and precision, as well as discussion of analytical methods for both XRF and ICP-MS at WSU, are given by Johnson and others (1999) and Knaack and others (1994), respectively. We prepared the Quaternary sand with 2 mm (mesh no. 10) and 0.075 mm (mesh no. 200) sieves at the DNR laboratory in Olympia, Washington prior to grinding at WSU, so that only the sand-size fraction was chemically analyzed. Although most nonglacial samples were well-sorted sand, sieving provides a better comparison between sand samples, eliminating or reducing erroneous results that may ensue from inclusion of fines and pebbles in the sand samples. As part of their quality check, WSU re-analyzed sample 15-8G and 15-33A using both XRF and 15-8G for ICP-MS methods. We present an average for both analyses in the Data Supplement. An additional suite of 12 samples were pulverized in an alumina shatterbox at the University of Puget Sound and then analyzed for trace elements by ICP-MS at ALS Minerals (Vancouver, B.C.). Three of these samples (15-4E, 15-26B, and 15-28D) were also analyzed by WSU and allow for inter-lab data comparison.

Table E1. Nd and Sr isotopic data. Errors shown in table are within-run statistics and represent error in the last significant digits. External reproducibility (σ) for Nd = ± 30 ppm and for Sr = ± 30 ppm. Sr and Nd isotope compositions are normalized to $^{86}\text{Sr}/^{88}\text{Sr} = 0.1194$ and $^{146}\text{Nd}/^{144}\text{Nd} = 0.7219$, respectively. $\epsilon\text{Nd}(t)$ is deviation from chondritic $^{143}\text{Nd}/^{144}\text{Nd}$ at the time of emplacement in units of parts per 10,000, assuming a present day ratio = 0.512638. Element concentrations (in ppm) are by inductively coupled plasma–mass spectrometry. Map unit ages (used in initial ratio calculations) are from this study except as follows: (1) Eian is assumed to be the same age as Eigd based on field relations, (2) Ages assigned to KJms_w samples 28G and 28D are those of Eigd; this is to assess whether these argillites were the source of Eigd magmas, (3) Bald Mountain age is from Tabor and others (2002), and (4) Mt. Pilchuck age is from M.P. Eddy (written communication, 2016). TDM is the depleted mantle model age (or crustal residence time) and is an estimate of the time elapsed since the Nd in the sample was extracted from the mantle. In the case of felsic rocks that formed by crustal melting, the TDM provides an estimate of the age of the source rocks.

Sample #	Latitude and Longitude	Map Unit	Age (Ma)	$^{143}\text{Nd}/^{144}\text{Nd}$	$\pm 1\sigma$	Sm (ppm)	Nd (ppm)	$^{143}\text{Nd}/^{144}\text{Nd}_i$	$\epsilon\text{Nd}(t)$	$\pm 1\sigma$	TDM (Ma)	$^{87}\text{Sr}/^{86}\text{Sr}$	$\pm 1\sigma$	Sr (ppm)	Rb (ppm)	$^{87}\text{Sr}/^{86}\text{Sr}_i$
15-26A	48.102172	Contact complex along the South Fork Stillaguamish River.														
	-121.951382	Eian	45.3	0.512793	10	3.42	13.6	0.512706	2.47	0.1	430	0.706787	12	211	74.2	0.706133
15-4E	48.102691	Medium grained hypidiomorphic granular biotite bearing hornblende granodiorite of the Granite Falls stock; collected along the Mountain Loop Highway.														
	-121.952393	Eigd	45.3	0.5129	11	3.2	14.2	0.512821	4.73	0.11	267	0.704068	14	243	42.5	0.703743
15-26G	48.102818	Medium grained hypidiomorphic granular biotite bearing hornblende granodiorite of the Granite Falls stock; collected near the Granite Falls fish ladder.														
	-121.954527	Eigd	45.3	0.512906	10	5.11	22.1	0.512825	4.81	0.1	256	0.704105	12	275	45.6	0.703796
15-28AF	48.065775	Western mélangé belt volcanoclastic metasandstone (not sample split; secondary sample at the same age site) (Appendix C).														
	-121.915424	KJms _w	166.7	0.513015	10	2.31	8.1	0.512649	4.46	0.1	90	0.704245	13	206	8.2	0.703973
15-28G	48.050485	Thinly bedded metasilstone and very fine metasandstone. Interpreted as distal turbidite facies.														
	-121.906021	KJms _w	45.3	0.512832	9	2.82	11.3	0.512736	3.19	0.09	370	0.705292	15	217	26.9	0.705037
15-28D	48.047693	Thinly bedded metasilstone and very fine metasandstone. Interpreted as distal turbidite facies.														
	121.902617	KJms _w	45.3	0.512837	12	3.45	11.8	0.512724	2.95	0.12	364	0.70531	11	157	29.9	0.704919
15-26H	48.076255	Trachyandesite flow collected from age site 26H (Figure M3, Appendix C)(not sample split; secondary sample at the same age site).														
	-121.982255	Evr	43	0.51295	9	4.08	19.3	0.512878	5.81	0.09	190	0.705037	20	171	125	0.703701
15-400A	48.066898	Coarse grained hypidiomorphic granular muscovite bearing biotite granite of the Bald Mountain pluton of Tabor and others (2002); collected in the adjacent Verlot quadrangle.														
	-121.836016	Bald Mountain	50	0.512726	9	4.03	13.2	0.512608	0.7	0.09	535	0.722546	8	23.5	183	0.70652
15-400C	48.062465	Fine to medium grained hypidiomorphic granular muscovite and biotite bearing granite of the Mount Pilchuck Stock (Tabor and others, 2002); collected in the adjacent Verlot quadrangle (Figure M3).														
	-121.804182	Mount Pilchuck	49.7	0.512636	11	9.1	41.4	0.512551	-0.42	0.11	675	0.713133	14	55.2	151	0.707545

Appendix E. Isotope Geochemistry

Isotopic analyses of Sr and Nd (9 samples) and Pb (3 samples) were performed at the University of Washington using a Nu Instruments multi-collector (MC) ICP-MS. Sr and Nd separations were performed following Nelson (1995), and the analytical procedures are described in Gaffney and others (2007) for Nd and in Brach-Papa and others (2009) for Sr. The procedures for Pb separation and subsequent MC-ICP-MS analysis are given in Harkins and others (2008). Sample localities are reported in Table E1.

In general, samples represent the freshest available material from representative exposures within each unit. Two samples each of Eigd and KJms_w, taken from different localities, were analyzed to assess the isotopic heterogeneity of these units, which was found to be minimal. Samples chosen for isotopic analysis were also analyzed for trace elements (Data Supplement) and where possible were also dated samples (Appendix C). The sample inventory in the Data Supplement spreadsheet provides the list of the various geochronology and geochemistry samples analyzed during our study including samples with multiple analyses. The results of the isotopic work reveal a wide range of initial ratios, indicating the Eocene magmas were derived from both mantle (or juvenile crustal) and older crustal material sources.

Table E2. Pb isotopic data. Th, U, and Pb concentrations by ICP-MS. External reproducibility (2σ) ± 125 , 150, and 200 ppm for $^{206}\text{Pb}/^{204}\text{Pb}$, $^{207}\text{Pb}/^{204}\text{Pb}$, and $^{208}\text{Pb}/^{204}\text{Pb}$, respectively. Pb isotope compositions are normalized to NIST-981 accepted values of $^{208}\text{Pb}/^{204}\text{Pb} = 36.721$, $^{207}\text{Pb}/^{204}\text{Pb} = 15.491$, $^{206}\text{Pb}/^{204}\text{Pb} = 16.937$. Initial ratios calculated for ages given in Table E1.

Sample	Unit	Th (ppm)	U (ppm)	Pb (ppm)	$^{206}\text{Pb}/^{204}\text{Pb}$	$^{207}\text{Pb}/^{204}\text{Pb}$	$^{208}\text{Pb}/^{204}\text{Pb}$	$^{206}\text{Pb}/^{204}\text{Pb}(\text{i})$	$^{207}\text{Pb}/^{204}\text{Pb}(\text{i})$	$^{208}\text{Pb}/^{204}\text{Pb}(\text{i})$
15-4E	Eigd	7.47	2.84	2.16	19.538	15.598	39.165	18.93454	15.56988	38.64224
15-28G	KJms _w	1.56	0.78	4	18.649	15.566	38.328	18.55249	15.56168	38.26417
15-400A	Bald Mtn. Pluton	8.39	6.77	14	19.322	15.635	38.862	19.07836	15.62332	38.7625